
Degree Project in Energy Technology

Second Cycle, 30 credits

# Ray-Tracing Simulation and Analysis of Bifacial PV with Multi-Albedo Surfaces

**MOHAMMED NABEEL HUMAYOON KABIR**

KTH School of Industrial Engineering and Management

Energy Technology - TRITA-ITM-EX 2025 111

Division of Heat and Power Technology

SE-100 44 STOCKHOLM

## Authors

Mohammed Nabeel Humayoon Kabir  mnhk@kth.se
Energy Technology
KTH Royal Institute of Technology

TRITA-ITM-EX 2025 111

## Place for Project

Stockholm, Sweden
Paris, France

## Examiner

Jeevan Jayasuriya
Stockholm, Sweden
KTH Royal Institute of Technology

## Supervisor

Alessandro Galleani
Feedgy (Quantom SAS)
Paris, France

**Master of Science Thesis**

**Department of Energy Technology**

**KTH 2025**

**Ray-Tracing Simulation and Analysis of Bifacial PV with Multi-Albedo Surfaces**

Mohammed Nabeel Humayoon Kabir

mnhk@kth.se

| Approved | Examiner | Supervisor |
|---|---|---|
| June 2025 | Jeevan Jayasuriya<br>Department of Energy Technology | Jeevan Jayasuriya<br>Department of Energy Technology |
| TRITA:<br>ITM-EX 2025:111 | Industrial Supervisor<br>Alessandro Galleani<br>Feedgy (Quantom SAS)<br>Paris, France | Contact person<br>Nabeel Humayoon<br>m.nabeel122@gmail.com |

TRITA – ITM-EX 2025:111
Stockholm, Sweden 2025

www.kth.se

# ABSTRACT

The global shift towards renewable energy has driven the advancement of bifacial photovoltaic (PV) systems, which generate electricity from both front and rear surfaces, capturing reflected light from the ground, known as albedo. This rear-side contribution significantly boosts energy yield, particularly when reflective surfaces are optimized. While traditional simulation tools like PVsyst approximate rear-side generation, they often oversimplify albedo's spatial and angular effects, leading to discrepancies with real-world performance. To overcome this, Sunsolve, a ray-tracing simulation tool, offers detailed modeling of light interactions, enabling more accurate predictions of bifacial gains over multi-albedo surfaces.

This thesis evaluates Sunsolve Yield's, further referred to as Sunsolve, accuracy for bifacial PV systems installed at a site in France, where albedo booster sheets of varying widths (3m, 4m, 5m, and 6m) were deployed under specific inverter MPPTs. Real-world data, including inverter outputs, weather conditions, and measured albedo values, served as the reference for validating Sunsolve's predictions. The analysis focuses on:

- Gain Yield Analysis, comparing the additional energy from boosters against a grass baseline.
- Simulated vs. Actual Comparisons, highlighting booster-induced gains through daily resampled scatter plots.
- Error Metric Evaluation using RMSE, SMAPE, $R^2$, and RMBE to measure Sunsolve's predictive accuracy.
- Sunny vs. Diffused Day Analysis, revealing variations in simulation accuracy under different irradiance conditions.

Results show that Sunsolve effectively captures albedo-induced bifacial gains, especially for larger booster configurations, but discrepancies arise from edge effects, spatial albedo variations, and inverter clipping. The study underscores the importance of site-specific properties and suggests enhancements like rear irradiance sensors and custom material inputs to improve simulation fidelity.

Overall, this research validates Sunsolve's capabilities while identifying pathways for optimizing both field setup and simulation accuracy in bifacial PV applications, paving the way for more reliable energy yield predictions in multi-albedo environments.

**Keywords:**
Bifacial Photovoltaics, Albedo Boosters, Ray-Tracing Simulation, Sunsolve, Multi-Albedo Surfaces, PV Performance Validation, Renewable Energy Modeling

# SAMMANFATTNING

Den globala övergången till förnybar energi har drivit på utvecklingen av bifaciala solcellssystem (PV), som genererar elektricitet från både fram- och baksida genom att utnyttja reflekterat ljus från markytan, så kallad albedo. Detta baksidesbidrag kan väsentligt öka energiproduktionen, särskilt när reflekterande ytor optimeras. Traditionella simuleringsverktyg som PVsyst uppskattar baksidesgenereringen, men förenklar ofta albedons rumsliga och vinklade effekter, vilket kan leda till avvikelser från verklig prestanda. För att hantera detta erbjuder Sunsolve – ett strålspårningsbaserat simuleringsverktyg – en mer detaljerad modellering av ljusinteraktioner och möjliggör därmed noggrannare prognoser av bifaciala vinster över ytor med varierande albedo.

Denna avhandling utvärderar Sunsolve Yields noggrannhet – hädanefter benämnt Sunsolve – för bifaciala PV-system installerade på en plats i Frankrike, där albedoförstärkande ark med varierande bredd (3 m, 4 m, 5 m och 6 m) placerades under specifika MPPT:er hos växelriktare. Fältdata såsom växelriktarens effekt, väderförhållanden och uppmätta albedovärden användes som referens för att validera Sunsolves prognoser. Analysen fokuserar på:

- Analys av energivinst, där extra energi från förstärkarna jämförs med en gräsreferens.
- Simulering vs. verklighet, genom dagliga omprovade spridningsdiagram.
- Felanalys med RMSE, SMAPE, $R^2$ och RMBE.
- Analys av soliga och diffusa dagar för att visa noggrannhetsvariationer.

Resultaten visar att Sunsolve effektivt fångar albedobaserade bifaciala vinster, särskilt för bredare förstärkarkonfigurationer. Vissa avvikelser orsakas av kantpåverkan, rumslig albedovariation och växelriktarbegränsningar. Studien understryker vikten av platsspecifika faktorer och föreslår förbättringar såsom bakre irradianssensorer och anpassade materialdata för ökad simuleringsprecision.

Sammanfattningsvis bekräftar denna forskning Sunsolves potential och visar vägar för att optimera både fältlayout och simuleringsnoggrannhet i bifaciala PV-system – vilket möjliggör mer tillförlitliga prognoser av energiproduktion i miljöer med flera albedoytor.

**Nyckelord:**
Bifacial solceller, Albedoförstärkare, Strålgångssimulering, Sunsolve, Multi-albedoytor, Validering av PV-prestanda, Modellering av förnybar energi

# ACKNOWLEDGEMENTS

I would like to express my sincere gratitude to everyone who supported and guided me throughout the course of this thesis and my academic journey.

First and foremost, I am deeply thankful to Marko Pavlov, Head of the IoT and Modeling wing of the R&D and Innovation Department at Feedgy, whose initial ideas and vision laid the foundation for this thesis. This project would not have existed without his insights and guidance. His involvement at every stage, from conception to execution, was instrumental in shaping the direction of my research. I am especially grateful for his consistent encouragement and his belief in this work, which provided me with the confidence to explore and build on novel concepts.

I also wish to express my heartfelt thanks to Alessandro Galleani, my supervisor at Feedgy, for his invaluable support, mentorship, and incredibly positive attitude. His experience, technical knowledge, and insightful feedback significantly contributed to the quality of this thesis. His open-mindedness and clarity in approach made working on this project an enjoyable and enriching experience.

To the entire Feedgy team and my colleagues at the company, thank you for fostering such a dynamic, welcoming, and innovative work environment. You made me look forward to what I do each day. The collaborative atmosphere, coupled with a culture of curiosity and creativity, helped me grow not only technically but also in how I think about problems. Working at Feedgy broadened my perspective and encouraged me to think outside the box, an approach I will carry forward in my career.

On the academic front, I am sincerely grateful to Professor Jeevan Jayasuriya, my examiner and professor at KTH, for his support and guidance throughout this journey. His thoughtful suggestions and timely feedback provided valuable academic perspective and direction, which helped shape the overall structure and clarity of this thesis. I deeply appreciate the time and attention he dedicated to reviewing my work and steering me in the right direction.

Lastly, I would like to express my deepest gratitude to my family. Their unwavering support and encouragement have made it possible for me to pursue my education in the field of renewable energy and bring this thesis to completion. Their constant presence has provided me with strength and stability throughout this journey. Their support allowed me to focus fully on both my academic and professional responsibilities while maintaining a healthy and fulfilling life outside of work and study. I am profoundly grateful for their trust, care, and unwavering belief in me.

To everyone who has been part of this journey- thank you!

# CONTENTS

# LIST OF TABLES



# LIST OF FIGURES

# List of Acronyms

| Acronym | Full Form |
|---|---|
| AC | Alternating Current |
| CSV | Comma-Separated Values |
| DC | Direct Current |
| DHI | Diffuse Horizontal Irradiance |
| DNI | Direct Normal Irradiance |
| GHI | Global Horizontal Irradiance |
| IV | Current-Voltage |
| MPPT | Maximum Power Point Tracker |
| NREL | National Renewable Energy Laboratory |
| POA | Plane of Array |
| PV | Photovoltaic |
| $R^2$ | Coefficient of Determination |
| RMBE | Relative Mean Bias Error |
| RMSE | Root Mean Square Error |
| RT | Ray Tracing |
| SMAPE | Symmetric Mean Absolute Percentage Error |
| UTC | Coordinated Universal Time |
| VF | View Factor |

# 1. INTRODUCTION

The global transition towards sustainable energy solutions has accelerated advancements in photovoltaic (PV) technologies, with bifacial PV systems emerging as a promising innovation. Unlike traditional mono-facial modules, bifacial modules generate electricity from both the front and rear surfaces, harnessing not only direct sunlight but also reflected light from the ground. This ability to utilize rear-side irradiance significantly boosts overall energy yield, especially in optimized environments where ground reflectance is enhanced. The extent of this rear-side contribution largely depends on the albedo properties of the surface beneath the panels. Natural surfaces such as grass, soil, or sand typically exhibit low albedo values, while engineered reflective surfaces, like white gravel, painted sheets, or custom-manufactured boosters, can substantially amplify rear-side irradiance, thereby enhancing bifacial power generation.

However, accurately predicting the energy yield of bifacial PV installations remains a considerable challenge due to the complex interplay of light reflections, module tilt, row spacing, and spatial variations in albedo. Traditional simulation softwares such as PVsyst incorporates rear-side generation through empirical models but often simplifies the angular and spatial distribution of reflected light. This approximation can lead to discrepancies between simulated outputs and actual field performance, particularly in scenarios involving heterogeneous albedo surfaces and complex terrain. To address these limitations, advanced ray-tracing simulation tools like Sunsolve, developed by an Australian company PV Lighthouse, have been introduced.[1] Sunsolve's ray-tracing capabilities allow for more granular modeling of light interactions, capturing multi-angle reflections, shadow effects, and variable surface textures with higher fidelity. This detailed representation is particularly valuable for bifacial systems, where rear-side contributions are sensitive to fine variations in reflected light.

## 1.1. Research Context and Objectives

This thesis is dedicated to evaluating the accuracy and reliability of Sunsolve's simulation capabilities for bifacial PV systems deployed over multi-albedo surfaces. The study is conducted at a bifacial PV site located in France, where albedo boosters of varying widths (3m, 4m, 5m, and 6m) were strategically installed beneath specific inverter MPPTs. These reflective sheets were designed to enhance rear-side irradiance, providing an ideal environment for studying the influence of controlled albedo modifications on bifacial energy yield. The unique field setup allows for the comparison of different booster widths in terms of their impact on rear-side generation, providing valuable insights into the optimization of albedo-enhanced PV installations.

Field data collected from the site, including weather measurements (GHI, DHI, DNI, ambient temperature, and wind speed) as well as inverter performance metrics for distinct MPPTs, serve as the primary reference for validating Sunsolve's simulation outputs. The study period spans from May 15 to August 13, 2024, with real-world albedo data available from June 13 to July 15, 2024, when the reflective boosters were operational. The analysis focuses on comparing the simulated MPPT power outputs against actual field measurements to assess the alignment and discrepancies in energy yield predictions. Furthermore, the grass scenario serves as the baseline reference for evaluating the gains introduced by the albedo boosters.

## 1.2. Research Questions

This study is guided by the following research questions aimed at assessing the predictive accuracy and optimization potential of Sunsolve's ray-tracing model:

1. How accurately does Sunsolve simulate bifacial PV energy yield under varying albedo conditions when compared to real field data?
2. What are the main sources of discrepancy between Sunsolve simulations and measured site performance?
3. How effective are albedo boosters of different widths in enhancing bifacial energy gains, and how well does Sunsolve capture this effect?
4. Can site-specific material properties and weather parameters improve the alignment of Sunsolve simulations with actual performance?
5. What optimizations can be made in Sunsolve’s ray-tracing parameters to enhance its predictive accuracy for bifacial PV systems?

## 1.3. Scope of Work

The primary scope of this thesis includes:

- Field Data Collection: Collecting the required field data, cleaning and processing the field data to pave the ground for seamless integration and analysis.
- Simulation Analysis: Performing detailed Sunsolve simulations for different albedo booster configurations (3m, 4m, 5m, 6m) and comparing the results against actual MPPT data from the site.
- Yield Gain and Time-Series Analysis: Evaluating time-series data for daily and hourly gains, assessing the consistency and magnitude of albedo-induced enhancements.
- Error Metrics and Validation: Calculating RMSE, SMAPE, $R^2$, and RMBE to quantify discrepancies and validate Sunsolve's accuracy.
- Sensitivity to Environmental Conditions: Investigating the impact of sunny and diffused days on simulation accuracy and yield variations.

## 1.4. Contributions of the Study

This thesis contributes to the understanding of:

- The practical effectiveness of albedo booster sheets of varying widths for bifacial PV optimization.
- The discrepancies and alignment between Sunsolve simulations and real-world performance metrics.
- The influence of cloud coverage and edge effects on MPPT power generation and how these can be adjusted for better simulation alignment.
- Opportunities for enhanced rear-side irradiance measurements using rear sensors and the potential for site-specific material properties in simulation models.
- Methodological improvements for future validation and simulation accuracy enhancements, particularly in the context of multi-albedo surfaces.

The findings from this research are expected to guide the design and simulation of bifacial PV systems, offering insights into optimizing albedo-based performance gains while improving the predictive accuracy of ray-tracing models like Sunsolve. Furthermore, it lays the groundwork for future improvements in field setup, simulation parameterization, and innovative research avenues to enhance the reliability of PV system simulations under variable albedo conditions.

# 2. LITERATURE REVIEW

## 2.1. Bifacial Photovoltaic System Technology

Bifacial photovoltaic (PV) technology has emerged as a significant advancement in the solar energy sector, offering the potential to enhance energy yield by capturing sunlight on both the front and rear sides of the solar module. Unlike traditional monofacial modules that only utilize the front surface for energy conversion, bifacial modules are designed to absorb light from both sides, thereby increasing the overall energy output. This section delves into the fundamental principles, advantages, and technological developments of bifacial PV systems. [2]

### 2.1.1. Fundamental Principles

Bifacial PV modules are typically constructed using transparent materials, such as glass, on both the front and rear sides, allowing light to penetrate and be absorbed by the photovoltaic cells from multiple directions. The rear side captures albedo light- sunlight that is reflected off the ground or surrounding surfaces- contributing to additional energy generation. The efficiency of bifacial modules is influenced by several factors, including the albedo of the installation surface, the height of the modules above the ground, and the tilt angle. Higher albedo surfaces, such as white concrete or snow-covered ground, can significantly enhance the rear-side irradiance, leading to increased energy output.

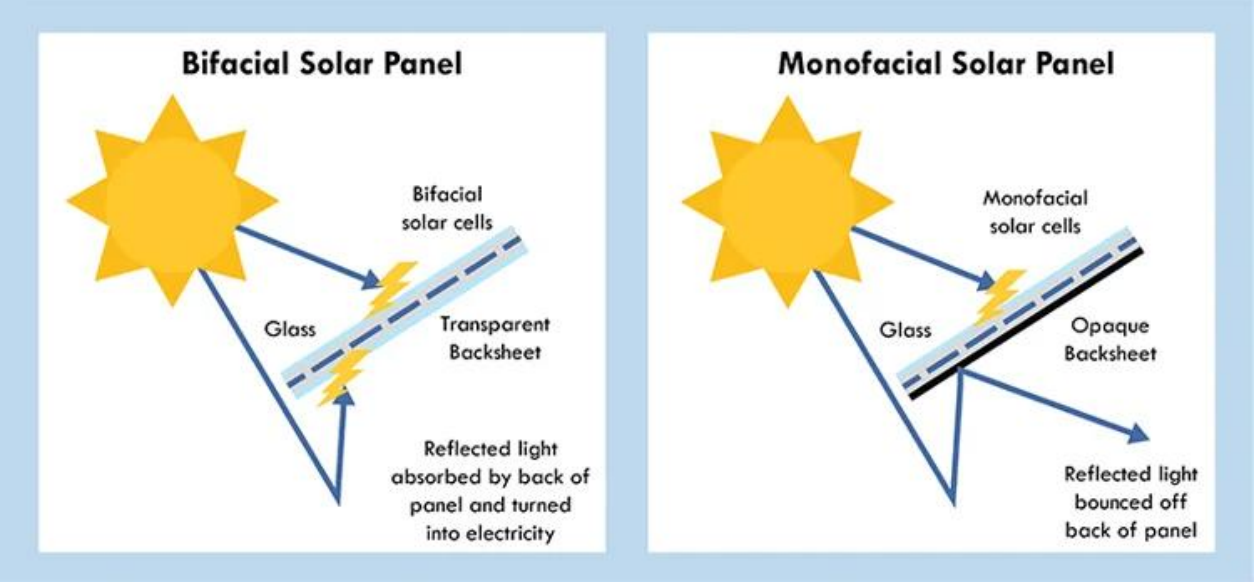


*Figure 1 MonoFacial and Bifacial PV Panels*

### 2.1.2. Advantages Over Monofacial Systems

The adoption of bifacial PV technology offers several advantages over conventional monofacial systems. [2]

- Increased Energy Yield: By harnessing light from both sides, bifacial modules can achieve higher energy output, with studies reporting gains ranging from 5% to 30%, depending on installation conditions.
- Improved Performance in Diffuse Light Conditions: Bifacial modules are more effective in capturing scattered and reflected light, making them suitable for regions with high diffuse irradiance.
- Enhanced Durability: The use of glass on both sides not only facilitates bifaciality but also improves the mechanical strength and longevity of the modules.
- Lower Levelized Cost of Electricity (LCOE): The increased energy production can lead to a reduction in LCOE, making bifacial systems more economically attractive over the system's lifetime. [2]

### 2.1.3. Technological Developments

Recent years have witnessed significant advancements in bifacial PV technology:

- Cell Technologies: Innovations such as Passivated Emitter and Rear Cell (PERC) [3], Passivated Emitter and Rear Totally Diffused (PERT) [4], and Heterojunction with Intrinsic Thin layer (HIT) [5] have been adapted for bifacial applications, enhancing efficiency and performance.
- Module Design: Manufacturers are optimizing module designs to maximize bifacial gain, including adjustments in frame design, encapsulant materials, and cell spacing.
- System Integration: The integration of bifacial modules with tracking systems has been explored to further augment energy capture by optimizing the angle of incidence throughout the day. [2]

### 2.1.4. Challenges and Considerations

Despite the promising advantages, bifacial PV systems present certain challenges:

- Measurement and Standardization: There is a lack of standardized testing procedures for bifacial modules, complicating performance assessment and comparison. [6]
- Modeling Complexity: Accurately modeling the performance of bifacial systems requires comprehensive data on site-specific albedo, shading, and other environmental factors.
- Installation Considerations: Optimal installation of bifacial modules necessitates careful planning regarding tilt angle, height, and ground surface properties to maximize rear-side irradiance.

Bifacial PV technology represents a significant stride in solar energy generation, offering enhanced efficiency and potential cost savings. While challenges remain in standardization and modeling, ongoing research and technological innovations continue to address these issues, paving the way for broader adoption of bifacial systems in various applications.

## 2.2. Influence of Albedo and Reflective Surfaces

Albedo, defined as the fraction of solar radiation reflected by a surface, plays a pivotal role in the performance of photovoltaic systems, especially bifacial modules that can capture light from both their front and rear surfaces. The reflectivity of the ground or surrounding surfaces directly influences the amount of irradiance reaching the rear side of bifacial panels, thereby affecting their overall energy yield. Understanding and optimizing albedo is crucial for enhancing the efficiency and reliability of PV installations.

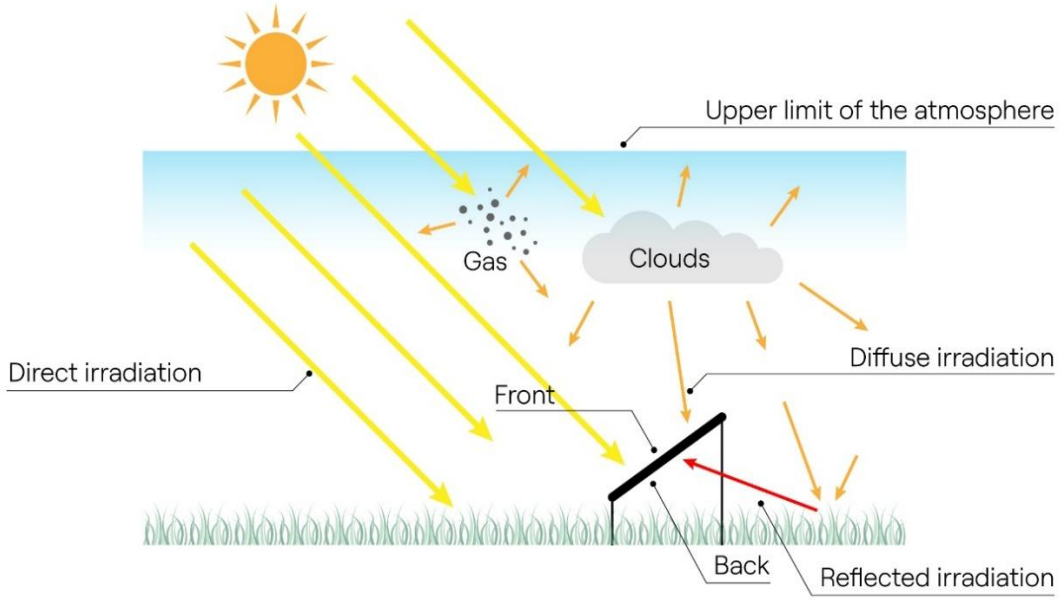


*Figure 2 Albedo in Solar PV systems [7]*

### 2.2.1. Albedo and Its Impact on PV Performance

The albedo of a surface varies based on its material and color. For instance, fresh snow has a high albedo of up to 0.9, while darker surfaces like asphalt have much lower values. In the context of PV systems, higher ground albedo can significantly boost the rear-side irradiance of bifacial modules. A study by Sun et al. (2017) demonstrated that increasing ground albedo from 0.25 to 0.5 could enhance bifacial gain by up to 30%, especially when modules are elevated above the ground. [8] [9]

Moreover, the type of ground cover affects albedo. Research indicates that surfaces like white concrete or reflective membranes can substantially increase albedo compared to

natural ground covers like grass. For example, a study by Amerisolar highlighted that using high-albedo materials beneath PV installations can lead to improved energy output. [10]

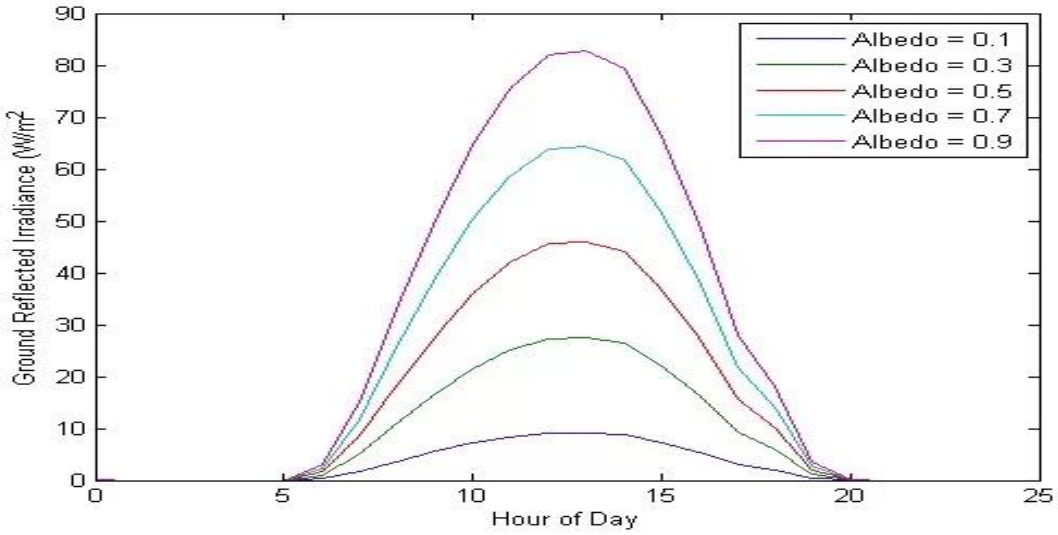


*Figure 3 Effects of Albedo on the Reflection of Solar Radiation (PVMC, 2019) [10]*

### 2.2.2. Reflective Surfaces and Albedo Boosters

Beyond natural ground reflectivity, artificial reflective surfaces, often termed albedo boosters, have been employed to enhance PV performance. These include materials like white gravel, reflective foils, or specially designed mirrors placed strategically around PV modules. A study by Enel Green Power emphasized the role of such reflective surfaces in optimizing energy production, especially in bifacial systems. [7]

Additionally, research by Tech Xplore (2024) discussed the integration of artificial ground reflectors in solar setups, noting improvements in system energy production and efficiency. The study found that these reflectors could make solar projects more economically viable by boosting energy yields. [11]

### 2.2.3. Dynamic Albedo and Environmental Considerations

Albedo is not a static property; it can change over time due to environmental factors such as snow cover, vegetation growth, or soiling. A study by Golroodbari et al. (2022) investigated the effect of dynamic albedo on the performance modeling of floating offshore PV systems, highlighting the importance of accounting for temporal albedo variations in accurate energy yield predictions. [12]

Furthermore, large-scale PV installations can themselves influence local albedo. Research published in Nature Communications (2024) indicated that extensive PV panel deployment might reduce local terrestrial albedo, potentially triggering a positive radiative forcing effect.

This underscores the need to consider the broader climatic implications of PV installations. [13]

### 2.2.4. Conclusion

Albedo and reflective surfaces are integral to the performance optimization of PV systems, particularly bifacial modules. By selecting appropriate ground materials and incorporating artificial reflectors, it is possible to enhance energy yields significantly. However, considerations regarding dynamic environmental changes and potential climatic impacts are essential for sustainable and efficient PV deployment.

## 2.3. Challenges in Modeling Bifacial Systems

Bifacial photovoltaic (PV) systems, which capture solar irradiance from both the front and rear sides of the module, have garnered significant attention due to their potential for increased energy yield. However, accurately modeling their performance, especially in environments with heterogeneous albedo conditions, presents several challenges. Traditional simulation tools often fall short in capturing the complexities associated with bifacial systems, necessitating the development and validation of more advanced modeling approaches.

### 2.3.1. Limitations of Traditional Simulation Tools

Conventional PV simulation software, such as PVSYST, has been widely used for modeling monofacial PV systems. However, its application to bifacial systems is limited. For instance, PVSYST's bifacial model is primarily based on a 2D approach, which may not accurately account for complex shading scenarios and varied ground reflectivity. Moreover, it lacks the capability to model multiple orientations within a single simulation, which is crucial for systems with varying module tilts and azimuths. These limitations can lead to inaccuracies in predicting the rear-side irradiance and, consequently, the overall energy yield of bifacial systems. [14]

Furthermore, the reliance on simplified assumptions, such as uniform ground albedo and neglecting the impact of nearby structures, can result in significant deviations between simulated and actual performance. This is particularly problematic in environments where the ground reflectivity varies spatially and temporally, such as in agricultural settings or regions with seasonal snow cover.

### 2.3.2. Challenges in Modeling Multi-Albedo Environments

Modeling bifacial PV systems in multi-albedo environments introduces additional complexities. The presence of surfaces with varying reflectivity, such as grass, concrete, and reflective membranes, affects the distribution of irradiance on the rear side of the modules. Traditional models often assume a constant albedo value, which does not capture the

dynamic nature of real-world conditions. This can lead to underestimation or overestimation of the bifacial gain.

Moreover, the angular dependence of reflected irradiance and the impact of module elevation and spacing further complicate the modeling process. Accurately capturing these factors requires detailed 3D modeling and ray-tracing techniques, which are computationally intensive and not typically incorporated into standard simulation tools. [15]

### 2.3.3. Advancements and the Need for Validation

To address these challenges, advanced modeling approaches, such as ray-tracing and view factor methods, have been developed. These methods offer more accurate representations of the complex interactions between solar irradiance, module geometry, and environmental conditions. For example, ray-tracing models simulate the path of individual light rays, accounting for reflections and shading effects, while view factor models estimate the proportion of irradiance exchanged between surfaces. [16]

However, the increased complexity of these models necessitates thorough validation against empirical data to ensure their reliability. Field measurements and experimental studies are essential for calibrating and validating these advanced models, particularly in diverse environmental conditions. This validation process is crucial for establishing confidence in the predictive capabilities of the models and for informing design decisions in bifacial PV system deployment. [17]

### 2.3.4. Conclusion

Accurate modeling of bifacial PV systems, especially in multi-albedo environments, remains a significant challenge. Limitations in traditional simulation tools necessitate the adoption of advanced modeling techniques, such as ray-tracing and view factor methods. However, these approaches require comprehensive validation through empirical studies to ensure their accuracy and reliability. Addressing these challenges is critical for optimizing the design and performance of bifacial PV systems in real-world applications.

## 2.4. Ray-Tracing Techniques for PV Simulation

The accurate simulation of bifacial photovoltaic (PV) systems necessitates advanced modeling techniques that can capture the complex interactions of light within these systems. Ray-tracing methods have emerged as a powerful tool in this context, offering detailed insights into the behavior of light as it interacts with various surfaces and materials. Unlike traditional modeling approaches, ray-tracing can account for the intricate geometries and varying albedo conditions often present in bifacial PV installations.

### 2.4.1. Fundamentals of Ray-Tracing in PV Applications

Ray-tracing is a computational technique that simulates the path of individual light rays as they travel through an environment, reflecting, refracting, or absorbing upon encountering different surfaces. In the context of PV systems, ray-tracing allows for the modeling of how sunlight interacts with both the front and rear surfaces of bifacial modules, as well as with the surrounding environment. This includes accounting for factors such as ground reflectivity (albedo), shading from nearby objects, and the angular distribution of incoming light.[18]

Tools like *bifacial_radiance*, developed by the National Renewable Energy Laboratory (NREL), utilize ray-tracing to model complex PV system layouts, including varying terrain and structural shading. These simulations can provide high-resolution data on irradiance distribution, which is critical for optimizing system design and predicting energy yield. [19]

### 2.4.2. Advantages Over Traditional Modeling Approaches

Traditional PV simulation tools, such as PVSYST, often rely on simplified assumptions and 2D models that may not accurately represent the complexities of bifacial systems. For instance, they might assume uniform albedo or neglect the impact of shading from adjacent rows. Ray-tracing, on the other hand, can model these factors in three dimensions, providing a more accurate representation of real-world conditions.[20]

A study by Grommes et al. demonstrated that combining ray-tracing with view factor models can enhance the accuracy of bifacial PV simulations. Their open-source tool, BifacialSimu, was validated against field data from installations in the USA and Germany, showing that the hybrid approach effectively captures both the detailed irradiance patterns and the overall energy yield. [21]

### 2.4.3. Computational Considerations

While ray-tracing offers increased accuracy, it is also computationally intensive. Simulating large-scale PV systems or conducting annual performance assessments can require significant processing time and resources. To address this, researchers have developed methods to accelerate ray-tracing simulations. For example, a study published in *Cell Reports Physical Science* introduced techniques to speed up Monte Carlo ray-tracing by nearly 90%, enabling more practical application of these methods in large-scale simulations. [22]

### 2.4.4. Integration with Other Modeling Techniques and Emerging Tools

Given the computational demands of ray-tracing, it is often beneficial to integrate it with other modeling approaches. Hybrid models that combine ray-tracing with view factor methods can balance accuracy and efficiency. For instance, using view factor models to

estimate the front-side irradiance and ray-tracing for the rear side can reduce computational load while maintaining high accuracy. This approach has been shown to be effective in studies focusing on complex albedo environments, where rear-side irradiance becomes increasingly significant [23]

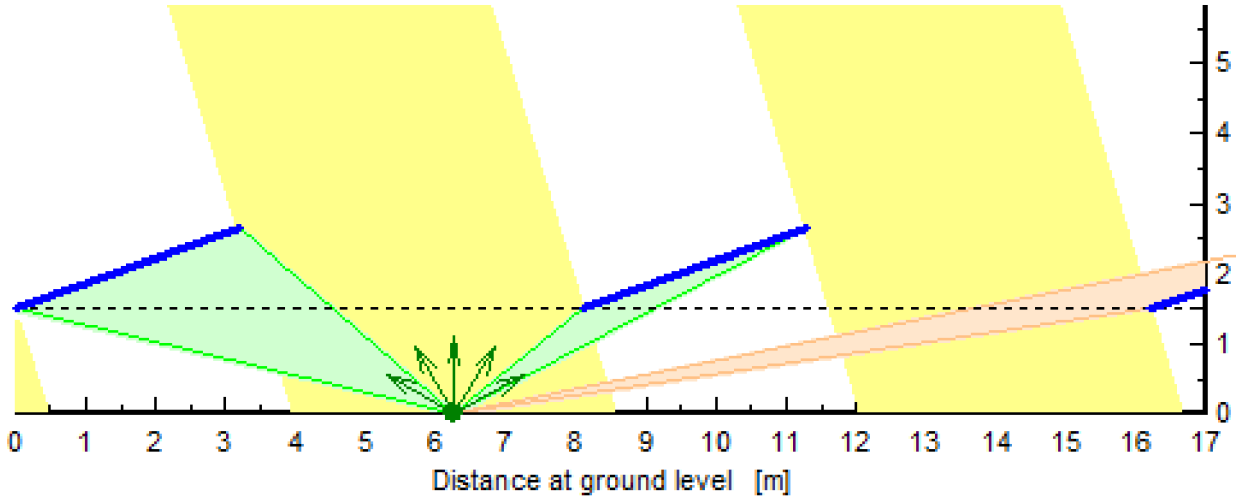


*Figure 4 Illustration of view factor to show how the rear side irradiance is evaluated. [23]*

Among emerging ray-tracing platforms, Sunsolve stands out for its application-specific focus on photovoltaic simulations. Developed by PV Lighthouse, Sunsolve offers 3D ray-tracing capabilities optimized for bifacial and vertical PV systems. It supports the modeling of arbitrary albedo distributions, shadow casting from nearby objects, and both direct and diffuse irradiance paths, making it particularly suitable for research into advanced albedo configurations such as reflective booster sheets. [1]

While not yet as extensively validated in academic literature as open-source tools like *bifacial_radiance*, Sunsolve is gaining traction in industry-focused projects for its intuitive UI and highly configurable simulation environment. Its primary limitation, however, lies in the limited accessibility of its backend algorithms, making it difficult to benchmark directly against open models without robust validation using field data, one of the key aims of this thesis.

### 2.4.5. Conclusion

Ray-tracing techniques represent a significant advancement in the simulation of bifacial PV systems, offering detailed and accurate modeling capabilities that surpass traditional methods. By capturing the complex interactions of light with module surfaces and environmental features, ray-tracing enables better system design and more reliable performance predictions.

Emerging tools like Sunsolve are pushing the boundaries of what can be modeled, particularly in systems with heterogeneous albedo surfaces. However, the lack of transparency in some commercial tools underscores the importance of validation studies - particularly those combining ray-tracing with real-world data - to ensure simulation reliability. Thus, integrating Sunsolve into this research not only serves as a performance evaluation of ray-tracing itself, but also contributes to the ongoing effort to improve bifacial PV modeling practices.

## 2.5. Review of Relevant Studies

The advancement of bifacial photovoltaic (PV) technology has necessitated rigorous research into accurate modeling techniques and performance assessments. This section reviews pivotal studies that have contributed to the understanding and optimization of bifacial PV systems.

### 2.5.1. Comparative Analysis of Modeling Techniques

A significant study by Ernst et al. (2024) conducted a comprehensive comparison between View-Factor (VF) and Ray Tracing (RT) models to evaluate their effectiveness in predicting bifacial irradiance. Utilizing an experimental dataset from the National Renewable Energy Laboratory (NREL) in Colorado, USA, the study found that while both models performed similarly for front-side irradiance, RT models provided more accurate predictions for rear-side irradiance, especially in complex environments with varying albedo and shading conditions. This highlights the importance of selecting appropriate modeling techniques based on specific system configurations and environmental factors. [15]

### 2.5.2. Enhancing Simulation Efficiency

Addressing the computational challenges associated with RT models, Ernst et al. (2021) proposed methods to accelerate Monte Carlo ray tracing simulations for large-scale solar systems. By optimizing the simulation algorithms, they achieved a reduction in computation time by nearly 90% without compromising accuracy. The study reported root-mean-square error values of 7.9% for front irradiance and 37.2% for rear irradiance when compared to field measurements. These advancements make RT models more feasible for practical applications in large PV installations. [22]

### 2.5.3. Experimental Performance Assessments

An experimental study by Tonita et al. (2023) introduced the Scaled Rear Irradiance (SRI) method to account for spectral albedo effects in bifacial PV systems. The research emphasized that traditional measurement standards often neglect the spectral characteristics of albedo, leading to inaccuracies in rear-side irradiance estimation. By incorporating spectral considerations, the SRI method provides a more accurate

representation of real-world operating conditions, facilitating better performance predictions and system designs. [24]

### 2.5.4. Impact of Environmental Factors

Ghafiri et al. (2024) conducted a year-long experimental study in the Canadian climate to evaluate the performance of bifacial PV modules. The research focused on the effects of snow coverage and local irradiance variations on energy yield. The study found that snow accumulation significantly impacted rear-side irradiance, leading to variations in energy output. Additionally, the research compared RT (Ray-Tracing) and 2D VF (View Factor) models, concluding that while RT models offered higher accuracy, VF models provided sufficient precision with reduced computational requirements for certain applications. [25]

### 2.5.5. Integration of Modeling and Experimental Data

A study by Grommes et al. (2023) combined RT and VF models to simulate irradiance and yield calculations of bifacial PV systems. By validating the simulation results with data from a single-axis tracked plant in the USA and a fixed-tilt plant in Germany, the research demonstrated that hybrid modeling approaches could effectively balance accuracy and computational efficiency. The study underscored the importance of integrating multiple modeling techniques to capture the complexities of bifacial PV systems accurately. [21]

These studies collectively underscore the critical role of accurate modeling and experimental validation in optimizing bifacial PV systems. The integration of advanced simulation techniques, consideration of environmental factors, and validation with real-world data are essential for enhancing the performance and reliability of bifacial photovoltaic installations.

# 3. METHODOLOGY

The methodology of this study is designed to evaluate the accuracy of Sunsolve's ray-tracing simulations for bifacial PV systems equipped with albedo boosters of varying widths. This evaluation is based on a detailed comparison with real-world field data collected from a bifacial PV installation located in France. The research workflow is structured to systematically capture site-specific characteristics, configure high-fidelity simulations, and perform robust data analysis to assess simulation reliability.

First, the Site Description and Experimental Setup provides an overview of the PV plant, including module configuration, inverter assignments, and MPPT structures. Special attention is given to the spatial arrangement of albedo booster sheets (3m, 4m, 5m, and 6m), installed beneath specific MPPTs, which are central to assessing rear-side energy gains. This is followed by the Albedo Booster Deployment Strategy, detailing the rationale behind booster placements and the expected impact on rear irradiance.

To validate simulations, comprehensive Field Data Collection was conducted, capturing inverter power output, site-specific weather parameters, and surface albedo measurements. These datasets form the baseline for comparing Sunsolve's predictions with actual performance. The Simulation Environment and Configuration section outlines the setup of Sunsolve's ray-tracing environment, replicating site conditions, module specifications, and booster layouts to ensure consistency with field measurements.

Finally, the Data Processing and Analysis section describes the methodology for synchronizing field and simulation data, applying correction factors for edge effects, and calculating performance metrics such as RMSE, SMAPE, $R^2$, and RMBE. These analyses enable a granular comparison of energy yield, gain percentages, and error distributions across varying albedo scenarios.

Together, this methodological framework provides a structured approach to quantifying the accuracy of Sunsolve's simulations, identifying discrepancies, and proposing enhancements for improved predictive reliability in multi-albedo bifacial PV systems.


## 3.1. Site Description and Experimental Setup

In order to validate the accuracy of energy yield predictions produced by the Sunsolve simulation tool, it was essential to obtain empirical performance data from a real-world bifacial photovoltaic (PV) system operating under varying albedo conditions. For this purpose, experimental access was granted to a section of a utility-scale solar PV installation located near Dijon, France. The selected site provided a suitable test environment to deploy albedo treatment scenarios and collect high-resolution inverter-level performance data for comparison against simulation outputs.

### 3.1.1. Site Location and Climatic Conditions

The solar plant is located close to the city of Dijon in eastern France. The site lies at an elevation of approximately 100 to 130 meters above sea level and experiences a temperate oceanic climate, which is characterized by moderately cold winters and warm summers. The region receives an annual average of 1,850 to 2,000 hours of sunshine, offering favorable conditions for photovoltaic energy generation. Precipitation is distributed throughout the year, with light snow occurring occasionally during winter months. However, snowfall is typically brief and non-persistent, exerting minimal impact on long-term solar irradiance. During the rainy seasons, the site may experience moist soil and wet grass, which could influence the reflective properties of the ground.

### 3.1.2. Ground Characteristics

The natural ground surface throughout the site is composed predominantly of ordinary grassland. This surface serves as the baseline (homogeneous low-albedo) condition for the study. During specific periods of the year, such as winter and spring, the grass may be wet due to precipitation or exhibit temporary snow coverage. However, for the majority of the year, the site presents a consistent and low-albedo reflective surface, representative of typical field conditions used in large-scale PV installations. This consistency in ground conditions is critical for assessing the effect of introducing engineered high-albedo treatments for energy yield enhancement.

### 3.1.3. PV Plant Configuration

The solar PV plant comprises bifacial monocrystalline silicon modules rated at 565 Wp each. These modules are mounted on a fixed-tilt ground-mounted support structure, with a tilt angle of 20 degrees facing South optimized for the site's latitude. The selected area's mounting arrangement involves two rows of 27 modules each (27 × 2 layout) forming a single table structure. The physical layout and geometric configuration of the mounting system are illustrated in Figure 5 and Figure 6 below, which provides a schematic representation of the module orientation and structural spacing.

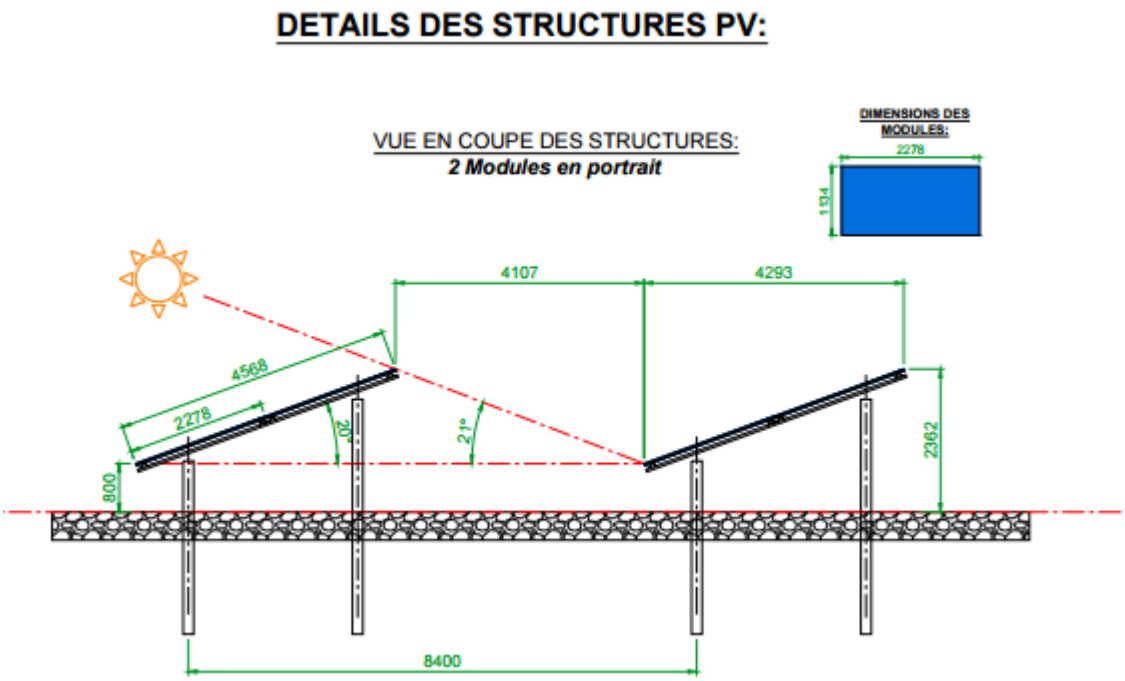


*Figure 5 Field PV Mounting System*

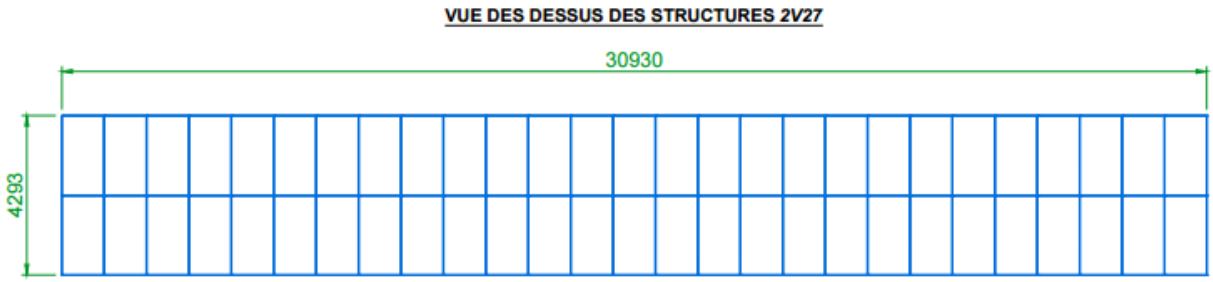


*Figure 6 PV Panel Configuration*

The plant operates using 45 string inverters, each rated at 200 kVA. Each inverter is connected to multiple module strings configured to maximize energy harvest while staying within operational voltage and current limits. The entire site was divided into 3 sections based on the transformer the section was connected to. Our experimental set up was based in section 1 of the site which was connected to transformer 1 (PTR 1). A section of the site layout is shown in Figure 7 , highlighting the string table arrangement and inverter distribution within the experimental area.


*Figure 7 Field PV Layout. The experimental zone is indicated with the green square.*

## 3.2. Albedo Booster Deployment Strategy

As part of the experimental setup, engineered albedo booster sheets were deployed beneath selected PV module tables to assess their influence on bifacial energy yield. These reflective surfaces were designed to enhance the rear-side irradiance received by the bifacial modules, enabling a controlled evaluation of yield improvements across varying albedo treatment lengths. The particular albedo booster sheets had a diamond mesh pattern to improve the

diffuse reflection from the surface. A picture of the sheet is shown in Figure 8 below for reference.

*Figure 8 Albedo Booster Sheet*

Ideally, for accurate comparative analysis and minimal site-to-site variability, all booster installations would be placed on identical string-table configurations within the same inverter and located in close proximity. This approach would ensure that the modules experience similar environmental and operational conditions. However, due to practical constraints and site limitations, the boosters were installed on the first PV table of several consecutive inverters instead. Each of these first tables consisted of two strings, which corresponded to MPPT 1 of the respective inverter. As these were located at the edge of the array block, they were subject to minor edge effects.

The albedo boosters were fabricated from high-reflectivity materials and installed with custom-designed ground anchors to ensure stability without significantly disturbing the underlying surface and minimal interference to surface reflection. Each booster sheet measured approximately 1.2 meters in width, and the total number of sheets placed beneath each PV table varied to create a range of albedo treatment lengths. Specifically, booster configurations included tables with 3, 4, 5, and 6 sheets, enabling the evaluation of albedo gains as a function of reflective surface coverage. The actual booster configuration details on site, after installation, are shown in the table and figures below. The booster sheet installation included some overlap between the sheets to facilitate anchoring to the ground.

| Zone | Table(s) | Inverter | Width(cm) |
|---|---|---|---|
| **1** | T1.21.1 + T1.21.2 | 1-14 | 315 |
| **2** | T1.20.1 + T1.20.2 | 1-13 | 419 |
| **3** | T1.17.1 | 1-10 | 523 |
| **4** | T1.16.1 | 1-9 | 630 |

*Table 1 Albedo Booster widths*

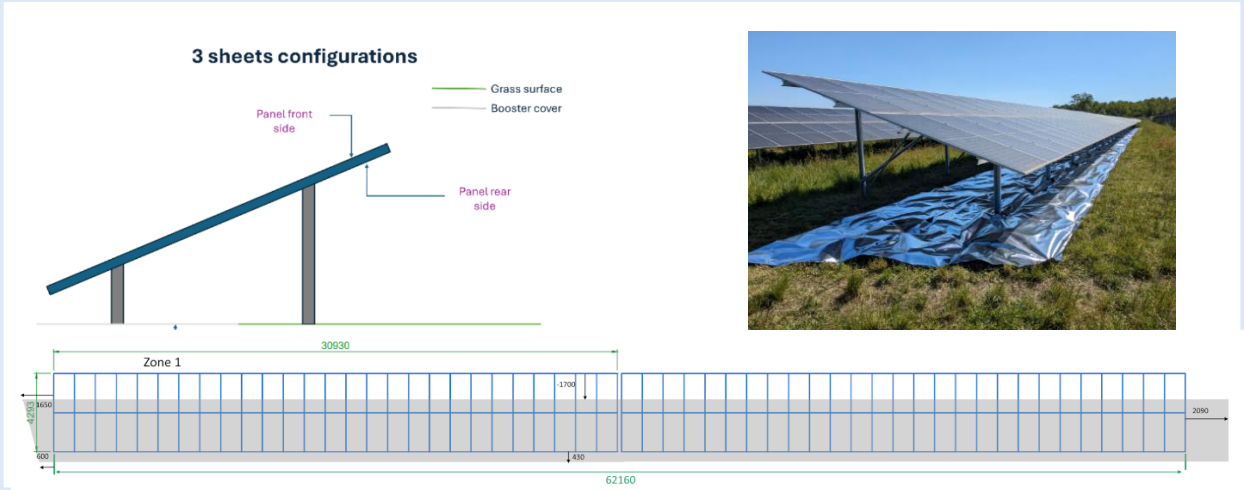


*Figure 9 Albedo 3-sheet configuration*

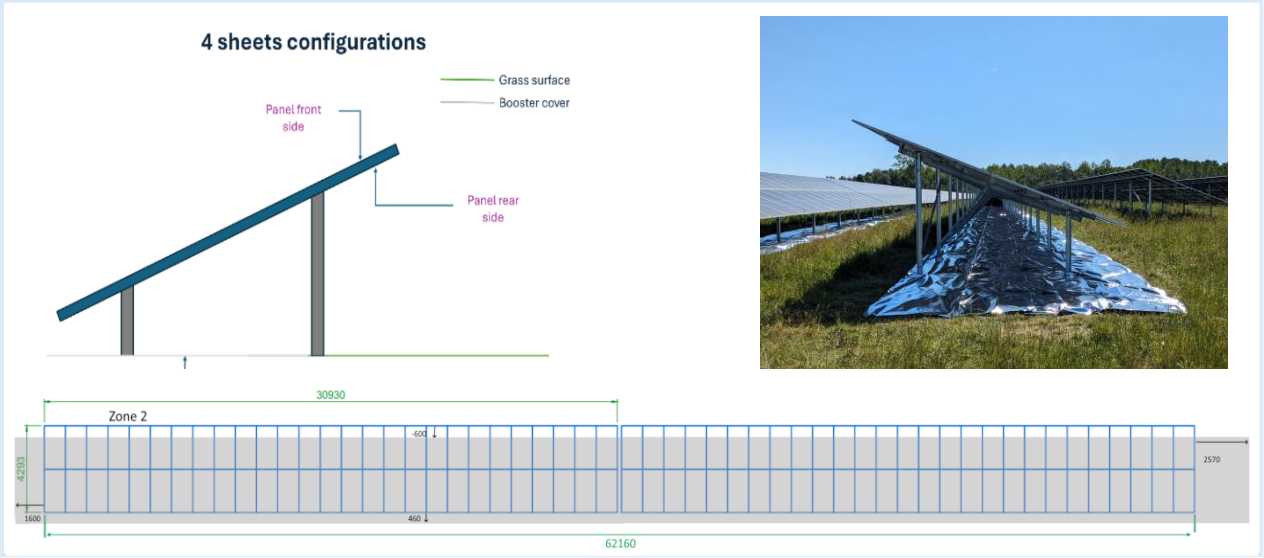


*Figure 10 Albedo 4-sheet configuration*

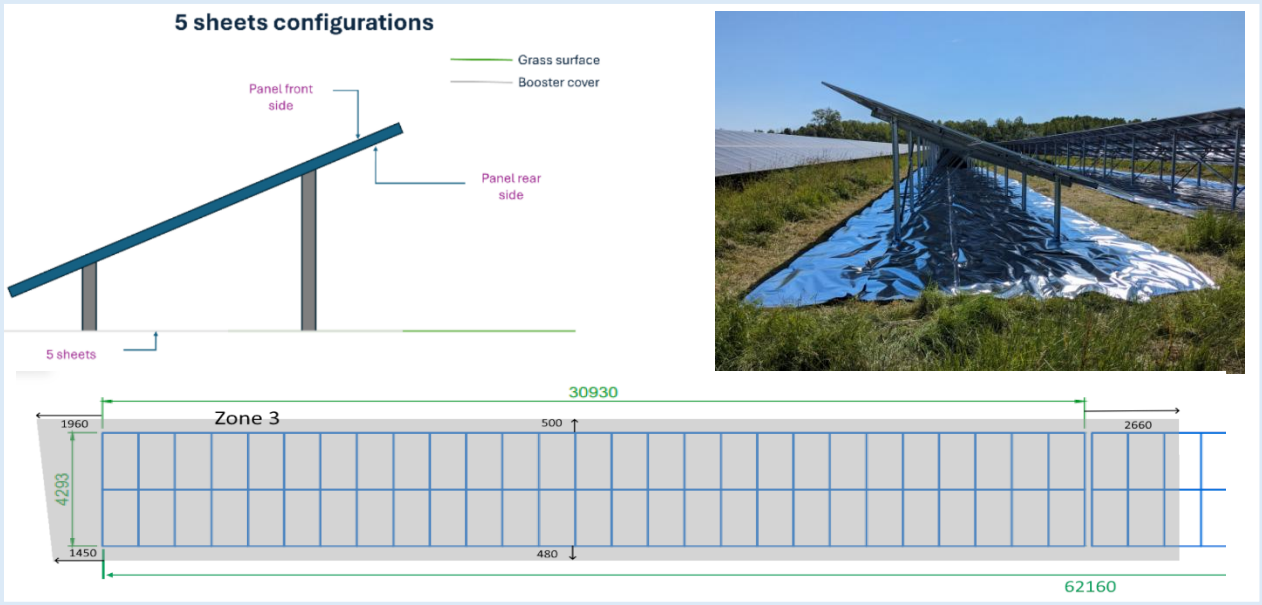


*Figure 11 Albedo 5-sheet configuration*

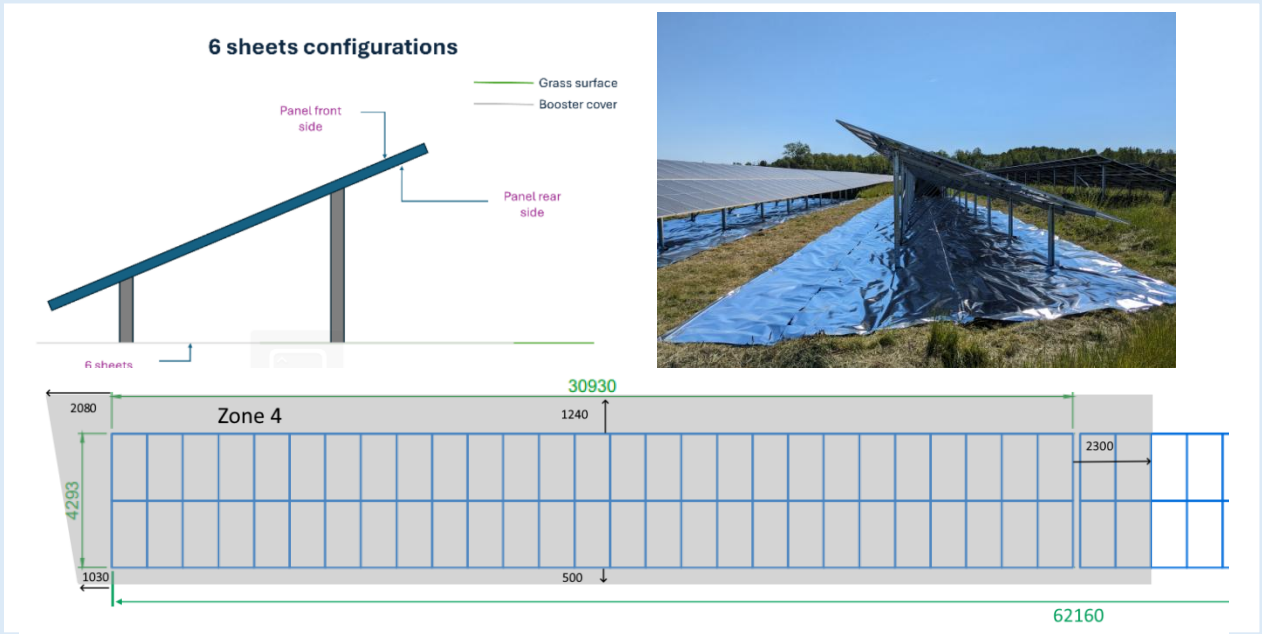


*Figure 12 Albedo 6-sheet configuration*

Before any physical installation, we conducted a site analysis to ensure that the increased rear irradiance would not introduce safety or performance risks. This included PVSyst simulations and an electrical load analysis to verify that the existing cable infrastructure could accommodate potential increases in current due to the added albedo. The final booster locations and their corresponding MPPTs were selected only after confirming system safety and compliance with design margins.

A schematic of the booster sheet installation layout is shown in Figure 13 below. Albedo booster sheets were installed on inverters 8 to 14, selected from a single section of the plant to minimize site variability. Notably, for inverters 9 and 10, which were configured to test 6-sheet and 5-sheet setups respectively, the option of equipping both MPPTs with boosters was ruled out due to cable current limitations. To avoid potential overcurrent issues, only one MPPT per inverter was fitted with booster sheets. In contrast, inverters 8, 11, and 12 were kept as control units with standard grass ground cover and no booster installation, serving as references for comparative yield analysis.

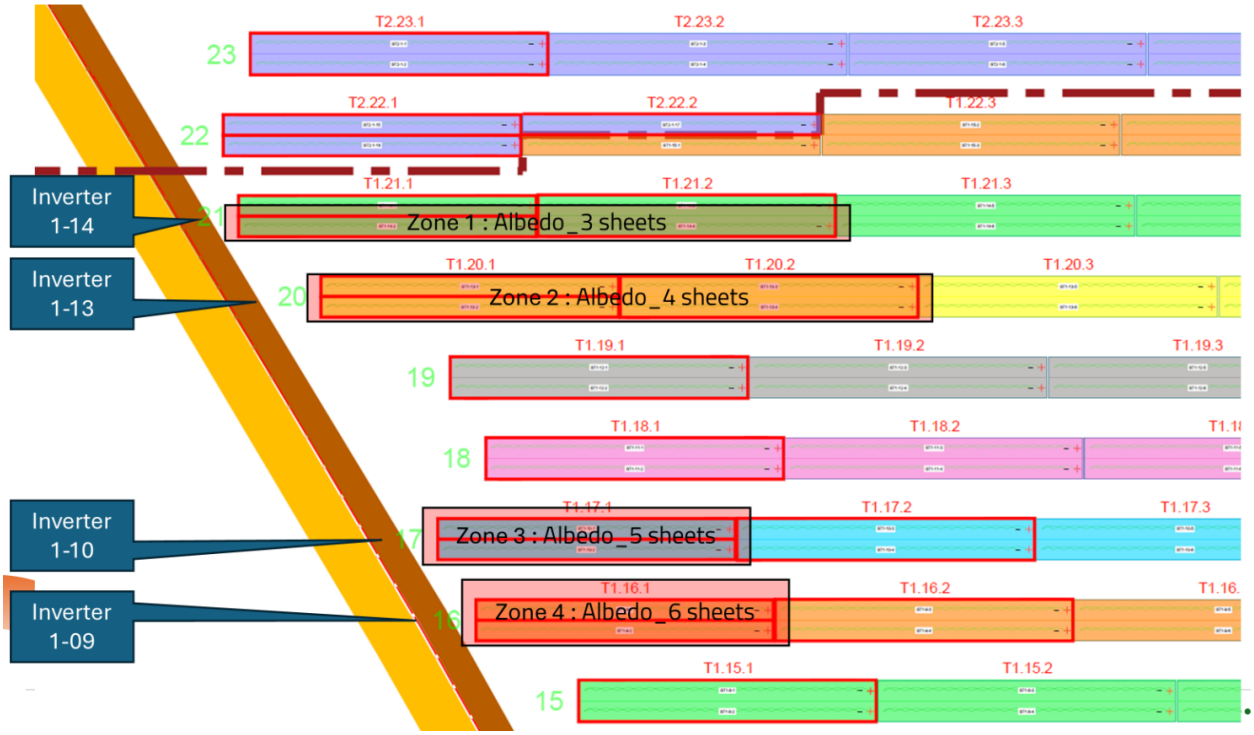


*Figure 13 Albedo Layout at Site*

This setup enabled the study to simulate a progressive increase in effective ground albedo and analyze the impact of increasing reflective area on the performance of bifacial modules. Control MPPTs on nearby inverters without booster treatment (i.e., with standard grass ground cover) were used as baseline references for relative performance comparisons.

## 3.3. Data Collection & Preparation

The albedo booster installations were active on the site for a limited duration, spanning from 13th June 2024 to 17th July 2024, primarily due to logistical and operational constraints. While this time window is relatively short from a performance assessment standpoint, it was the maximum feasible duration for field testing under the given site conditions. As such, it

represents a focused period of observation during which data was collected for validation and comparison.

### 3.3.1. Inverter Data

We obtained detailed inverter-level data for each of the selected inverters involved in the study. The data included:

- Inverter AC Power output (kW)
- String-level voltage and current measurements for all 18 string inputs of each inverter

This data granularity at the MPPT and string level was crucial for evaluating the effect of booster sheet installation on specific sections of the PV array.

### 3.3.2. Satellite Weather Data

To broaden the scope of the analysis and to support simulation validation, we also obtained satellite-based weather data from SODA for the same time frame.[26] This data set included:

- GHI, DHI, and DNI
- Ambient temperature
- Wind speed and direction
- Rainfall
- Air pressure

### 3.3.3. Field Weather Data

In addition to electrical performance data, we had access to the site's weather monitoring infrastructure. The site was equipped with a comprehensive weather monitoring system, which included:

- Pyranometers – Strategically installed across three different sections of the PV plant (PTR1, PTR2, and PTR3) to measure Global Horizontal Irradiance (GHI) independently at multiple points.
- A central weather station that provided continuous measurements of:
    - Global Horizontal Irradiance (GHI)
    - Ambient temperature
    - Wind speed and direction
    - Relative humidity
    - Air pressure

| TIMESTAMP | wind_speed_m/s | ambient_temp_°C | relative_humidity | irradiance_w/m2_LuftWS | air_pressure_hPa | irradiance_w/m2_Ptr1 | irradiance_w/m2_Ptr2 | irradiance_w/m2_Ptr3 |
|---|---|---|---|---|---|---|---|---|
| 2024-01-01 00:00:00 | 4.200 | 5.9000 | 0.83700 | NaN | 987.500 | NaN | NaN | NaN |
| 2024-01-01 00:15:00 | 5.200 | 6.2000 | 0.81300 | NaN | 987.650 | NaN | NaN | NaN |
| 2024-01-01 00:30:00 | 5.300 | 5.9000 | 0.82500 | NaN | 987.700 | NaN | NaN | NaN |
| 2024-01-01 00:45:00 | 6.600 | 6.2000 | 0.81250 | NaN | 987.650 | NaN | NaN | NaN |
| 2024-01-01 01:00:00 | 6.700 | 6.1000 | 0.82100 | NaN | 987.600 | NaN | NaN | NaN |
| ... | ... | ... | ... | ... | ... | ... | ... | ... |
| 2024-09-29 22:45:00 | 0.661 | 10.4775 | 0.95716 | NaN | 994.121 | NaN | NaN | NaN |
| 2024-09-29 23:00:00 | NaN | NaN | NaN | NaN | NaN | NaN | NaN | NaN |
| 2024-09-29 23:15:00 | 0.687 | 10.5600 | 0.96084 | NaN | 994.363 | NaN | NaN | NaN |
| 2024-09-29 23:30:00 | 0.554 | 10.7360 | 0.96060 | NaN | 994.000 | NaN | NaN | NaN |
| 2024-09-29 23:45:00 | NaN | NaN | NaN | NaN | NaN | NaN | NaN | NaN |

*Table 2 Field Weather Data*

To obtain the weather data required for pre-processing and simulations we also made some initial processing with these data as follows:

## Global Horizontal Irradiance (GHI) Processing

One of the critical weather inputs for the simulations and yield analysis is the Global Horizontal Irradiance (GHI). At the site, GHI data was collected from four independent pyranometers:

- Three individual pyranometers of the same make, positioned at the PTR1, PTR2, and PTR3 sections of the PV plant.
- One pyranometer mounted on the central weather station, located on the roof of the PTR1 transformer.

During initial data observations, it became apparent that the GHI values recorded by the three individual pyranometers (PTR1, PTR2, and PTR3) were consistently higher than those measured by the weather station pyranometer, as shown in Figure 14 below. This discrepancy is likely attributed to differences in pyranometer brand, sensor sensitivity, and potential calibration variances. Notably, the pyranometers at PTR1, PTR2, and PTR3 were of identical make, while the weather station pyranometer was of a different brand, potentially leading to variations in absolute irradiance measurements despite following a similar daily irradiance pattern.

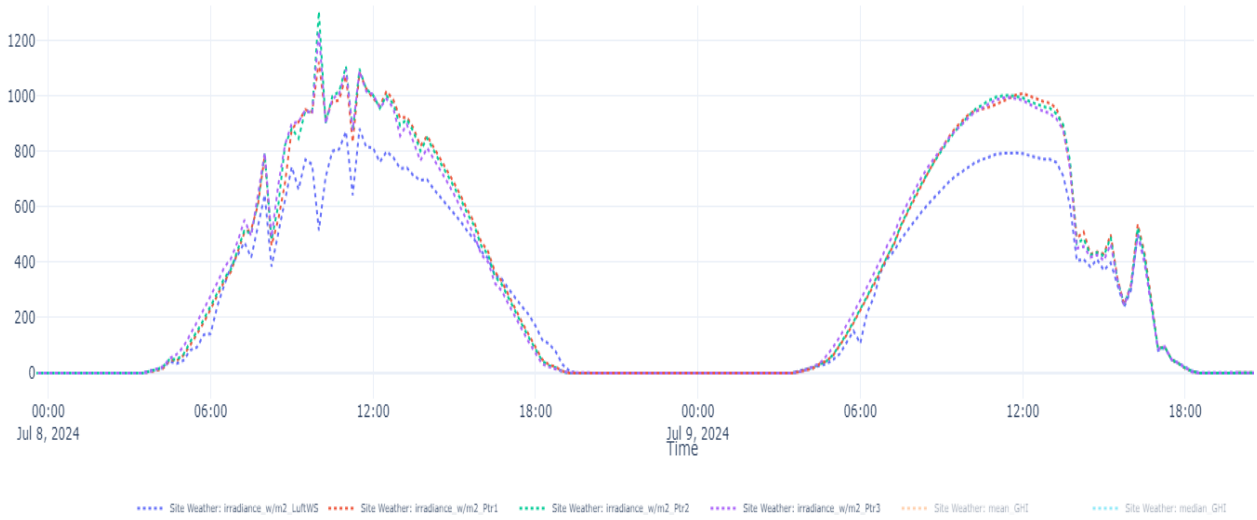


*Figure 14 Site Irradiance Data*

To address this inconsistency and enhance the reliability of the GHI input for simulations, we adopted a mean-based correction approach:

- Since PTR1 is the closest to the albedo booster installation and the primary monitoring area, it was given primary consideration.
- PTR2, the second closest pyranometer, was also included due to its similar irradiance pattern.
- Finally, the weather station pyranometer was incorporated to balance the dataset, acknowledging its different calibration characteristics.

The GHI input used for the simulation and analysis was then calculated as the mean of the GHI values from PTR1, PTR2, and the weather station pyranometer. This averaging approach effectively neutralized the brand-related biases and provided a representative GHI dataset.

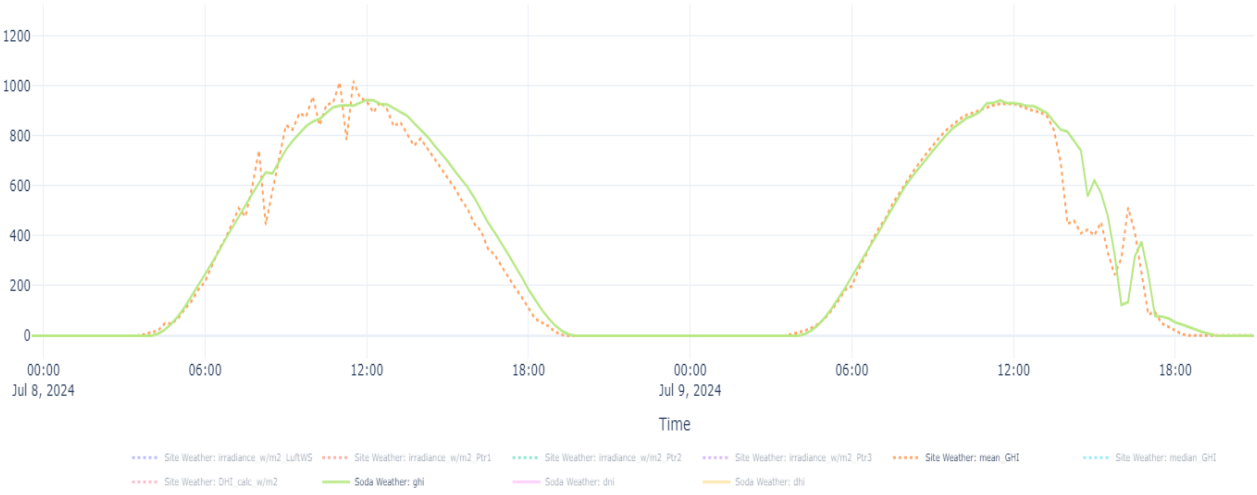


*Figure 15 Site Mean GHI and satellite GHI*

Moreover, this averaged GHI data was found to be in closer agreement with satellite-based GHI estimations (SoDa-Helioclim) [26], suggesting that the mean calculation offered a more realistic and site-specific irradiance profile. This adjustment allowed for a more consistent and reliable weather input in the simulations, directly influencing the accuracy of the modeled power outputs and comparative analyses.

## Calculation of Diffuse Horizontal Irradiance (DHI)

For Sunsolve to accurately simulate the performance of the PV system, it requires either Diffuse Horizontal Irradiance (DHI) or Direct Normal Irradiance (DNI) in conjunction with Global Horizontal Irradiance (GHI). Since our site weather station did not directly measure DHI, it became necessary to calculate DHI from the available GHI data. This was done by leveraging satellite-based weather data from SODA, which includes GHI and DHI measurements.

### Methodology for DHI Calculation

The calculation of the site-specific DHI was performed through the following steps:

*1. Synchronizing Timestamp Indices:*

The first step involved aligning the timestamps of the site weather data (cessey_weather_df) and the satellite weather data (Soda_weather_data). This ensures that both datasets are directly comparable for each time instance, preventing any time shift errors during calculations.

The intersection of the timestamps from both datasets was taken, and only the common entries were retained for further analysis.

*2. Calculating the Diffuse Fraction from SODA Data:*

To estimate the diffuse component of the site's GHI, the diffuse fraction was first calculated using SODA's satellite data:

$$\text{Diffuse Fraction} = \frac{\text{DHI (SODA)}}{\text{GHI (SODA)}}$$

This represents the proportion of GHI that is diffused rather than direct sunlight.

Any division by zero errors or undefined values (infinity or NaN) were handled by replacing them with zero, ensuring that the calculation remained valid.

*3. Estimating DHI for the Site:*

Once the diffuse fraction was determined, it was applied to the mean GHI values derived from the site pyranometers (as discussed previously). This allowed us to calculate the site-specific DHI as follows:

$$\text{DHI (Site)} = \text{Mean GHI (Site)} \times \text{Diffuse Fraction (SODA)}$$

This step effectively transposes the diffuse behavior observed in satellite data onto the site-specific GHI measurements, resulting in a realistic DHI estimation.

Any negative values produced during this multiplication were clipped to zero since irradiance cannot be negative.

*4. Updating the Site Weather DataFrame:*

Finally, the newly calculated DHI values were integrated back into the main cessey_weather_df dataframe, ensuring that the DHI column was updated and aligned with the common timestamps.

The choice to use SODA's satellite-derived diffuse fraction was driven by the absence of direct DHI measurement at the site. By mapping the satellite-based diffuse behavior onto our site GHI values, we ensured a realistic approximation of diffuse irradiance while maintaining consistency with actual site-specific solar exposure.

This calculated DHI now serves as a critical input for Sunsolve, enhancing the accuracy of the simulation models, especially during cloudy or high-scattering conditions where diffuse light significantly contributes to bifacial gains.

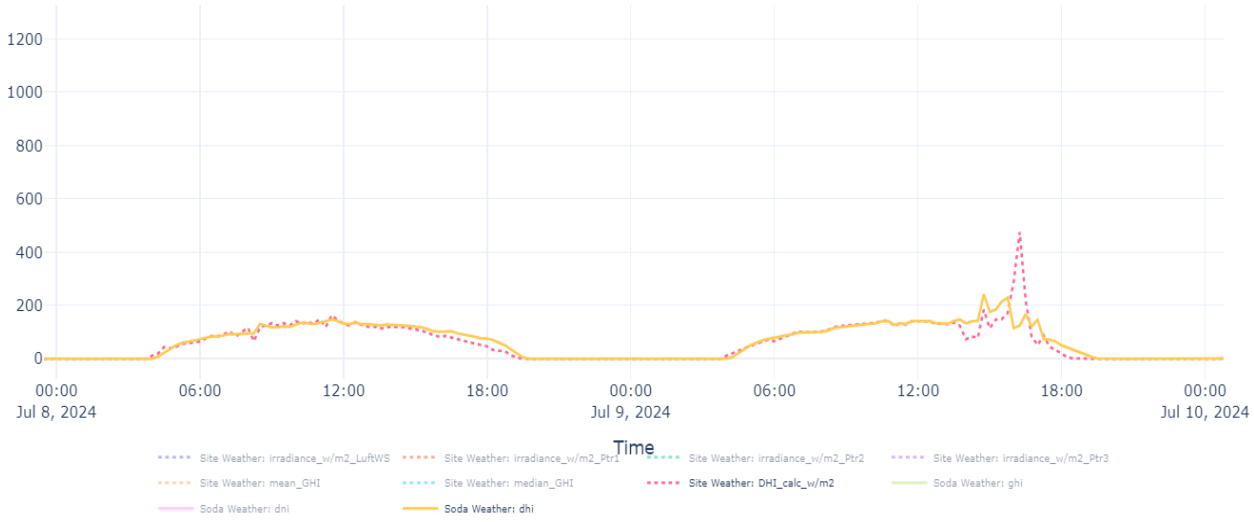


*Figure 16 Satellite DHI and site calculated DHI*

This detailed environmental data allowed for accurate cross-referencing of system performance with weather conditions across the observation period.

All the data streams-both from the field and satellite sources-were available at 15-minute intervals and recorded in UTC timestamps, ensuring consistent temporal alignment across datasets for preprocessing, comparison, and simulation input.

### 3.3.4. Data Cleaning, Outlier Detection, and Alignment

Before integrating the weather datasets into Sunsolve, a rigorous data preprocessing stage was performed to enhance the reliability of the simulation outputs. This stage involved:

1. Data Cleaning:
    - Removal of corrupted entries, missing timestamps, and erroneous spikes that could skew simulation accuracy.
    - Replacement of missing values using appropriate interpolation methods to maintain dataset continuity.
2. Outlier Detection:
    - Identification of abnormal weather readings, such as unexpected jumps in Global Horizontal Irradiance (GHI), Direct Normal Irradiance (DNI), or Diffuse Horizontal Irradiance (DHI) that fell outside typical diurnal patterns.
    - Verification of outlier points with secondary data sources to confirm whether they represented true anomalies or sensor errors.
3. Timestamp Alignment and Range Matching:
    - Both field and satellite datasets were carefully aligned with respect to their timestamps, ensuring synchronized 15-minute intervals throughout the entire simulation period.
    - Temporal gaps were handled through linear interpolation where appropriate or removed, while overlapping data points were merged consistently.
    - The range of data was clipped to the specific dates of interest for the simulation window, matching Sunsolve's requirements for smooth processing.
4. Column Selection and Setup:
    - The weather parameters required for Sunsolve simulation-GHI, DNI, DHI, ambient temperature, wind speed, and air pressure-were extracted and organized in the appropriate format.

### 3.3.5. Input Preparation for Simulation

After the weather data was thoroughly cleaned, verified, and aligned, the final processed weather file was generated. This structured dataset, containing only the necessary weather parameters, was then configured to match Sunsolve's input specifications.

This comprehensive collection of real-time field data and high-resolution satellite weather inputs formed the backbone of the analysis and validation process for this study.

## 3.4. Simulation Environment and Configuration

### 3.4.1. Introduction to Sunsolve Yield and Rationale for Selection

In the realm of photovoltaic (PV) system modeling, selecting an appropriate simulation tool is paramount, especially when dealing with complex scenarios such as bifacial modules operating over heterogeneous ground surfaces. For this study, we have chosen Sunsolve Yield (referred to in this report as Sunsolve), developed by PV Lighthouse, as our primary simulation software. This decision is grounded in Sunsolve's advanced capabilities in handling multi-albedo environments, its detailed modeling approach, and its flexibility in simulating various system configurations.

Sunsolve is a physics-based simulation tool designed to model the performance of PV systems with high accuracy. Unlike traditional tools that rely on simplified view factor models, Sunsolve employs a comprehensive ray-tracing engine that accounts for the intricate interactions of light within a PV system. This includes considerations for mounting structures, wavelength-dependent albedo, and the spectral response of PV modules. Such detailed modeling is particularly beneficial when assessing bifacial systems, where rear-side irradiance plays a significant role in overall energy yield. [27]

One of the standout features of Sunsolve is its ability to model spatially varying albedo. In real-world scenarios, the ground beneath a PV array may not have uniform reflectivity due to variations in surface materials, vegetation, or artificial reflectors. Sunsolve allows users to define different albedo values across the simulation domain, enabling a more realistic representation of the operating environment. This is crucial for our study, which involves analyzing the impact of albedo booster sheets of varying lengths installed beneath selected PV tables. [1]

In contrast, PVsyst, a widely used PV simulation software, has limitations in this regard. PVsyst allows for the definition of a single albedo value for the entire ground surface, which does not accurately capture the effects of non-uniform ground reflectivity. As noted in the PVsyst forum, "There is only one albedo value to describe the ground properties. Furthermore, the current bifacial view factor models are based on a cross section of the table rows, and don't allow to describe changes of properties along the row". This limitation makes PVsyst less suitable for studies involving heterogeneous albedo conditions. [28]

Moreover, Sunsolve offers a user-friendly graphical interface, allowing for the easy configuration of system details, including module specifications, mounting structures, and environmental conditions. The software's simulation engine is optimized for speed, enabling the modeling of complex systems in a matter of minutes. Unlike many traditional ray-tracing software tools, Sunsolve performs its complex ray-tracing calculations in parallel using

cloud computing resources. This cloud-based approach allows for significantly faster simulations. This efficiency facilitates the exploration of multiple scenarios and the optimization of system configurations for maximum yield in reasonable time periods. [29]

Sunsolve's capabilities extend to the calculation of bifacial factors with high accuracy, which can be used in conjunction with other simulation tools like PVsyst. PV Lighthouse provides a step-by-step guide on determining PVSyst bifacial inputs using Sunsolve. This interoperability allows for the integration of Sunsolve's detailed modeling results into broader simulation workflows. [30]

In summary, the selection of Sunsolve for this study is driven by its advanced modeling capabilities, particularly in handling multi-albedo environments, its detailed ray-tracing approach, and its flexibility in simulating various system configurations. These features make it an ideal tool for accurately assessing the performance of bifacial PV systems under complex ground reflectivity conditions.

### 3.4.2. Simulation Algorithms and Methods in Sunsolve

#### Optical Solving

Sunsolve employs a sophisticated simulation framework that integrates Monte Carlo ray tracing with thin-film optics modeling to analyze the optical behavior of photovoltaic systems. This hybrid approach enables detailed assessments of light interactions within complex solar module architectures, accounting for phenomena such as reflection, transmission, absorption, and photogeneration.

##### Monte Carlo Ray Tracing

At the core of Sunsolve's simulation methodology is the Monte Carlo ray tracing algorithm. This statistical technique involves the generation of a large number of rays, each representing a photon or a packet of photons, to model the probabilistic nature of light propagation and interaction within the solar module. Each ray is assigned specific properties, including wavelength, intensity, direction, and polarization, and is traced through the system as it undergoes various interactions. [31]

The simulation process begins with the emission of a "packet" of rays, typically comprising 5,000 individual rays. These rays are propagated through the system, and at each interface-such as module surfaces, encapsulant layers, or structural components like torque tubes-the algorithm calculates the probabilities of reflection, transmission, and absorption based on the Fresnel equations and the material properties involved. A random decision, weighted by these probabilities, determines the path of each ray, simulating the stochastic nature of photon interactions.

This process continues iteratively, with rays being traced through successive interactions until they either exit the system, their intensity falls below a predefined threshold (e.g., 0.01% of the initial intensity), or they reach a maximum number of interactions (e.g., 1,000). The outcomes of these simulations-such as the number of rays absorbed, transmitted, or reflected-are aggregated to provide statistical estimates of the system's optical performance.

Monte Carlo ray tracing is particularly advantageous for modeling complex geometries and materials, as it can accommodate arbitrary shapes and inhomogeneous media without requiring simplifications that might compromise accuracy. This makes it a powerful tool for simulating real-world photovoltaic systems with intricate designs and diverse material compositions. [32]

### Thin-Film Optics Modeling

In addition to ray tracing, Sunsolve incorporates thin-film optics modeling to account for interference effects and wavelength-dependent behavior in multilayer structures. This is achieved through the transfer-matrix method (TMM), a mathematical approach used to analyze the propagation of electromagnetic waves through stratified media. [33]

The TMM involves representing each layer in a multilayer stack with a matrix that describes how it modifies the amplitude and phase of incident light. By multiplying these matrices, one can determine the overall effect of the entire stack on the incident light, including the reflectance, transmittance, and absorptance spectra. This method is particularly effective for modeling thin-film coatings, anti-reflective layers, and other optical elements commonly used in photovoltaic modules.

By integrating TMM with Monte Carlo ray tracing, Sunsolve can simulate both the macroscopic behavior of light propagation and the microscopic interference effects within thin films. This comprehensive approach allows for accurate predictions of optical losses and gains, enabling the optimization of module designs for enhanced performance.

### Absorption Modeling with Beer's Law

To model the attenuation of light as it travels through absorbing materials, Sunsolve applies Beer's Law (also known as the Beer-Lambert Law). This principle describes the attenuation of light as it passes through an absorbing medium. The law is mathematically expressed as:

$$A = \log_{10}\left(\frac{I}{I_0}\right) = \varepsilon \cdot c \cdot l$$

where:

- A is the absorbance (dimensionless),
- $I_0$ is the incident light intensity,

- I is the transmitted light intensity,
- ϵ is the molar absorptivity or extinction coefficient ((L·mol$^{-1}$·cm$^{-1}$),
- c is the concentration of the absorbing species (mol·L$^{-1}$),
- l is the path length of the light through the material (cm)

Beer's Law implies that the reduction in light intensity is exponential with respect to the thickness and concentration of the absorbing medium.

In Sunsolve's ray-tracing simulations, Beer's Law is used to model the absorption of light as rays pass through semi-transparent layers like module glass or encapsulants. For each ray that intersects an absorbing layer, the transmitted intensity is calculated based on the path length within the material and its absorption properties. This is crucial for estimating realistic power generation, as absorbed light in silicon contributes to electron–hole pair generation, while absorption in non-active materials results in energy loss.

In Sunsolve, this is integrated into the ray-tracing procedure, where every ray's intensity is updated upon passing through an interface using:

$$I = I_0 \cdot 10^{-\varepsilon \cdot c \cdot l}$$

This allows Sunsolve to account for realistic energy losses and gains during multi-interface interactions in bifacial PV setups.

### Optical Simulation Workflow

To summarize, the simulation workflow in Sunsolve involves the following steps:

1. A 'packet of rays' is created. The default number of rays in a packet is 5000. Each ray in this packet is assigned a wavelength, an intensity, a direction, and a starting location above the system.
2. Each light ray proceeds along a straight line until it intersects with an interface, such as the surface of a module, the ground, or a torque tube.
3. At this interaction, and at all future interactions with an interface,
    - reflectance, transmittance and absorptance are calculated, where the value of each depends on the wavelength λ and the electric field (polarisation), as well as on the complex refractive index of the materials on either side of the interface and any thin films that lie between them;
    - the intensity of the ray is reduced by the value of the absorptance;
    - the magnitudes of reflectance and transmittance are translated into probabilities;
    - a random decision, weighted by those probabilities, is taken to select whether to reflect or transmit the ray at the interface;

    - a new direction is calculated and ascribed to the ray depending on whether the ray is reflected or transmitted, and on the scattering model assigned to that interface;
    - The ray continues until it intersects another interface.
4. If the ray passes through an absorbing layer, its intensity is reduced by applying Beer's law. This reduction in intensity is usually considered as a loss (e.g., due to absorption in the glass of a module), but when the ray passes through a semiconductor like silicon, the absorption can equate to the photogeneration of electron–hole pairs and therefore the reduction in intensity can be considered as a gain.
5. Steps 2–4 are repeated for each ray until
    - the ray is lost from the system by being reflected to the sky;
    - the ray's intensity decreases below a threshold (the default is 0.01%); or
    - the ray has intersected with the maximum allowable number of interfaces (the default is 1000).
6. The gains (photogeneration) and losses (reflection, transmission, parasitic absorption) are recorded for each ray and summed and averaged to give the results of the ray packet.
7. Steps 1–6 are repeated for as many ray packets that are required for the total number of rays to equal the value entered at 'Rays per solar angle' on the Options tab. The total gains and losses are averaged and sent to the user interface.
8. This entire procedure is repeated for as many solar angles needed to solve the requested period of the energy yield.

Thus, the global gains and losses are determined by averaging a large number of rays. With a sufficiently large number of rays, the Monte Carlo simulation converges to the physical model.

## Electrical Solving in Sunsolve

Sunsolve determines the electrical performance of solar cells and modules by solving an equivalent-circuit model, yielding the current-voltage (JV) characteristics. From the JV curve, key performance metrics such as maximum power point ($P_{MP}$), short-circuit current density ($J_{SC}$), and open-circuit voltage ($V_{OC}$) are extracted. These outputs are accessible under the 'JV' tab in the Sunsolve interface.

### Inputs to the Equivalent-Circuit Model

The parameters required for the equivalent-circuit model are specified in the 'Circuit' tab. While most inputs are user-defined, two parameters can be either user-specified or computed by Sunsolve: the series resistance ($R_s$) and the light-generated current density ($J_L$).

*Series Resistance (Rs)*

The series resistance accounts for resistive losses within the solar cell and can be determined in two ways: [34]

1. Direct Specification: If electrodes are not enabled in the 'Electrodes' tab or if the 'Calculate grid resistance' option is unchecked in the 'Circuit' tab, the user can directly input the total series resistance value (Rs).
2. Calculated Grid Resistance: When electrodes are enabled and 'Calculate grid resistance' is checked, Sunsolve computes the grid resistance component (Rsg) based on electrode geometry and material properties. The user provides the non-grid series resistance (Rs), and the total series resistance is then:

$$Rs = Rsn + Rsg$$

This approach allows for a more accurate representation of resistive losses, especially in complex electrode configurations.

*Light-Generated Current Density ($J_L$)*

The light-generated current density represents the photocurrent produced within the solar cell due to incident illumination. It is calculated by integrating the product of the incident photon flux (Jph(λ)), the absorptance of the active region (A(λ)), and the collection efficiency (η(λ)) over all wavelengths:

$$J_L = \int_0^\infty J_{ph}(\lambda) \cdot A(\lambda) \cdot \eta(\lambda)\, d$$

Here:

- Jph(λ): Incident photon current density, defined by the illumination conditions.
- A(λ): Spectral absorptance of the active region, determined via ray tracing.
- η(λ): Wavelength-dependent collection efficiency, specified in the 'Circuit' tab.

For bifacial cells, Sunsolve distinguishes between front and rear illumination, calculating separate contributions:

$$J_L = J_{LF} + J_{LR}$$

Where $J_{LF}$ and $J_{LR}$ are the front and rear light-generated current densities, respectively.

## General Procedure

The electrical solving process in Sunsolve involves the following steps:

1. Optical Simulation: Ray tracing is employed to determine the spectral absorptance of the active region for both front $\left(\mathrm{A_F}(\lambda)\right)$and rear ($\mathrm{A_R}(\lambda)$) illumination.

2. Photocurrent Calculation: Using the absorptance data, incident photon flux ($J_{ph}(\lambda)$), and collection efficiencies ($\eta_F(\lambda)$, $\eta_R(\lambda)$), Sunsolve computes the front and rear light-generated current densities:

$$J_{LF} = \int_0^\infty J_{ph}(\lambda) \cdot A_F(\lambda) \cdot \eta_F(\lambda)\, d$$

$$J_{LR} = \int_0^\infty J_{ph}(\lambda) \cdot A_R(\lambda) \cdot \eta_R(\lambda)\, d$$

$$J_L = J_{LF} + J_{LR}$$

3. Series Resistance Determination: Sunsolve calculates the grid resistance ($R_{sg}$) based on electrode parameters and adds it to the user-defined non-grid resistance ($R_{sn}$) to obtain the total series resistance (Rs).
4. Equivalent Circuit Solution: With $J_L$, $R_s$, and other circuit parameters, Sunsolve solves the equivalent-circuit model to generate the JV curve.
5. Performance Metrics Extraction: From the JV curve, key electrical outputs such as $P_{MP}$ , $J_{SC}$, and $V_{OC}$ are determined.

Notably, if only electrical parameters in the 'Circuit' tab are modified, Sunsolve recalculates the JV curve without rerunning the optical simulation, as the absorptance ($A(\lambda)$) remains unchanged.

### Temperature Effects

Solar cells often operate at temperatures higher than standard test conditions (typically 25 °C or 298 K). Sunsolve allows users to input circuit parameters at a nominal temperature (Tnom) and then adjusts these parameters to the actual operating temperature (T) using temperature coefficients, following the methodology employed in PVsyst .[35]

The adjustments are as follows:

*Light-Generated Current Density:*

$$J_L = J_{L,\text{nom}}[1 + \mu_{IL}(T - T_{\text{nom}})]$$

Here:

- $J_{\text{l}}$ - Light-generated current density
- $J_{\text{lnom}}$ - Nominal light-generated current density
- $\mu_{\text{il}}$ - Temperature coefficient for the light-generated current
- $T$ - Actual operating temperature
- $T_{\text{nom}}$ - Nominal reference temperature

*Ideality Factor of the Primary Diode:*

$$m_1 = m_{1,\text{nom}}[1 + \mu_{m1}(T - T_{\text{nom}})]$$

Here:

- $m_1$ - Primary diode ideality factor
- $m_{1\text{nom}}$ - Nominal ideality factor at reference temperature
- $\mu_{m1}$ - Temperature coefficient for the ideality factor
- $T$ - Actual operating temperature
- $T_{\text{nom}}$ - Nominal reference temperature

*Saturation Current Density of the Primary Diode:*

$$J_{01} = J_{01nom}\left(\frac{T}{T_{nom}}\right)^3 \exp\left[\frac{qE_g}{m_1 k}\left(\frac{1}{T} - \frac{1}{T_{nom}}\right)\right]$$

Here: [36]

- $J_{01}$ - Recombination current of the primary diode
- $J_{01\text{nom}}$ - Nominal recombination current
- $T$ - Actual operating temperature
- $T_{\text{nom}}$ - Nominal reference temperature
- $q$ - Electron charge
- $E_g$ - Band gap of the semiconductor
- $m_1$ - Ideality factor of the primary diode
- $k$ - Boltzmann's constant [37]

This approach assumes that other circuit parameters, such as series resistance (Rs) and shunt resistance (Rsh), remain unaffected by temperature variations. [38]

### 3.4.3. Simulation Steps

#### Weather Data Input

Sunsolve requires a range of weather inputs to perform accurate simulations of photovoltaic yield. The software provides multiple options for importing weather data, including its own database, third-party APIs, or custom CSV files. Since we are working with both actual field measurements and satellite data for additional simulation comparisons, we opt for the custom CSV import method. [39]

### Weather Data Requirements and Input Configuration:

To set up weather data in Sunsolve, the following steps are performed:

- Location Details:
  Before importing the weather data, basic geographic and temporal details of the site need to be specified:
  - Location Name: Identifier for the simulation site.
  - Latitude and Longitude: Exact coordinates for accurate solar position calculations.
  - Timezone: Local timezone for aligning the timestamp data.
  - Altitude: Elevation of the site above sea level, which can influence atmospheric attenuation.
- Weather Data Parameters:
  The software requires certain minimum weather parameters for effective simulation:
  - Timestamp: In UTC format for consistency.
  - Global Horizontal Irradiance (GHI): Measures the total solar radiation received per unit area.
  - Ambient Temperature: To calculate module temperature and its effect on performance.
  - Wind Speed: Important for thermal modeling and cooling effects on modules.
  - DHI or DNI: At least one of Diffuse Horizontal Irradiance (DHI) or Direct Normal Irradiance (DNI) must be provided to simulate sunlight distribution accurately.

  Optional weather parameters:
  - Air Pressure, Relative Humidity, Rainfall: These parameters can be included for more detailed analysis but are not mandatory for running the simulations.

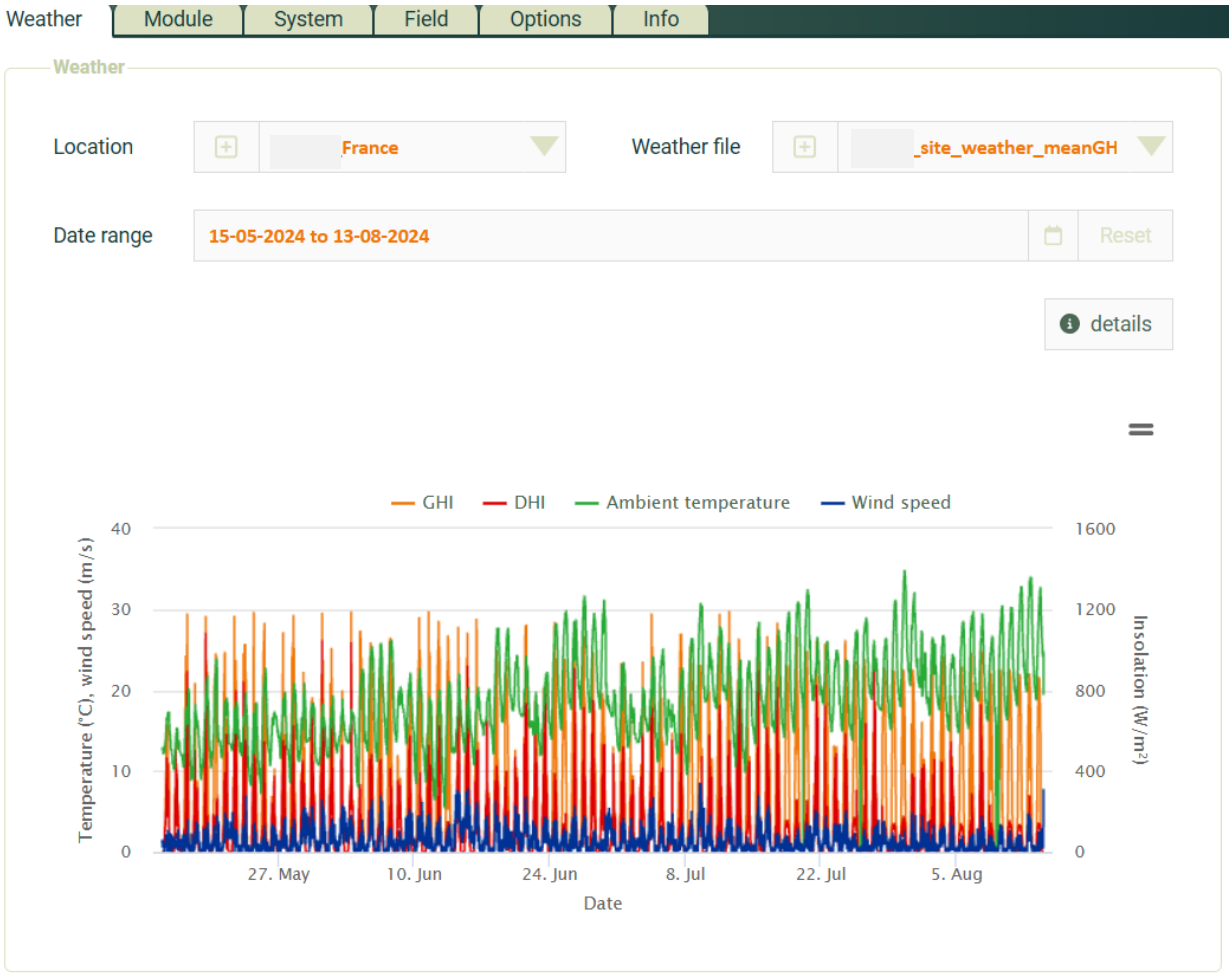


*Figure 18 Weather Configuration in Sunsolve*

### Data Import and Visualization:

- Sunsolve allows users to easily upload CSV files with the specified weather data.
- The software provides a visualization tool to inspect the imported weather data directly, enabling quick detection of any anomalies or gaps. This is particularly useful to verify the consistency of the data before running simulations.
- The software also flags missing or improperly formatted data during the import process to ensure the simulation runs smoothly.

### Simulation Date Range and Year Limitations:

After data import, users can define the date range for which the simulation should be executed.

Sunsolve has a unique concept called Simulation Year, which is equivalent to 365 days calculated hourly (365 days × 24 hours = 8,760 time steps).

The number of "Simulation Years" is calculated based on the total number of time steps in the imported weather data: For instance, if the weather data has a 15-minute interval, one year of data corresponds to 4 simulation years in Sunsolve (4 × 8,760 time steps). This means that if you import a single year of weather data with 15-minute intervals, Sunsolve will simulate it as four separate "years" in the software.

It is important to optimize the date range to fit within Sunsolve's monthly simulation quota, as excessive simulation years can deplete the monthly limit faster than anticipated.

### Integration with Ray-Tracing Calculations:

Once the weather data is successfully imported and the date range is specified, Sunsolve uses this information to determine the trajectory of the rays during simulations.

## PV Panel Configuration

After successfully importing and verifying the weather data, the next step in configuring the simulation environment in Sunsolve involves specifying the photovoltaic (PV) panel characteristics.

### PV Panel Specification:

For our simulation, we utilized 565 Wp bifacial panels, identical to those installed at the actual site. Sunsolve offers multiple methods to input PV module data:

- Manual Entry: Inputting parameters directly from the PV module datasheet.
- PAN File Import: Uploading a PAN file, typically provided by the module manufacturer.
- Sunsolve File Import: Importing panel details from a previously simulated Sunsolve file.

Given that we had access to the PAN file from the supplier, we opted to import it directly. This method ensures that the module's specifications, including electrical characteristics, are accurately represented in the simulation. Sunsolve allows for editing these parameters post-import to align with specific design requirements, such as adjusting optical and electrical characteristics.

### Module Configuration Types:

Sunsolve provides two distinct module configuration options:

1. Simple Module Configuration: This approach involves using the PAN file or datasheet details to define the module. It focuses on electrical parameters without delving into detailed optical properties.
2. Complex Module Configuration: This advanced configuration incorporates detailed optical properties, including glass reflectance and transmittance. By simulating how rays interact with the module's materials, it offers a more comprehensive analysis.

However, this method requires intricate data, often proprietary and not readily available to end-users. [40]

In our project, the emphasis was on assessing the impact of albedo boosters. Given the unavailability of detailed optical data and to maintain consistency with the actual site conditions, we proceeded with the simple module configuration using the PAN file. All parameters from the PAN file were retained without modifications to replicate the real-world scenario accurately.

#### Visualization and Verification:

Post-import, Sunsolve facilitates the visualization of the module's I-V curve, allowing for verification of the specifications and ensuring that the module behaves as expected within the simulation environment.

### PV System Configuration

Sunsolve offers a comprehensive and intuitive platform for configuring photovoltaic (PV) systems, accommodating various system types and structural components. This flexibility is crucial for accurately simulating different installation scenarios and optimizing system performance.

#### System Types

Sunsolve supports three primary PV system configurations:

- Fixed Tilt Systems: These systems have modules installed at a constant tilt angle and azimuth throughout the year. The structural components include posts, rafters, and purlins. This configuration is straightforward and cost-effective, making it suitable for many installations.
- Single-Axis Trackers: Modules in this setup rotate around a single axis to follow the sun's path, enhancing energy capture. The structure comprises posts, rails, and torque tubes. Single-axis trackers can increase energy yield by 15–25% compared to fixed-tilt systems, depending on location and design specifics. [41]
- Waves Configuration: This unique arrangement features modules tilted in opposing directions, forming a wave-like pattern. The structure includes ballast blocks, rails, and joints. This design can optimize land use and energy production in specific scenarios.

Our test site has a fixed tilt system. So, we shall focus on the fixed tilt configuration and detail out the different specifics of this configuration.

*Fixed tilt Mounting Structure Configuration*

Within Sunsolve, the mounting structure can be precisely defined, encompassing: [42]

- Posts: Vertical supports anchoring the system to the ground.
- Rafters: Horizontal beams attached to the posts, providing support for purlins.
- Purlins: Horizontal members mounted on rafters, to which PV modules are affixed.

Fixed systems are defined by purlins, rafters and posts. Modules are positioned on top of the purlins (or on top of the rafters if no purlins are used). Purlins are positioned on top of the rafters with no gap between them. Posts are attached to the rafters.

Users can specify dimensions, shapes, orientations, and materials for each component. Material selection is significant, as it influences the reflectivity and, consequently, the albedo effect impacting bifacial modules.

### PV Panel orientation

Landscape/portrait: This definition is intended to simplify the inputs for the most common system and module configurations. It assumes that the module cell layout is defined as shown in the image below:

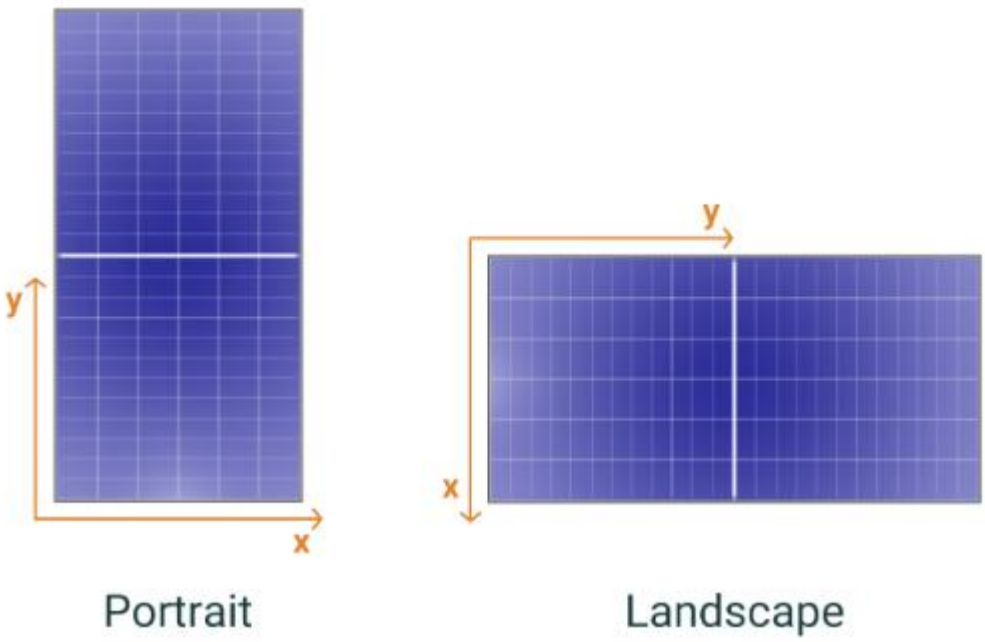


*Figure 19 Orientation of PV Panels*

Figure 21 below defines the dimensions of the 'unit system' as well as the lateral and vertical spacing between modules. The dimensions of the unit-system are defined by the row pitch and lateral spacing, noting that the lateral module separation is included in the unit-system width.

Figure 20 shows the layout of a system when it's represented by the unit system of Figure 21. The system contains infinitely many unit systems , which in this example contains 2 × 4 modules, and therefore it extends infinitely in both directions.

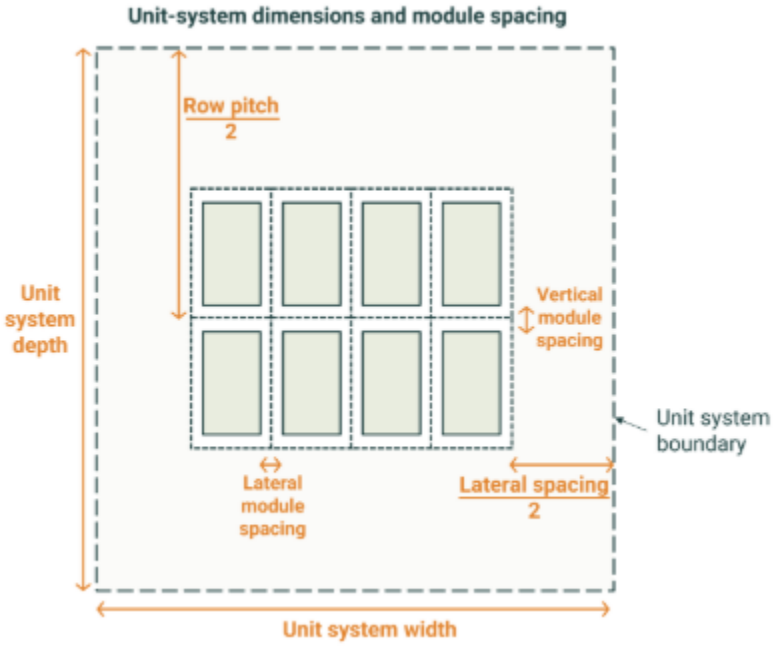


*Figure 21 Unit PV System Dimensions*

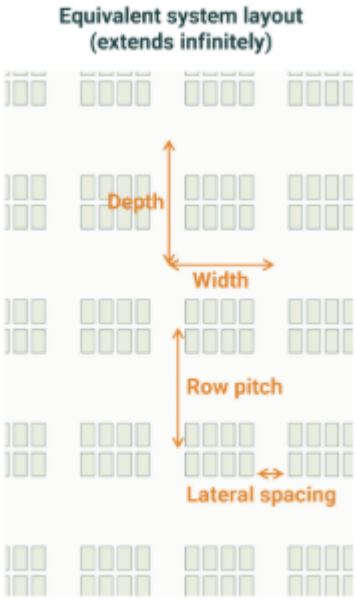


*Figure 20 System Dimensions*

For a large PV system, e.g., a system with hundreds of modules, we're most interested in the performance of a 'central module'. A central module is a module that's sufficiently far from all sides of the system that it is unaffected by edge effects. (Edge effects tend to be significant in the first and last row of a system, and in the five modules at either end of a row.)

To simulate a central module, simulate a unit system with a single module and zero module spacing, and then set appropriate unit-system dimensions. The figures below show an example unit system (left) and its equivalent system (right), which extends infinitely in X and Y directions.

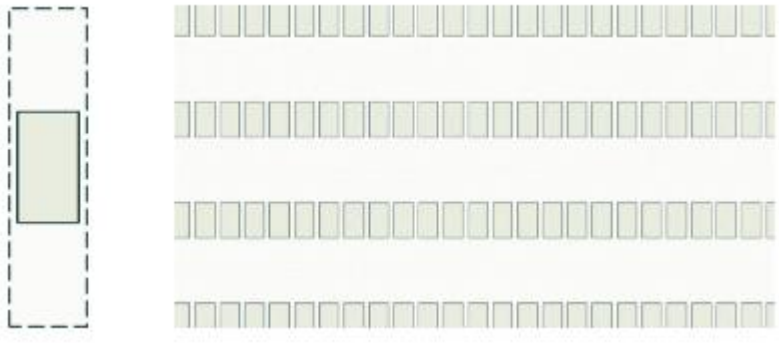

*Figure 22 Unit PV system in Sunsolve*

### Mounting Structure Configuration in Sunsolve

Once the mounting structure configurations were understood and defined within Sunsolve, we moved towards replicating the actual physical setup of the PV system from the site into the simulation environment. While Sunsolve provides robust options to configure mounting structures directly within its platform, we opted for a more precise and site-accurate approach.

To achieve this, we designed the module mounting structure of the 27 x 2 panel table configuration in SketchUp. This step was crucial because SketchUp allowed us to precisely replicate the structural layout as it exists on-site, including every dimension and component of the physical mounting setup. This was important not only for maintaining geometric accuracy but also for ensuring that reflective surfaces and shading behaviors were captured exactly as they would occur in reality.

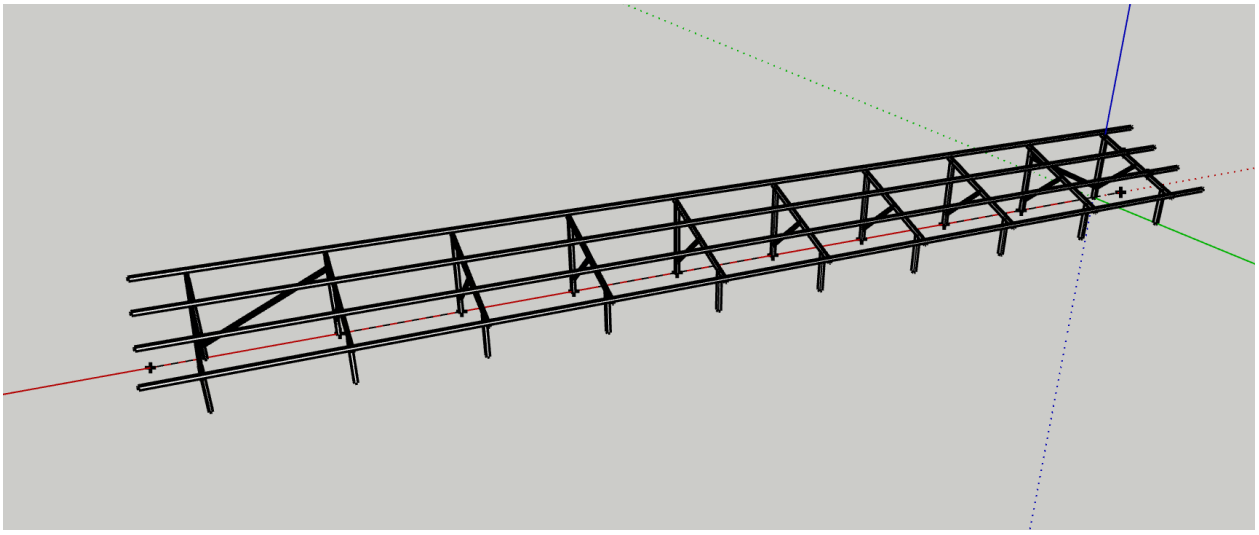

*Figure 23 Module Mounting Structure Design in SketchUp*

*Integration into Sunsolve*

After completing the design in SketchUp, the mounting structure was imported into Sunsolve as a custom object. Sunsolve's platform supports the import of external 3D objects, which made it possible to seamlessly integrate the SketchUp model into the simulation environment. This custom object was then aligned with the PV module configurations that were set up within Sunsolve.

In Sunsolve, the PV module parameters were carefully defined to match the actual field conditions:

- Module Layout: The number of panels was set according to the field configuration, with 27 modules in the horizontal axis and 2 modules in the vertical axis, creating the 27 × 2 arrangement.
- Panel Spacing: We input the exact horizontal and vertical spacing between the panels, ensuring that the array density and layout were replicated accurately.
- Tilt Angle and Azimuth: The tilt angle and azimuth direction were configured to mirror the actual site setup, aligning with the same orientation used in the field installation.
- Height from Ground: The ground clearance of the panels was specified as per the actual mounting structure at the site, which is critical for simulating shading and albedo effects accurately.

Because the mounting structure was precisely designed in SketchUp and exported directly into Sunsolve, it fit perfectly under the defined panel configuration, with no need for further adjustments. This alignment validated that the simulation environment mirrored the real-world spatial relationships between the mounting structure and the panels, which is essential for realistic ray-tracing calculations.

*Material Definition for Accurate Ray-Tracing*

To enhance the accuracy of Sunsolve's ray-tracing simulation, we specified the material properties of the mounting structure. The structure was defined as galvanized steel: the same material used at the actual site. This definition is critical because Sunsolve's ray-tracing engine accounts for surface properties like reflectivity and absorption, impacting the rear-side irradiance of bifacial modules. Specifying galvanized steel allowed the simulation to replicate how light interacts with the structure, including reflections that contribute to rear-side gain.

*Positioning and Final Adjustment*

After the SketchUp model was imported:

- The structure was positioned directly beneath the PV module configuration within Sunsolve.

- Minor adjustments were made to ensure perfect alignment, confirming that the module mounting structure from SketchUp integrated seamlessly into the Sunsolve panel setup.
- This integration verified that the mounting structure and panel configurations were spatially accurate, mirroring the physical layout on-site.

By combining a custom-modeled structure from SketchUp with precise panel configuration in Sunsolve, we ensured that the simulation environment was as close to reality as possible. This detailed replication allowed Sunsolve's simulations to realistically model albedo effects, shadowing, and reflections, resulting in a highly accurate simulation environment. This setup laid a robust foundation for performance analysis that closely represents on-site conditions.

## Albedo Configuration in Sunsolve

### Grass Reference System

Following the configuration of the PV modules and mounting structures, the next critical step involved defining the albedo properties of the ground surface within Sunsolve. For the reference system, which features natural grass as the ground surface, our team had previously validated the albedo value through a comparative simulation approach. This process entailed simulating the actual scenario in Sunsolve and exporting the results to PVSyst for varying albedo values. By comparing these simulations to actual yield data, we determined that an albedo value of 23.8% for grass provided the closest match to real-world performance. This value was subsequently used in Sunsolve to simulate the grass reference system accurately.

Additionally, Sunsolve allows for the specification of ground slope. Given that our experimental site is situated on flat terrain, we set the ground slope parameter to 0 degrees, ensuring that the simulation accurately reflects the site's topography.

### Albedo Booster Systems

To assess the impact of enhanced ground reflectivity, we introduced albedo booster sheets into the simulation. These sheets were modeled as custom objects within Sunsolve, with dimensions and thicknesses mirroring those used on-site. The positioning of these booster sheets along the X and Y axes in Sunsolve was meticulously adjusted to replicate their actual placement in the field.

It's important to note that while the booster sheets were categorized as 3-sheet, 4-sheet, 5-sheet, and 6-sheet configurations, the actual widths on-site were not simply multiples of individual sheet widths. This discrepancy arose because the sheets were slightly overlapped to secure them to the ground effectively. To ensure accurate replication, we measured the

actual widths of the overlapped sheets on-site and used these measurements to define the custom albedo objects in Sunsolve. Each albedo booster scenario was simulated separately in Sunsolve, just like the grass reference simulation, to facilitate comparative analysis.

### Material Properties and Reflectance Configuration

The albedo booster sheets were composed of aluminum, a material known for its high reflectivity. However, when laid over grass, the sheets exhibited wrinkles and undulations due to the underlying terrain, affecting their reflective properties. Initially, we utilized Sunsolve's built-in 'weathered aluminum' material for the simulation. This approach did not yield results that aligned closely with actual site performance.

- The optical properties of the aluminum sheets were determined through trial and error within SunSolve, using reference values based on typical behavior of similar reflective materials. After a few iterations, the following parameters were selected as they provided the best match between simulated and actual performance across all scenarios: Reflectance: 0.7
- Absorptance: 0.3
- Scattering: Set to constant with wavelength
- Lambertian Fraction Distribution: 0.5

The Lambertian distribution is a model that describes how light reflects off a surface such that the apparent brightness is the same regardless of the observer's angle. This model is particularly useful for simulating diffuse reflections from rough surfaces. A Lambertian fraction of 0.5 indicates that half of the reflected light follows a Lambertian (diffuse) distribution, while the remaining half may follow a different (e.g., specular) distribution. This setting effectively captures the semi-diffuse reflective behavior of the wrinkled aluminum sheets. [43]

This configuration provided simulation results that closely matched the actual performance observed on-site. While future work may involve conducting further laboratory tests to obtain wavelength-dependent reflectance data for even more precise simulations, the current approach using average reflectance values has proven effective for the purposes of this thesis.

### Heterogeneous Albedo Configurations

It's noteworthy that all simulations involving albedo booster sheets employed heterogeneous albedo configurations. This means that the ground surface in the simulation comprised regions with differing albedo properties-specifically, natural grass areas and aluminum booster sheet areas. This setup contrasts with the homogeneous albedo

configuration used in the grass reference simulation, where the entire ground surface was modeled with a uniform albedo values.

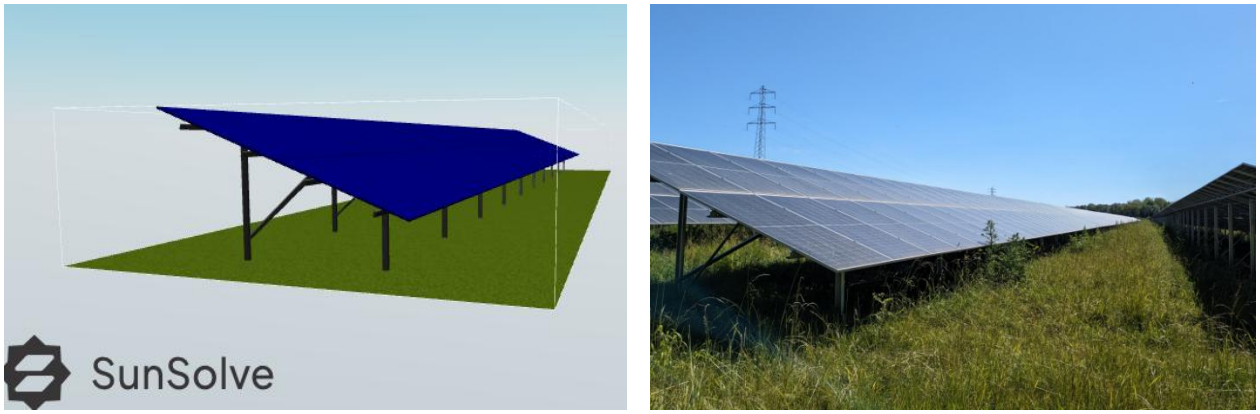


*Figure 24 Grass System design in Sunsolve*

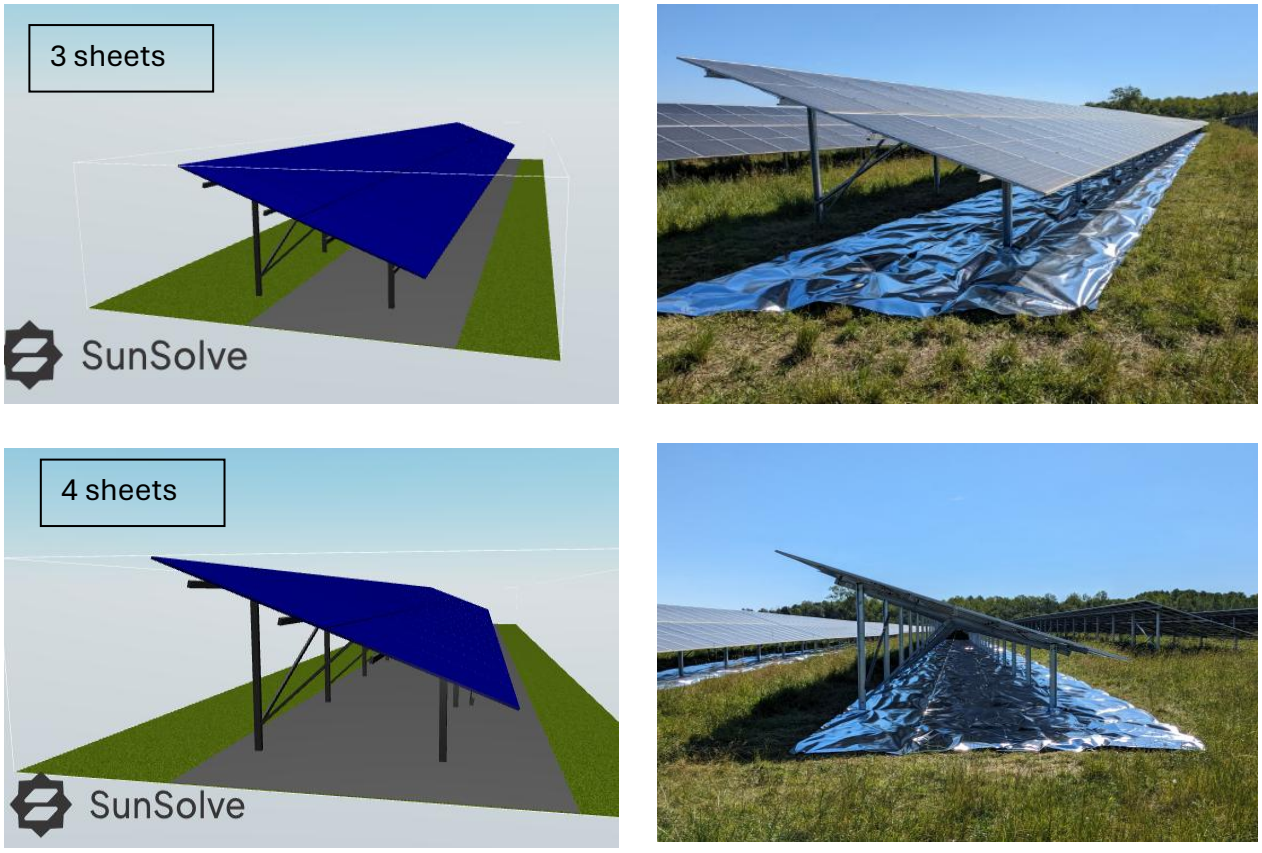


*Figure 25 Albedo 3 and 4 sheet design in Sunsolve*

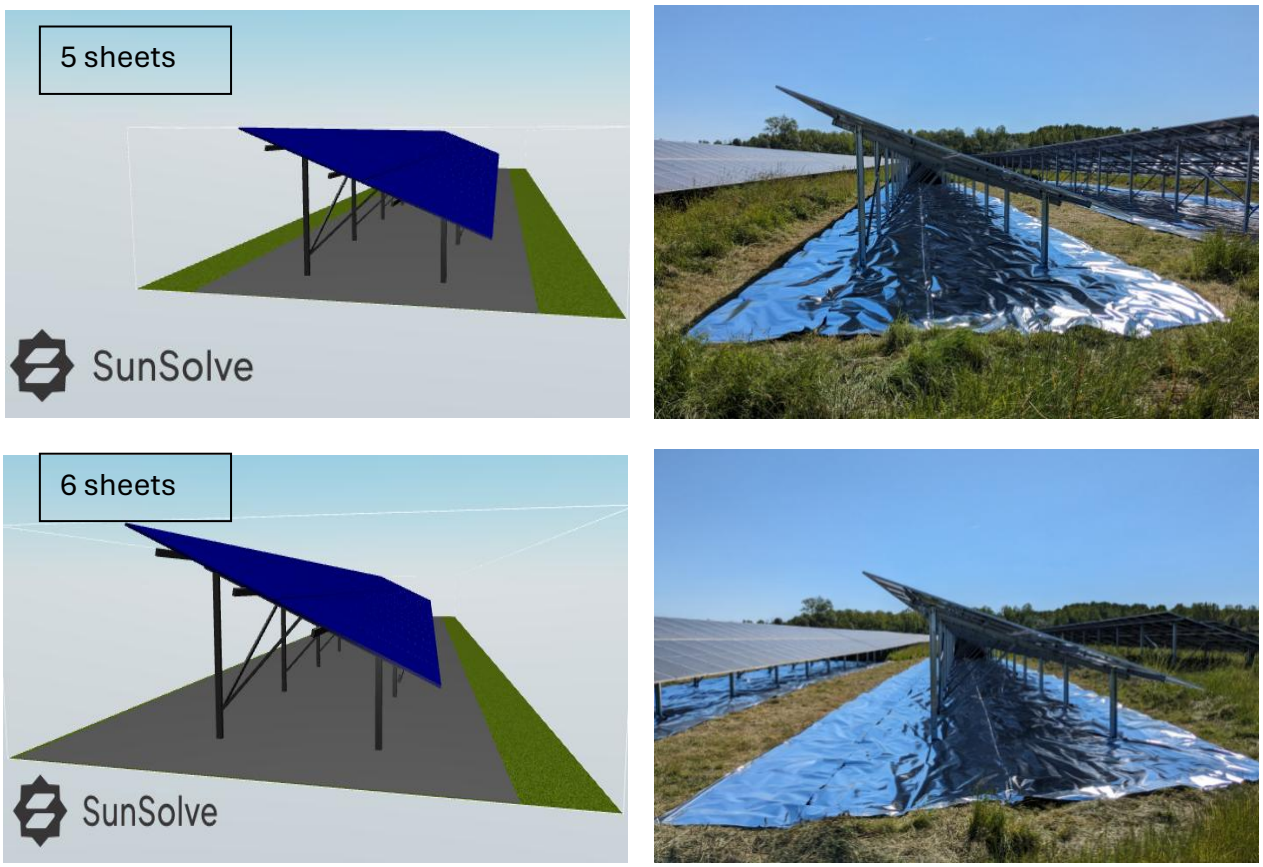


*Figure 26 Albedo 5 and 6 sheet design in Sunsolve*

By accurately modeling both the physical placement and optical properties of the albedo booster sheets, the simulations provide a reliable basis for analyzing the impact of enhanced ground reflectivity on PV system performance.

### Thermal Inputs Configuration

In addition to configuring the PV modules, mounting structures, and albedo settings, Sunsolve also allows for the definition of thermal inputs for the simulation. The thermal model plays a crucial role in determining the module's operating temperature, which directly impacts the system's electrical yield. In Sunsolve, the default thermal model used is the Faiman Thermal Model. This model is widely utilized in PV simulations for its simplicity and effectiveness in estimating module temperatures under varying environmental conditions. [44]

The Faiman model estimates the module temperature (Tm) based on the following equation: [45]

$$Tm = Ta + \frac{G \cdot (1 - \eta)}{U0 + U1 \cdot v}$$

Where:

- Ta = Ambient temperature (°C)
- G = Solar irradiance ($W/m^2$)
- η = Module efficiency
- U0 = Heat loss coefficient (no wind, $W/m^2 \cdot K$)
- U1 = Heat loss coefficient (wind-dependent, $J \cdot s \cdot m^{-3} \cdot K^{-1}$)
- v = Wind speed (m/s)

The default values for the Faiman thermal model in Sunsolve are:

- $U_0 = 25\ W/m^2 \cdot K$ ; $U_1 = 1.2\ J \cdot s \cdot m^{-3} \cdot K^{-1}$

These are the same as the default values in PVSyst when reliable hourly wind speed data is available. This alignment allows for consistent thermal loss calculations across both simulation platforms. For our simulation, we retained these default values to ensure comparability with PVSyst and maintain accuracy in the thermal behavior representation of the PV modules.[46]

### String Definition

Sunsolve allows for the definition of the number of strings and the number of panels within each string. In the simulation setup, the total number of panels specified is distributed across all string combinations. For example, if the configuration consists of 27 × 2 panels (a total of 54 panels), these panels are used for all defined string arrangements. If the number of string panels exceeds the total simulated panels, Sunsolve reuses the ray-tracing simulations for those panels accordingly.

In our setup, we have configured 2 strings of 27 panels each, representing a single PV array table that mirrors our actual site layout. The first string of 27 panels is assigned to the upper row, and the second string to the lower row within the simulation structure. If we wanted to simulate a third string of 15 panels, the first layer of panels in the simulation would be reused to accommodate this additional string. This modular approach enables flexible string configurations while maximizing the use of simulation results.

Sunsolve provides flexibility in defining the Solve Type for simulations, allowing users to choose between three levels: Module Level, DC String Level, and AC Level. This selection determines the granularity at which electrical characteristics are calculated and analyzed.

1. Module Level: At the module level, Sunsolve performs ray tracing and electrical calculations individually for each solar panel. This detailed analysis considers the IV characteristics, temperature effects, and shading impacts on a per-module basis.

2. DC String Level: In the DC String Level configuration, modules are grouped into electrical strings as defined in the layout. Ray tracing is performed for each module, and the resulting IV curves are combined into string-level IV curves, reflecting the performance of series-connected modules. This level is particularly useful for analyzing MPPT behavior and string-specific losses.
3. AC Level: At the AC Level, Sunsolve aggregates string IV curves into an array-level IV curve, which is then connected to an inverter model. This final step simulates DC-to-AC conversion, capturing inverter efficiency and any associated conversion losses.

For our analysis, we specifically focus on the DC String Level, aligning with individual MPPT data from the field to achieve higher fidelity in performance comparisons.

### Ray Count Configuration

Sunsolve also provides the option to configure the number of rays traced during simulations. The ray count directly influences the precision of the optical calculations-higher ray counts improve accuracy but require more computational power. By default, Sunsolve uses an optimized number of rays per solar angle to balance accuracy and simulation time. For our simulations, we utilize the default Sunsolve ray count, which has been validated to provide a good trade-off between precision and efficiency. [47]

This controlled ray distribution ensures that optical behaviors like absorption, reflection, and transmission are captured effectively, leading to realistic electrical outputs in the final simulation results.

### Diffuse Light Transposition Models

Sunsolve calculates the transposition of diffuse light and solar position based on the models specified during simulation configuration. Diffuse light transposition is crucial in accurately modeling the energy yield of photovoltaic (PV) systems, as it adjusts the incident irradiance on tilted surfaces based on the nature of the diffuse light scattering in the atmosphere. Sunsolve provides five primary methods for transposition of diffuse light:

#### 1. Isotropic Sky Model

The Isotropic Sky Model is the simplest and most widely used diffuse light transposition model, introduced by Liu and Jordan (1960). [48] It assumes that diffuse irradiance is uniformly distributed across the entire sky dome, regardless of weather conditions. This means the intensity of diffuse light is considered equal in all directions. The diffuse irradiance $I_d$ on a tilted surface in this model is represented as: [49]

$$I_d = DHI \frac{1 + \cos \beta}{2}$$

where:

- $I_d$ – Diffuse irradiance
- $\beta$ – Tilt angle of the surface
- DHI – Diffuse Horizontal Irradiance

This model is most appropriate for fully overcast conditions, where diffuse light is scattered evenly. [50]

### 2. Hay and Davies Model

The Hay and Davies Model was introduced to improve upon the Isotropic Model by accounting for the anisotropic nature of sky diffuse irradiance. It considers the circumsolar region (the area close to the sun) as more intense than the rest of the sky dome. The model divides the sky into three components:[51]

1. An isotropic background
2. A circumsolar brightening region
3. A horizon brightening term

The transposition formula is given as:

$$I_d = DHI \cdot \left[ A \cdot R_b + (1 - A) \cdot \frac{1 + \cos(\beta)}{2} \right]$$

where:

- $I_d$ - Diffuse irradiance on the tilted surface (W/m$^2$)
- $DHI$ - Diffuse Horizontal Irradiance (W/m$^2$)
- $A$ - Anisotropy index, calculated as DNI/DNI$_{extra}$
- $Rb$ - Ratio of beam radiation on tilted surface to that on horizontal surface
- $\beta$ - Surface tilt angle from horizontal (degrees)

This model accounts for enhanced light intensity in the circumsolar region and is particularly useful in clearer conditions.[52]

### 3. Perez Models (1987, 1990, SAM Version)

The Perez Models are the most advanced diffuse transposition models provided in Sunsolve. They offer enhanced accuracy by accounting for circumsolar and horizon brightening effects and the anisotropic nature of diffuse light. Three versions are implemented in Sunsolve:

- Perez (1987) – The original model, accounting for circumsolar effects.[53]
- Perez (1990) – An improvement over the 1987 version, with refined calculations for clear and overcast skies.[54]
- Perez (SAM) – An adaptation of the 1990 Perez model by NREL for its System Advisory Model (SAM). [55]

The general form of the Perez model for tilted surface irradiance is given by: [56] [57]

$$I_d = DHI \times \left[(1 - F_1)\left(\frac{1 + \cos(\beta)}{2}\right) + F_1\left(\frac{a}{b}\right) + F_2 \sin(\beta)\right]$$

where:

- $F_1$ - Circumsolar brightness coefficient
- $F_2$ - Horizon brightness coefficient
- $a$ - Incidence-weighted solid angle sustained by the circumsolar region as seen by the tilted surface
- $b$ - Incidence-weighted solid angle sustained by the circumsolar region as seen by the horizontal surface
- $\beta$ - Tilt angle of the surface from horizontal (degrees)

Ray tracing in Sunsolve independently handles the absorption of direct and diffuse light within the unit-system. These transposition models are specifically applied during the yield calculation to modify the DHI (Diffuse Horizontal Irradiance) and DNI (Direct Normal Irradiance) components as defined in the weather files, ensuring realistic representation of light interactions with the solar array.

## Solar Position Models in Sunsolve

Sunsolve provides various models to calculate the sun's position in the sky during simulations. The software accounts for three critical components to accurately model solar positioning: Solar Vector, Solar Refraction, and Solar Time. These models enable the simulation to predict the solar zenith and azimuth angles, which are essential for evaluating solar irradiance on tilted surfaces.

### 1. Solar Vector Models

The solar vector models calculate the sun's geometric position in the sky, unaffected by atmospheric refraction. Sunsolve includes the following options:

1. Reda and Andreas (2004) – This model, developed by Reda and Andreas, is the most precise option available, with an accuracy of ±0.0003° for zenith and azimuth angles. The algorithm, based on Meeus (1998) calculations, is valid between the years 2000 BCE and 6000 CE, making it highly reliable for long-term simulations. [58]
2. Blanco-Muriel (2001) – This model calculates solar positioning with an accuracy of 0.5 minutes of arc. It is computationally efficient and was widely used between 1999 and 2015. [59]
3. Michalsky (1988) – This model, with a subsequent erratum in 1998, provides reliable solar vector calculations but is slightly less accurate compared to Reda and Andreas. [60]

4. Walraven (1979) – First introduced in 1979 with a correction the same year, this model is a classic solar vector calculation method but with lesser accuracy compared to modern approaches. [61]
5. Spencer (1971) – Implemented from *Reno (2012)*, this is an older model with simple trigonometric calculations. [62]
6. ASCE (2012) – Also implemented from *Reno (2012)*, this is a basic model often used in simplified solar calculations. [63]
7. PVSyst (as of Apr-2023) – This is the solar position algorithm currently described in PVSyst's documentation. It is primarily used for PV system simulations in industry. [64]

Sunsolve modifies these algorithms to exclude refraction so that its impact can be computed separately.

### 2. Solar Refraction Models

Solar refraction is the bending of sunlight as it passes through Earth's atmosphere, altering the sun's apparent position. Sunsolve provides three models to account for this effect:

1. None – No atmospheric refraction correction is applied.
2. Reda and Andreas (2004) – This model includes highly accurate refraction corrections, integrated with its solar vector calculations. The algorithm adjusts the solar position based on altitude, air pressure, and temperature. If these parameters are not specified in the weather file, default values are used. [58]
3. Zimmerman (1981) – A less complex model for solar refraction, suitable for simpler simulations. [65]

### 3. Solar Time Models

Sunsolve also allows users to configure the solar time for simulations. Solar time is critical for aligning the solar vector calculations with the Earth's rotation and geographic location. It converts UTC (Coordinated Universal Time) and legal time to local solar time. The options available are:

1. Reno (2012) – This is the default algorithm in Sunsolve. It provides high accuracy for converting standard time to solar time. [63]
2. Blanco-Muriel (2001) – This method is also available for solar time conversion, extending the accuracy of its solar vector model. [59]
3. PVSyst – The algorithm used in the PVSyst tool for synchronizing solar vector data with local time. [64]

## Overriding with User-defined Solar Position

Sunsolve also allows users to override the computed solar vector and refraction models by providing custom solar zenith (or elevation) and solar azimuth values directly through the weather file. Selecting "Load from weather" in the Sunsolve configuration menu enables this override. This feature is particularly useful for experiments requiring exact sun positioning based on measured data rather than modeled calculations.

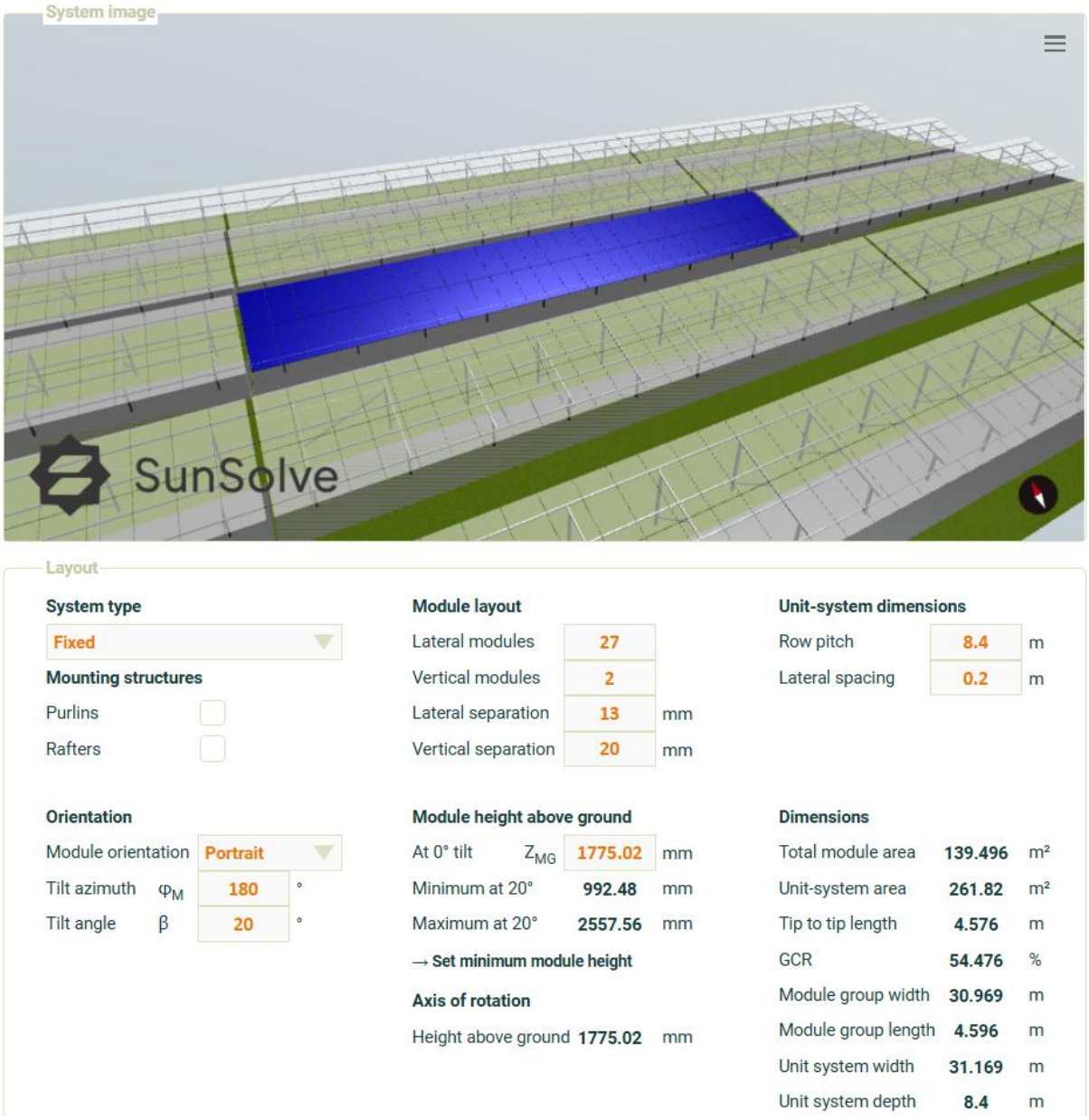


*Figure 27 Overview of the system in Sunsolve*

### 3.4.4. Simulation Output

With all input configurations specified-encompassing module layout, transposition models, solar position calculations, and ray-tracing parameters-the Sunsolve simulation is executed. Depending on the complexity of the model and the chosen ray configurations, the simulation may take anywhere from a few minutes to slightly longer to complete. Once finalized, Sunsolve generates an Output section.

#### Summary

The primary section of the output is dedicated to the summary energy yield for the specified simulation period. This includes the following key performance indicators:

- Total Energy Yield: The total amount of electrical energy generated by the PV system over the simulation timeframe.
- Specific Yield: The energy generated per installed kW of capacity, reflecting the efficiency of the system relative to its size.
- Performance Ratio (PR): A measure of the system's effectiveness, calculated as the ratio of the actual output to the theoretical maximum output under ideal conditions.
- Bifacial Performance Ratio (BPR): If bifacial panels are used, this metric evaluates the energy contribution from the rear side of the panels relative to the front side.
- Average Daily Specific Yield: The average daily energy production per installed kW over the simulation period.
- Bifi Optical Gain: This parameter quantifies the additional energy gain achieved by the rear side of the bifacial panels due to ground reflectance and albedo effects.

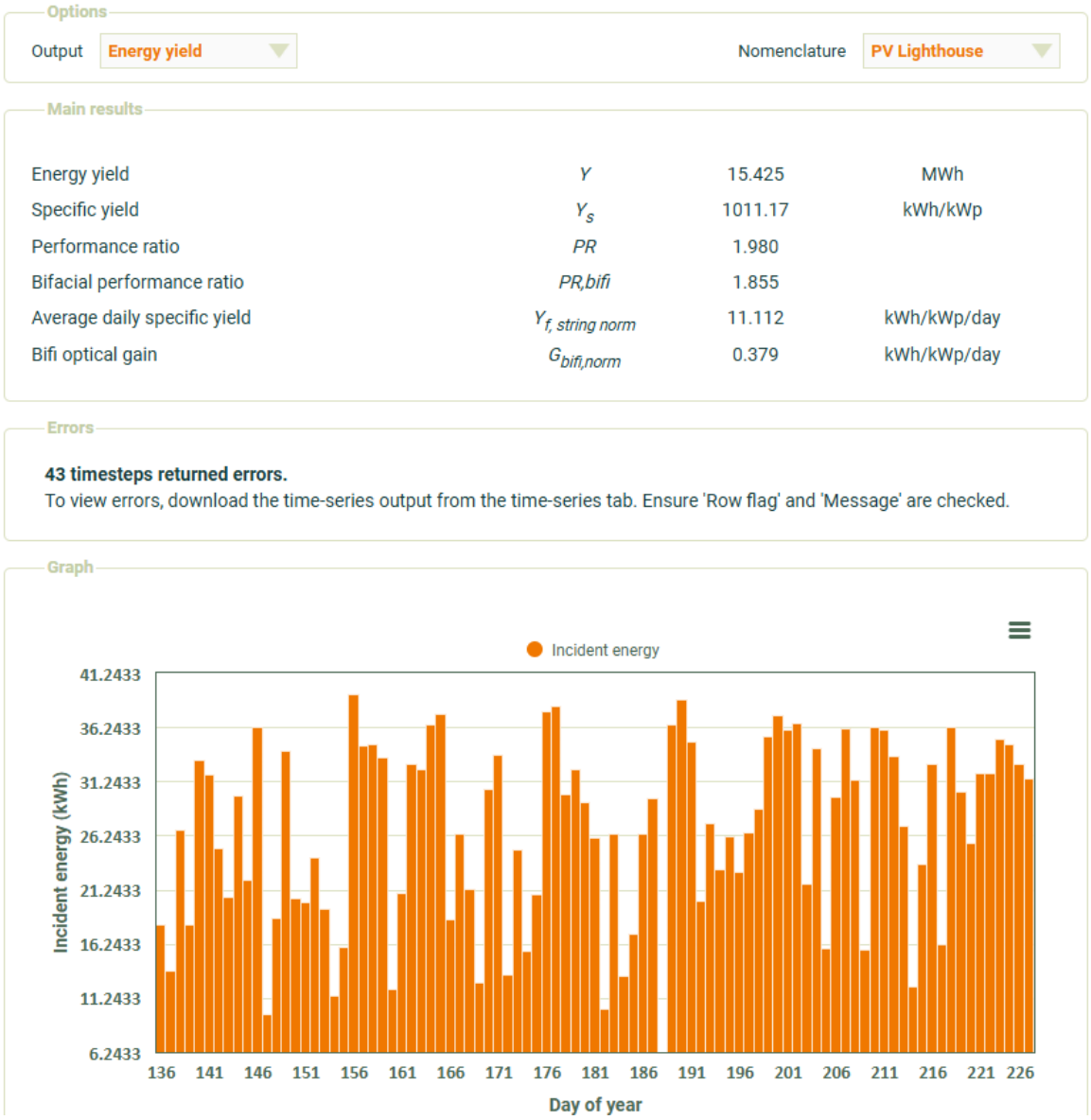


*Figure 28 Sunsolve Output Summary*

The output summary also includes interactive graphical representations of the yield data. These plots allow for dynamic exploration of various aspects of the simulation, such as energy generation trends, bifacial gain contributions, and system performance over time. Users can zoom, pan, and filter data to analyze specific intervals or conditions.

Furthermore, Sunsolve automatically performs a set of error checks during the simulation process. If any discrepancies or calculation issues arise-such as improper module connections, invalid ray-tracing paths, or insufficient weather data: they are clearly flagged in the output summary. This immediate feedback enables quick identification and resolution of potential issues.

### Time-Series CSV Export

The second segment of the Sunsolve output process involves generating a time-series CSV file that encapsulates the simulation's detailed performance data. This export option allows users to select the specific parameters they want to include in the final CSV, providing a high degree of customization for post-simulation analysis.

#### Configuration Options for CSV Generation

When setting up the CSV export, Sunsolve offers several customization options:

1. Date Configuration:

Date Type: Users can choose the timestamp format for the output data, with options for:

   - UTC (Coordinated Universal Time) – the standard time reference.
   - Legal Time – local time adjusted for daylight saving, if applicable.
   - Solar Time – time based on the actual position of the sun in the sky.

Date Format: The date format can be set to a timestamp or customized to any preferred format, providing flexibility for different analysis tools.

2. Output Options: Sunsolve enables users to select the granularity of the output data. The available options include:
   - Module Summary – Aggregated performance metrics for all modules.
   - Module Details – Detailed data for each individual module.
   - String Summary – Combined results for each string of modules.
   - String Details – Fine-grained electrical performance data for each module string.

For our project, we specifically select String Details since it provides the most comprehensive breakdown of electrical parameters for each string:- crucial for our comparative analysis with field data.

#### Electrical Parameters and Weather Data

In addition to electrical outputs, the CSV generation allows users to include weather data columns as required for further analysis. The critical DC electrical parameters we export include:

- Pmp, With Mismatch, at $T_{op}$: Maximum power point (Pmp) adjusted for module mismatch, at the operating temperature.
- Vmp: Voltage at maximum power point.
- Imp: Current at maximum power point.
- Voc: Open-circuit voltage.

- Isc: Short-circuit current.
- Mismatch Losses: Quantifies power losses due to electrical mismatch between modules in the same string.

The inclusion of these parameters ensures that the exported data is well-suited for deeper performance analysis and comparison against field measurements.

#### PVSyst Compatibility

An additional feature of Sunsolve is its PVSyst export compatibility. During the CSV configuration, users can select specific output data formatted to seamlessly integrate with PVSyst. This enables cross-software analysis and allows Sunsolve results to be directly imported into PVSyst for further simulation or reporting, streamlining the validation process.

#### CSV Generation and Further Processing

Once the desired parameters are selected, Sunsolve generates the time-series CSV file, which is ready for export. This file serves as the foundation for further processing, analysis, and validation steps in our project.

### 3.4.5. Simulation Scenarios and Data Generation

Based on the established modeling criteria and configurations, simulations were conducted for the grass (baseline) scenario as well as for each of the albedo-boosted configurations. These simulations were performed using two distinct weather datasets:

1. Cleaned and processed field-measured weather data, collected directly from on-site sensors.
2. Satellite-based weather data, obtained from high-resolution satellite observations.

Upon completion of the simulations, Sunsolve generated CSV output files for each albedo scenario under both weather datasets. This resulted in a structured collection of output files representing the modeled performance for:

- Grass (Baseline) – Field Weather | Satellite Weather
- Albedo 3m – Field Weather | Satellite Weather
- Albedo 4m – Field Weather | Satellite Weather
- Albedo 5m – Field Weather | Satellite Weather
- Albedo 6m – Field Weather | Satellite Weather

Each CSV file contained detailed time-series data of irradiance, electrical output, module temperatures, and performance metrics across the specified simulation window.

An example of the structure of the csv files is shown below:

| | A | B | C | D | E | F | G | H | I | J | K | L |
|---|---|---|---|---|---|---|---|---|---|---|---|---|
| 1 | DateTime (UTC) | GHI (W/m2) | DHI (W/m2) | DNI (W/m2) | Ambient temperature (°C) | Wind velocity (m/s | String [1] Power (W) | String [1] Vmp (V) | String [1] Imp (A) | String [2] Power (W) | String [2] Vmp (V) | String [2] Imp (A) |
| 2 | 2024-05-14T23:00:00. | 0 | 0 | 0 | 12.99999428 | 1.399999976 | 0 | 0 | 0 | 0 | 0 | 0 |
| 3 | 2024-05-14T23:15:00. | 0 | 0 | 0 | 12.89998817 | 1.100000024 | 0 | 0 | 0 | 0 | 0 | 0 |
| 4 | 2024-05-14T23:30:00. | 0 | 0 | 0 | 12.89998817 | 1.5 | 0 | 0 | 0 | 0 | 0 | 0 |
| 5 | 2024-05-14T23:45:00. | 0 | 0 | 0 | 12.74999428 | 1.5 | 0 | 0 | 0 | 0 | 0 | 0 |
| 6 | 2024-05-15T00:00:00. | 0 | 0 | 0 | 12.70000648 | 0.600000024 | 0 | 0 | 0 | 0 | 0 | 0 |
| 7 | 2024-05-15T00:15:00. | 0 | 0 | 0 | 12.70000648 | 1.350000024 | 0 | 0 | 0 | 0 | 0 | 0 |
| 8 | 2024-05-15T00:30:00. | 0 | 0 | 0 | 12.60000038 | 0.899999976 | 0 | 0 | 0 | 0 | 0 | 0 |
| 9 | 2024-05-15T00:45:00. | 0 | 0 | 0 | 12.55001259 | 1.100000024 | 0 | 0 | 0 | 0 | 0 | 0 |
| 10 | 2024-05-15T01:00:00. | 0 | 0 | 0 | 12.60000038 | 0.600000024 | 0 | 0 | 0 | 0 | 0 | 0 |
| 11 | 2024-05-15T01:15:00. | 0 | 0 | 0 | 12.45000648 | 0.949999988 | 0 | 0 | 0 | 0 | 0 | 0 |
| 12 | 2024-05-15T01:30:00. | 0 | 0 | 0 | 12.39998817 | 0.899999976 | 0 | 0 | 0 | 0 | 0 | 0 |
| 13 | 2024-05-15T01:45:00. | 0 | 0 | 0 | 12.35000038 | 0.649999976 | 0 | 0 | 0 | 0 | 0 | 0 |
| 14 | 2024-05-15T02:00:00. | 0 | 0 | 0 | 12.20000648 | 1.299999952 | 0 | 0 | 0 | 0 | 0 | 0 |
| 15 | 2024-05-15T02:15:00. | 0 | 0 | 0 | 12.10000038 | 0.949999988 | 0 | 0 | 0 | 0 | 0 | 0 |
| 16 | 2024-05-15T02:30:00. | 0 | 0 | 0 | 12.10000038 | 0.600000024 | 0 | 0 | 0 | 0 | 0 | 0 |
| 17 | 2024-05-15T02:45:00. | 0 | 0 | 0 | 12.14998817 | 0.800000012 | 0 | 0 | 0 | 0 | 0 | 0 |
| 18 | 2024-05-15T03:00:00. | 0 | 0 | 0 | 12.10000038 | 0.899999976 | 0 | 0 | 0 | 0 | 0 | 0 |
| 19 | 2024-05-15T03:15:00. | 0 | 0 | 0 | 12.14998817 | 0.550000012 | 0 | 0 | 0 | 0 | 0 | 0 |
| 20 | 2024-05-15T03:30:00. | 0 | 0 | 0 | 12.20000648 | 0.699999988 | 0 | 0 | 0 | 0 | 0 | 0 |
| 21 | 2024-05-15T03:45:00. | 0 | 0 | 0 | 12.30001259 | 0.150000006 | 0 | 0 | 0 | 0 | 0 | 0 |
| 22 | 2024-05-15T04:00:00. | 2.733333349 | 0 | 0 | 12.39998817 | 0.699999988 | 0 | 0 | 0 | 0 | 0 | 0 |
| 23 | 2024-05-15T04:15:00. | 7.099999905 | 7.099999905 | 0 | 12.24999428 | 0.25 | 0 | 0 | 0 | 0 | 0 | 0 |
| 24 | 2024-05-15T04:30:00. | 12.5666666 | 11.86532402 | 16.47856331 | 12.20000648 | 0.300000012 | 165.6528625 | 1073.076172 | 0.154371917 | 157.7242584 | 1056.377075 | 0.149306804 |
| 25 | 2024-05-15T04:45:00. | 19.08333397 | 18.00108337 | 13.32355118 | 12.39998817 | 0.300000012 | 271.9552612 | 1071.530884 | 0.253800631 | 263.4453735 | 1069.239502 | 0.246385723 |
| 26 | 2024-05-15T05:00:00. | 41.40000153 | 38.96207047 | 20.08488846 | 12.49999428 | 0 | 583.4866333 | 1105.67627 | 0.527719021 | 560.0164185 | 1102.966553 | 0.507736742 |
| 27 | 2024-05-15T05:15:00. | 79.41666412 | 74.42943573 | 30.7124424 | 12.74999428 | 0.200000003 | 1080.878296 | 1128.229614 | 0.958030522 | 1053.995117 | 1126.028564 | 0.93602854 |

*Table 3 Sunsolve CSV output*

These generated datasets, alongside the actual inverter results collected from the field, form the foundation of our analysis and observations. By structuring the results this way, we establish a clear comparison between:

- Simulated vs. Actual inverter performance
- Field weather vs. Satellite weather predictions
- Baseline grass scenario vs. albedo-boosted scenarios

## 3.5. Data Processing and Analysis

We utilize Python within the VSCode environment for the processing, analysis, and visualization of datasets we have. The first step in this process is to input and structure the datasets for each albedo scenario.

### 3.5.1. Sunsolve Data

#### Input and Organization of Simulation Files

The Sunsolve simulation files are first defined in a structured manner using a dictionary, where each key represents a specific simulation group (in this case, "Sunsolve_data"), and the values are further dictionaries containing the albedo scenarios and their corresponding filenames. This structure helps to efficiently loop through each simulation, load the datasets, and process them systematically.

#### Reading and Processing CSV Files

Each CSV file corresponding to the albedo simulations (grass, albedo_3m, albedo_4m, albedo_5m, and albedo_6m) is then loaded into memory. The timestamp column is renamed to TIMESTAMP for clarity and parsed into a standardized datetime format. These timestamps

are then set as the index of the DataFrame to enable time-based operations like resampling or time slicing.

Additionally, we calculate the total MPPT power for each albedo scenario by summing the power outputs from String 1 and String 2 of the inverter. The formula used is:

MPPT(W)=String [1] Power (W) + String [2] Power (W)

These power values are stored as new columns named:

"MPPT(W)_grass",

"MPPT(W)_albedo_3m",

"MPPT(W)_albedo_4m",

"MPPT(W)_albedo_5m", and

"MPPT(W)_albedo_6m" ; for their respective scenarios.

### Merging the DataFrames

All the individual MPPT power series for each scenario are combined into a single DataFrame, which is then stored in a variable called Sunsolve_data. This structure allows for easy comparison and analysis of MPPT outputs across different albedo conditions.

### Adding Weather Data to the Combined DataFrame

To perform more detailed analysis, we also include the weather data from the grass simulation file, as it contains the relevant meteorological parameters for the site. The weather data columns included are:

- DHI ($W/m^2$) : - Diffuse Horizontal Irradiance
- GHI ($W/m^2$) : - Global Horizontal Irradiance
- DNI ($W/m^2$) : - Direct Normal Irradiance

The weather columns are extracted from the grass simulation file, indexed by their corresponding timestamps, and then merged with the Sunsolve_data DataFrame. This ensures that the MPPT power outputs are fully aligned with the corresponding weather conditions at each timestamp, facilitating a synchronized analysis.

### Final Output Structure

The final Sunsolve_data DataFrame now includes:

1. Weather Data :- DHI, GHI, and DNI values.
2. MPPT Power Data for each albedo simulation :- grass, albedo_3m, albedo_4m, albedo_5m, and albedo_6m.

The basic structure is shown below:

| TIMESTAMP | DHI (W/m2) | GHI (W/m2) | DNI (W/m2) | MPPT(W)_grass | MPPT(W)_albedo_3m | MPPT(W)_albedo_4m | MPPT(W)_albedo_5m | MPPT(W)_albedo_6m |
|---|---|---|---|---|---|---|---|---|
| 2024-05-14 23:00:00 | 0.0 | 0.0 | 0.0 | 0.0 | 0.0 | 0.0 | 0.0 | 0.0 |
| 2024-05-14 23:15:00 | 0.0 | 0.0 | 0.0 | 0.0 | 0.0 | 0.0 | 0.0 | 0.0 |
| 2024-05-14 23:30:00 | 0.0 | 0.0 | 0.0 | 0.0 | 0.0 | 0.0 | 0.0 | 0.0 |
| 2024-05-14 23:45:00 | 0.0 | 0.0 | 0.0 | 0.0 | 0.0 | 0.0 | 0.0 | 0.0 |
| 2024-05-15 00:00:00 | 0.0 | 0.0 | 0.0 | 0.0 | 0.0 | 0.0 | 0.0 | 0.0 |

*Table 4 Sunsolve Data Overview*

### 3.5.2. Loading of Field and Satellite Weather Data

Along with the Sunsolve simulation outputs, we also load two crucial datasets:

1. Soda Satellite Weather Data
2. Actual Site Weather Data

Both datasets were preprocessed and cleaned to ensure alignment with the 15-minute timestamp intervals used in the Sunsolve simulations. This step ensures perfect synchronization between the weather inputs and the simulation timestamps for accurate analysis.

### 3.5.3. Loading of Inverter Datasets

The next step involves loading the actual inverter datasets from the site. We are specifically working with eight inverters:

- inv_7, inv_8, inv_9, inv_10, inv_11, inv_12, inv_13, inv_14

The CSV files corresponding to these inverters are loaded and processed. We only extract the necessary columns, including:

- Date and Time - Renamed to TIMESTAMP and set as the index for time-based operations.
- Power AC (kW) - Represents the AC power output of the inverters.
- DC Voltage (V) and DC Current (A) for each string (1 to 18) of the inverter.
- Solar Irradiance Reference ($W/m^2$) for monitoring incoming sunlight levels.

We also perform data cleanup during this stage:

- Negatives are converted to positives since these values sometimes appear with minor negative fluctuations due to sensor calibration issues.
- For specific inverters, we set current values to zero for certain strings that are known to always be inactive. This avoids false readings from these inputs that could skew analysis.

### Calculation of DC Power for Each String

To analyze MPPT-level power, we first calculate the DC Power (Pdc) for each string of each inverter. The formula used is:

$$P_{\text{dc}} = V_{\text{dc}} \times I_{\text{dc}}$$

where:

- Vdc is the DC Voltage of the string, and
- Idc is the DC Current of the string.

Each string's power output is calculated and added to a new DataFrame for each inverter:

- Pdc_inv_7 - Contains power for each string in inverter 7
- Pdc_inv_8 - Contains power for each string in inverter 8
- ...
- Pdc_inv_14 - Contains power for each string in inverter 14

### Aggregation of Strings into MPPT Power Outputs

Each inverter is equipped with multiple strings, which are grouped in pairs to form Maximum Power Point Tracking (MPPT) zones. The power for each MPPT is calculated by summing the power outputs of the corresponding string pairs:

$$P_{\text{MPPT}} = P_{\text{dc, String1}} + P_{\text{dc, String2}}$$

This aggregation step produces MPPT-level power data for each inverter:

- mppt_Pdc_inv_7 - Contains MPPT power data for inverter 7
- mppt_Pdc_inv_8 - Contains MPPT power data for inverter 8
- ...
- mppt_Pdc_inv_14 - Contains MPPT power data for inverter 14

Each of these DataFrames is indexed by timestamp, fully synchronized with the weather and simulation data.

### Selection of Inverters and MPPTs for Each Albedo Scenario

Now that we have MPPT-level power data for each inverter, we select specific inverters and MPPTs that correspond to each albedo scenario, as follows:

- Grass: Inverter 8, MPPT 1
- Albedo 3m: Inverter 14, MPPT 1
- Albedo 4m: Inverter 13, MPPT 1
- Albedo 5m: Inverter 10, MPPT 1
- Albedo 6m: Inverter 9, MPPT 1

The grass reference inverter can also be chosen as 7, 11 or 12 as well. We chose inverter 8 as the grass reference because its position is closest to Inverter 9 which houses the longest width albedo booster (6 sheets)

This selection is done by dynamically accessing the corresponding MPPT power columns from the previously processed DataFrames and consolidating them into a single DataFrame called inv_data.

The final structure of inv_data includes the MPPT power outputs of the selected inverters, aligned with the specified albedo scenarios. This structured DataFrame is ready for further analysis and comparison against the Sunsolve simulation results.

An overview of the inv data structure is shown below:

| | grass | albedo_3m | albedo_4m | albedo_5m | albedo_6m |
|---|---|---|---|---|---|
| TIMESTAMP | | | | | |

*Figure 29 Inverter Data Structure*

### 3.5.4. Further Data Cleaning and Synchronization

#### Synchronizing the Timestamps

To ensure accurate comparisons between the Sunsolve simulation data and the field inverter data, we first identify the common timestamps present in both datasets. This step is crucial since both datasets must be aligned to the exact same time intervals for meaningful analysis.

The common timestamps are extracted by performing an intersection of the index (timestamp) of both inv_data and Sunsolve_data.

We then reindex both DataFrames to include only the timestamps that are common. A visual check was also conducted to make sure there were no discrepancies. This removes any mismatched or out-of-sync data points that could distort the analysis.

#### Handling Missing Values

After reindexing, any missing values are filled with zeros. This step is especially important for:

- The Sunsolve simulation data (Sunsolve_data) - To ensure there are no NaN gaps in the GHI or other simulation parameters.
- The Inverter power data (inv_data) - So that any missing power production is considered as zero output, preventing analysis issues.

### Removing Daylight Non-Production Periods

One major cleanup step is to remove timestamps where the simulation predicts sunlight (daylight), but the inverters are not producing power. This can happen if the inverter is offline, disconnected, or faulty.

To identify these periods, we:

1. Check for Global Horizontal Irradiance (GHI) levels above 50 W/m$^2$. This is a threshold indicating daylight conditions.
2. Check if any inverter in the inv_data is not producing power (values ≤ 0) during these daylight hours.
3. If both conditions are met, we mark these timestamps for removal.

These non-producing times are then dropped from the DataFrame (inv_data) to prevent skewing the yield analysis. A message is printed to indicate how many timestamps were removed.

### Final Synchronization Check

After cleaning, we perform another synchronization check to ensure that both datasets remain perfectly aligned:

- We again intersect the indexes of both inv_data and Sunsolve_data.
- Both DataFrames are reindexed and filled with zeros to match perfectly.

At this stage, the datasets are cleaned, synchronized, and filtered for proper daylight comparison. We are now ready to move on to compare the simulation and field data for yield analysis and validation.

## 3.5.5. Classifying Days Based on Sky Conditions

The performance of albedo boosters in bifacial PV systems is heavily influenced by the irradiance conditions on any given day. These reflective surfaces are designed to amplify the ground-reflected light that reaches the rear side of the bifacial modules. However, their effectiveness varies significantly depending on the nature of the sunlight:

- On clear, sunny days, most of the incoming solar energy is in the form of direct normal irradiance (DNI), which predominantly reaches the front side of the modules. The role of the albedo booster is less impactful because the back-side illumination primarily depends on the ground's reflectivity of sunlight.
- Conversely, on diffused sky days:- where the sunlight is scattered across the sky dome- albedo boosters become substantially more effective. The diffused light is reflected more uniformly from the albedo sheets, enhancing the rear-side exposure of the modules and improving overall energy yield.

- For mixed (miscellaneous) days, the impact fluctuates as conditions vary between sunny and cloudy, necessitating a separate analysis to capture these dynamics.

To understand the real contribution of albedo boosters under different conditions and to quantify their performance enhancement, it is essential to classify days based on irradiance patterns. This classification allows for a more granular analysis of the relative performance gains across clear, diffused, and mixed sky conditions.

The following steps are employed to classify the available days:

## Resampling Data to Daily Averages

To begin the classification of sky conditions, we first resample the Sunsolve simulation data to daily averages. This allows us to observe the average irradiance levels (GHI, DNI, DHI) for each day, making it easier to distinguish between clear, diffused, and mixed days. The Daily plots of GHI, DHI and DNI are shown in Figure 30, below:

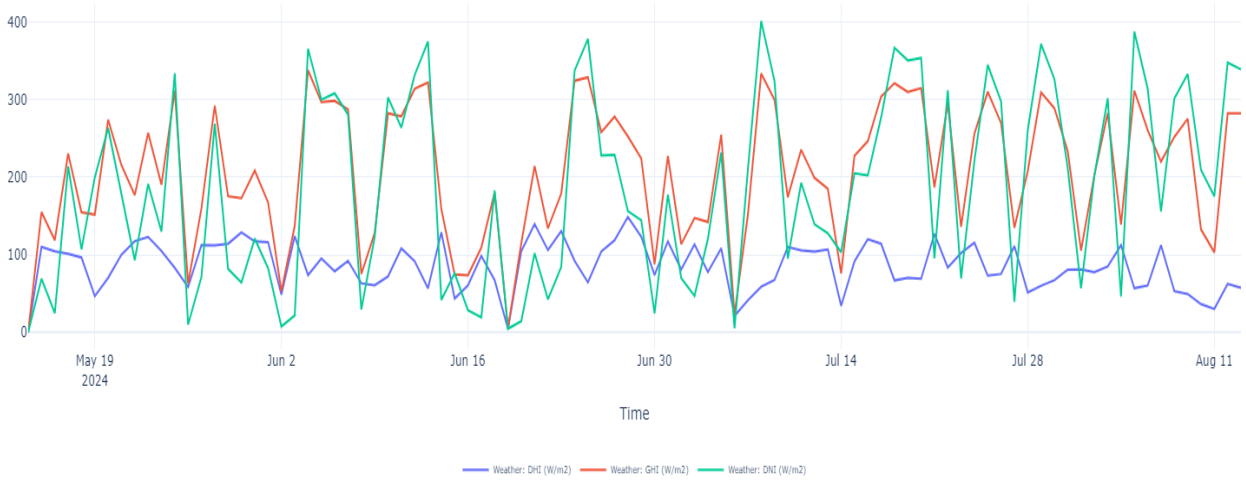


*Figure 30 Daily Irradiance Plot*

## Defining Thresholds for Sky Conditions

The threshold for classification is set based on the site conditions we observed and to get the best filters based on the site conditions. We set the following irradiance thresholds to classify the days:

*Clear Sky Days*

- Global Horizontal Irradiance (GHI) > 300 W/m$^2$
- Direct Normal Irradiance (DNI) > 350 W/m$^2$
- Diffuse Horizontal Irradiance (DHI) < 100 W/m$^2$

These thresholds are indicative of days with strong direct sunlight and minimal cloud cover.

*Diffused Sky Days*

- Direct Normal Irradiance (DNI) < 15 W/m$^2$
- Global Horizontal Irradiance (GHI) > 50 W/m$^2$

This condition is typical for overcast or cloudy days, where sunlight is mostly scattered and not direct.

*Miscellaneous (Mixed) Sky Days*

- These are days that do not fit the above two categories and generally have variable or unstable sky conditions.

## Classifying the Days

Using the daily average values from the Sunsolve dataset, we:

1. Identify Clear Sky Days by applying the thresholds for GHI, DNI, and DHI.
2. Identify Diffused Sky Days using the conditions for low DNI and sufficient GHI.
3. Extract all days from the dataset and identify those that do not fit either category as Miscellaneous Days.

*Figure 31 Sunny(left), Diffused(middle) and Miscellaneous Days(right)*

The classified days are then converted to DatetimeIndex for easy matching with the inverter data.

## Filtering Inverter and Sunsolve Data Based on Classification

Once the days are categorized, we filter the main datasets (inv_data and Sunsolve_data) based on the sky condition:

- Clear Sky Data: All timestamps that fall within the identified clear sky days.
- Diffused Sky Data: All timestamps that belong to diffused days.
- Miscellaneous Sky Data: All remaining timestamps that belong to mixed conditions.

## Summary of Classification

Finally, a summary of the classification is printed out, indicating:

- The total number of days analyzed.

- The number of days classified as Clear, Diffused, and Miscellaneous.
- The shapes of the filtered DataFrames for both the inverter data and Sunsolve data.

```
Total number of days: 92
Clear sky days: 9
Diffused sky days: 3
Miscellaneous sky days: 80

All inverter data shape: (8348, 5)
Clear sky inverter data shape: (864, 5)
Diffused sky inverter data shape: (260, 5)
Misc sky inverter data shape: (7224, 5)

All SUNSOLVE data shape: (8348, 8)
Clear sky SUNSOLVE data shape: (864, 8)
Diffused sky SUNSOLVE data shape: (260, 8)
Misc sky SUNSOLVE data shape: (7224, 8)
```

*Figure 32 Summary of Day Classification*

This step confirms that the data has been successfully separated into three distinct categories, setting the stage for targeted analysis based on specific sky conditions.

### 3.5.6. MPPT Gain Calculations and Smoothing

After classifying the days based on sky conditions (clear, diffused, and mixed), we move on to calculate the MPPT gain for each scenario (albedo_3m, albedo_4m, albedo_5m, albedo_6m) with respect to the grass reference. This is done for both simulated and actual datasets, with grass serving as the baseline for comparison.

#### Simulated Gain Calculation

We start with the simulated data from Sunsolve:

- The reference scenario is the grass simulation, and for each albedo scenario, the gain is calculated as the percentage increase or decrease relative to grass:

$$\text{Gain (\%)} = \frac{(\text{MPPT Power (Albedo Scenario)} - \text{MPPT Power (Grass)})}{\text{MPPT Power (Grass)}} \times 100$$

- A threshold logic is applied to filter out erroneous or unrealistic gain values during low irradiance hours (before 6 AM and after 6 PM) and when the MPPT power is too low (< 550 W) or the absolute difference between the two is too small (< 1 W).
- If these conditions are met, the gain is set to 0 for those timestamps, as power differences during very low light are unreliable.
- Finally, the simulated gains for each scenario are stored in a DataFrame, with NaN values replaced by 0.

### Actual Gain Calculation

Next, we compute the gain for the actual field data:

- The reference for actual data is also grass, but this is sourced from a different inverter than the albedo boosters in the field. This is important as each inverter might perform differently due to varying irradiance or string configurations.
- The gain formula is the same as the simulated case, but a slightly higher MPPT power threshold (700 W) is used before filtering, to account for the field-based variability.
- The same threshold logic is applied, setting gains to 0 if the conditions are met.
- The final results are organized in a DataFrame, similarly replacing NaNs with 0.

### Sky Classification and Gain DataFrames:

The gain calculations are performed for the entire dataset and also separately for the clear-sky and diffused-sky classified days. This allows us to analyze the performance improvements of albedo boosters under different sky conditions:

- df_simulated_gain, df_actual_gain - Complete dataset
- df_simulated_gain_sunny, df_actual_gain_sunny - Clear-sky days
- df_simulated_gain_diffused, df_actual_gain_diffused - Diffused-sky days

### Smoothening the Actual Gain Data

The next step is to smooth the actual gain time series for better trend analysis. This is particularly important because the grass reference is from a different inverter, so transient spikes and drops can appear in the actual gain, not necessarily due to albedo changes but because of inherent inverter behavior. Further, The albedo boosters also collected a lot of debris and dirt over the installation period which could significantly affect the behavior of the rear irradiation and subsequently cause some erratic patterns.

To mitigate this, we apply a rolling average window (4-time steps) to smooth out these fluctuations and make the comparison with simulations more meaningful. The rolling average works by taking the average of a defined number of consecutive data points centered around each timestamp. In our case, with a window size of 4 and center alignment, each point is smoothed by averaging its own value along with the two preceding and one following points. Mathematically, the smoothed gain at time t, represented as $G_{smooth}(t)$, is calculated as:

$$G_{smooth}(t) = \frac{1}{N}\sum_{i=-1}^{2} G(t+i)$$

where G(t) represents the gain at time t, and N is the number of valid points within the window. At the boundaries of the dataset, the window adjusts dynamically to include only

the available points. This smoothing process reduces sharp noise and transient fluctuations, making the trend in the gain data more apparent and improving the reliability of comparisons against simulation outputs.

Additionally, we adjust the smoothed curve:

- For each day, we detect non-zero power production and set the gain to 0 before the first valid reading and after the last valid reading.
- This ensures that only valid production times are considered, avoiding artificial gain spikes during early morning or late evening when production is effectively zero.

We generate the smoothed gains for:

- The complete dataset
- Clear-sky days
- Diffused-sky days

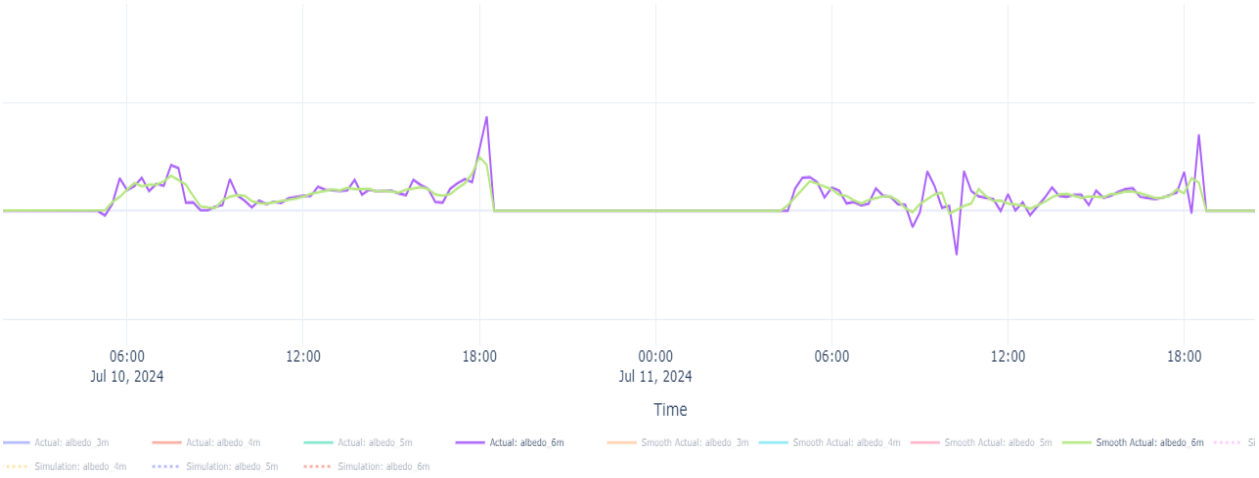


*Figure 33 Smooth (green) vs Actual Inverter gains (violet)*

We can use these gain datasets to plot time-series graphs and analyze the gain yields for each scenario under different sky conditions.

### 3.5.7. Gain Yield Calculation

To evaluate the actual performance boost provided by the albedo boosters, we calculate the gain yield for each scenario compared to the grass reference. Unlike individual scenario yields, the gain yield focuses specifically on the boost effect from the albedo sheets, normalizing the results against the grass scenario for both simulation and actual measurements.

## Why Gain Yield Instead of Absolute Yield?

- In field data, each inverter's MPPT behavior can differ slightly even under similar conditions.
- There is also AC power clipping that can affect the absolute yield measurement.
- By comparing relative gains against the same reference (grass), we cancel out individual inverter differences and clipping effects, providing a more standardized view of the booster impact.

## Procedure

1. Select the Time Window: The function allows you to specify a time range for the analysis. If not provided, it defaults to the entire dataset range. We will analyze for the date range where the albedo boosters were installed at the site.
2. Data Filtering: Both Sunsolve simulation data and field inverter data are filtered to match the specified date range.
3. Define Scenarios: The scenarios considered for analysis are:
    - Grass (baseline reference)
    - Albedo 3m, 4m, 5m, and 6m
4. Calculate Energy Yield (kWh): For each scenario, the energy yield is computed using the MPPT power values and the time step duration (15-minute intervals = 0.25 hours):

$$1000E_{\text{kWh}} = \frac{\sum(P_{\text{MPPT}} \times \Delta t)}{1000}$$

where $P_{\text{MPPT}}$ is the MPPT power in watts, and $\Delta t$ is the time step in hours.

5. Compute Gain Percentage The yield for each scenario is compared to the grass reference to find the gain percentage:

$$\text{Gain (\%)} = \frac{(E_{\text{Scenario}} - E_{\text{Grass}})}{E_{\text{Grass}}} \times 100$$

This is done separately for simulated and actual data.

6. Calculate Error Percentage: The difference between the simulated gain and the actual gain is recorded as the absolute error percentage:

$$\text{Absolute Error (\%)} = \text{Simulated Gain (\%)} - \text{Actual Gain (\%)}$$

7. Organize Results into a Table: All calculated values are stored in a structured table with the following columns:
    - Scenario
    - Actual Energy (kWh)
    - Simulated Energy (kWh)

- Actual Gain % vs Grass
- Simulated Gain % vs Grass
- Absolute Error %

### Result Overview

The final DataFrame, gain_yield_table, neatly presents:

- The total energy produced for each scenario,
- The percentage gains over the grass reference,
- And the deviation between simulated and actual performance.

This allows us to clearly compare the effectiveness of the albedo boosters in both simulated conditions and real-world performance.

## 3.5.8. Absolute Yield Calculation with Clipping Adjustment

In this step, we shift our focus to calculating the absolute yields for each scenario, comparing the actual measured yields against the simulated Sunsolve yields, mainly for the time-period when albedo boosters were installed at the site. However, there is a crucial difference between the two datasets:

- The actual inverters have a known AC power clipping limit of 215 kW (which is about 25.7 kW per MPPT).
- In the simulations, this clipping effect is not naturally represented, leading to an overestimation of power during high irradiance periods.

Therefore, we first apply clipping adjustments to the simulated MPPT data before calculating the yields to create a fair comparison.

### Clipping Adjustment for Simulated Data

The following steps were taken to account for clipping in the Sunsolve simulation data:

1. We define the clipping threshold and the target compression range: Clipping starts at 25.7 kW for each MPPT, and the values are linearly mapped to a range between 25.7 kW and 26.5 kW.
2. For each MPPT scenario (grass, albedo_3m, albedo_4m, albedo_5m, and albedo_6m), the code identifies all values exceeding the threshold.
3. If clipping is detected, it calculates the actual minimum and maximum values of the over-threshold points. These values are linearly scaled down to fit within the specified range, mimicking real-world inverter clipping behavior.

4. Finally, the adjusted values are written back into a new DataFrame (Sunsolve_data_clipped), ensuring the clipping effect is represented in the simulation data.

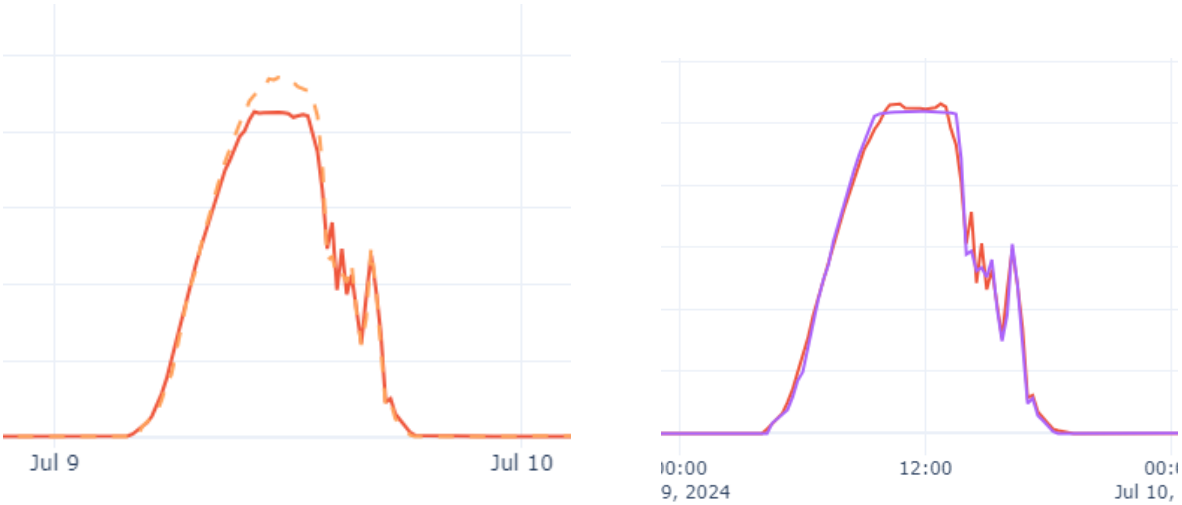


*Figure 34 Actual Inverter data vs Unclipped(left) and Clipped(right) Simulation Data*

We do this way instead of direct clipping at a fixed value to better simulate the actual MPPT clipping of the inverters which can vary depending on values of the other MPPTs of the inverter.

## Absolute Yield Calculation

Once clipping is applied, we move on to calculate the absolute yields for both the actual inverter data and the clipped Sunsolve simulation data. The process is as follows:

1. Filter the Data: The data is filtered to match the specified time range (2024-06-13 to 2024-07-15). This ensures we are analyzing yields only during the booster installation period.
2. Energy Yield Calculation: For each scenario:
    - The MPPT power values are multiplied by the time interval (15 minutes or 0.25 hours).
    - The total energy is then summed and converted to kWh.

$$E_{kWh} = \frac{\sum(P_{MPPT} \times \Delta t)}{1000}$$

where $P_{MPPT}$ is the power in watts, and $\Delta t$ is the time step in hours.

3. Baseline (Grass) Reference: The absolute energy yield for grass is used as the reference for calculating percentage errors.
4. Error Calculation: The absolute yield differences between the simulated and actual data are calculated for each scenario:

$$\text{Error (\%)} = \frac{(\text{Simulated Yield} - \text{Actual Yield})}{\text{Actual Yield}} \times 100$$

This metric helps us understand how well the simulations align with real-world performance.

5. Organize into a DataFrame: All the results are compiled into a structured table (yield_summary) with the following columns:
    - Actual Yield (kWh) - Field-measured energy for each scenario.
    - Simulated Yield (kWh) - Clipped Sunsolve simulation energy.
    - Error Percentage (%) - Difference between the two.

### 3.5.9. Error Metrics for Validation and Analysis

Now we move on to defining the error metrics used for the validation and comparison of simulated and actual datasets. These metrics are crucial for quantifying the accuracy and reliability of the Sunsolve simulation outputs against the measured field data across different albedo booster configurations. The error metrics allow for detailed analysis under different sky conditions- diffuse, sunny, and mixed days, enabling us to understand the performance of the model under varying irradiance scenarios.

The following error metrics are used for evaluation:

#### 1. Root Mean Square Error (RMSE)

The Root Mean Square Error (RMSE) is a standard measure of the average magnitude of the error between predicted (simulated) and observed (actual) values. It is calculated as the square root of the mean of the squared differences: [66]

$$\text{RMSE} = \sqrt{\frac{1}{n}\sum_{i=1}^{n}(S_i - A_i)^2}$$

Where:

- Si – Simulated MPPT power for each time step
- Ai – Actual MPPT power for each time step
- n – Number of time steps

*Interpretation:*

- Lower RMSE values indicate better agreement between the simulation and the actual data.
- Since errors are squared, large deviations are penalized more heavily, making RMSE sensitive to outliers.

## 2. Symmetric Mean Absolute Percentage Error (SMAPE)

Symmetric Mean Absolute Percentage Error (SMAPE) measures the average magnitude of absolute errors in percentage terms, relative to the average of actual and simulated values. Unlike traditional MAPE, SMAPE is symmetric and bounded, making it more reliable when handling values near zero: [67]

$$\text{SMAPE} = \frac{100}{n}\sum_{i=1}^{n}\frac{|S_i - A_i|}{(|S_i| + |A_i|)/2}$$

*Interpretation:*

- Lower SMAPE indicates better model performance.
- It is particularly useful when the magnitude of values is low, as it normalizes errors by the average of actual and simulated values.

## 3. Coefficient of Determination ($R^2$ Score)

The Coefficient of Determination, or R2R^2R2, indicates how well the simulated values approximate the actual data. It is defined as: [68]

$$R^2 = 1 - \frac{\sum_{i=1}^{n}(A_i - S_i)^2}{\sum_{i=1}^{n}(A_i - \bar{A})^2}$$

Where:

- Si – Simulated MPPT power
- Ai – Actual MPPT power
- $\bar{A}$ – Mean of actual MPPT power

*Interpretation:*

- An $R^2$ value of 1 indicates a perfect fit.
- Values closer to 1 imply high predictive accuracy, while values near 0 indicate poor performance.
- Negative values can occur when the model is worse than a simple average.

## 4. Relative Mean Bias Error (RMBE)

The Relative Mean Bias Error (RMBE) measures the average bias between the simulated and actual values, expressed as a percentage of the actual average: [69]

$$\text{RMBE} = \frac{\sum_{i=1}^{n}(S_i - A_i)}{\sum_{i=1}^{n} A_i} \times 100$$

*Interpretation:*

- Positive RMBE indicates the model overestimates power generation.
- Negative RMBE indicates underestimation.
- Ideally, RMBE should be close to 0, reflecting unbiased predictions.

# 4. Observations and Baseline Analysis

## 4.1. Site Weather Characteristics During Study Period

The study was conducted at a ground-mounted photovoltaic (PV) system site in France, with data collected from January 1 to September 30, 2024. The albedo boosters were installed between June 13 and July 15, 2024. This period corresponds to the summer months, characterized by longer daylight hours and higher solar irradiance, which are conducive to PV performance. We would have preferred a much longer dataset to obtain more reliable results. However, we could install the albedo test set-up only for this period due to site and client restrictions.

Temperature and Humidity: During June and July, the site experienced average high temperatures ranging from approximately 21.8°C to 24.5°C, with average lows between 11.6°C and 13.8°C. Relative humidity levels were moderate, averaging around 82% in June and 76% in July. These conditions are typical for the region during summer and are favorable for PV system operation. [70]

Precipitation and Cloud Cover: Precipitation during the installation period was moderate, with June receiving about 67 mm of rainfall over 18.4 days, and July receiving approximately 52 mm over 16.7 days. Cloud cover was relatively low, contributing to increased solar irradiance reaching the PV panels. [71]

Solar Irradiance: The period from mid-June to mid-July falls within the peak solar irradiance season for the region. Average daily incident shortwave solar energy during this time was approximately 6.7 to 6.8 $kWh/m^2$. This high level of solar energy availability is ideal for assessing the performance impact of albedo boosters. [72]

Wind Conditions: Average wind speeds during June and July were moderate, around 11.3 km/h. Such wind conditions are generally favorable for PV systems, as they can aid in cooling the panels, potentially improving efficiency. [72]

Implications for Albedo Booster Performance: The installation period's weather conditions, characterized by high solar irradiance, moderate temperatures, and low precipitation, provided an optimal environment for evaluating the effectiveness of albedo boosters. The ground-mounted system, initially installed over grass, benefited from the increased reflectivity introduced by the albedo boosters, potentially enhancing the bifacial PV modules' performance.

In summary, the favorable weather conditions during the albedo booster installation period were conducive to maximizing the potential benefits of increased ground albedo, thereby providing a reliable basis for assessing their impact on PV system performance.

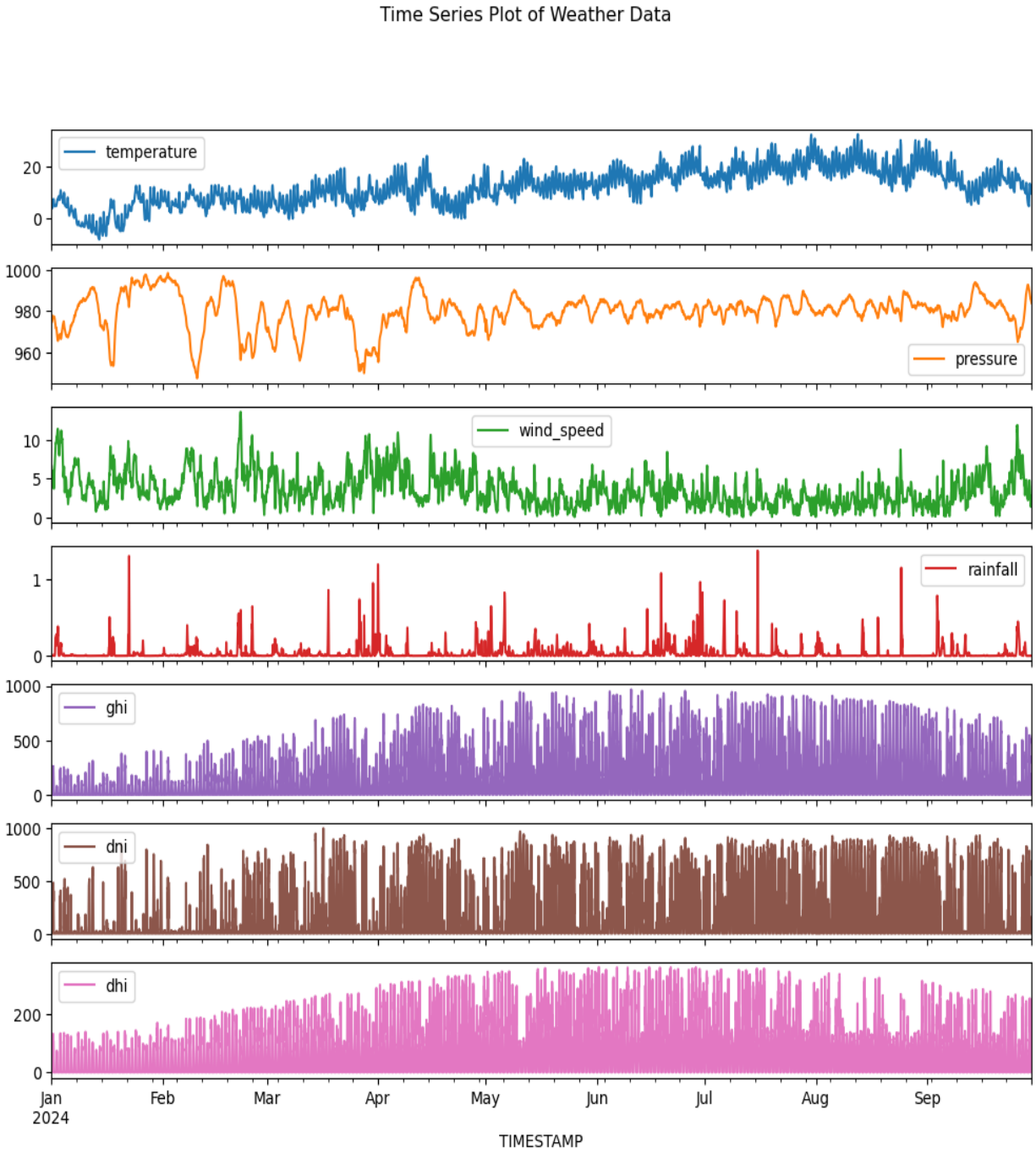


*Figure 35 Weather Data Overview*

## 4.2. Trends in Sunsolve and Field Results

Examining the Sunsolve simulation data alongside actual inverter measurements provide valuable insights into the performance of the bifacial PV system under different albedo booster configurations. By plotting the MPPT power outputs of each scenario (grass, albedo_3m, albedo_4m, albedo_5m, and albedo_6m) against the corresponding weather data, particularly Global Horizontal Irradiance (GHI), several important trends can be observed consistently in both Sunsolve simulations and field results.

### 4.2.1. Correlation Between GHI and MPPT Power Outputs

One of the first and most evident observations is the strong correlation between GHI and the MPPT power outputs for all scenarios, both in Sunsolve simulations and the actual field data. This close alignment occurs because Sunsolve's simulation engine is based on detailed ray-tracing and transposition models that account for both direct and diffuse components of solar irradiance, while the field results naturally respond to real-time irradiance conditions.

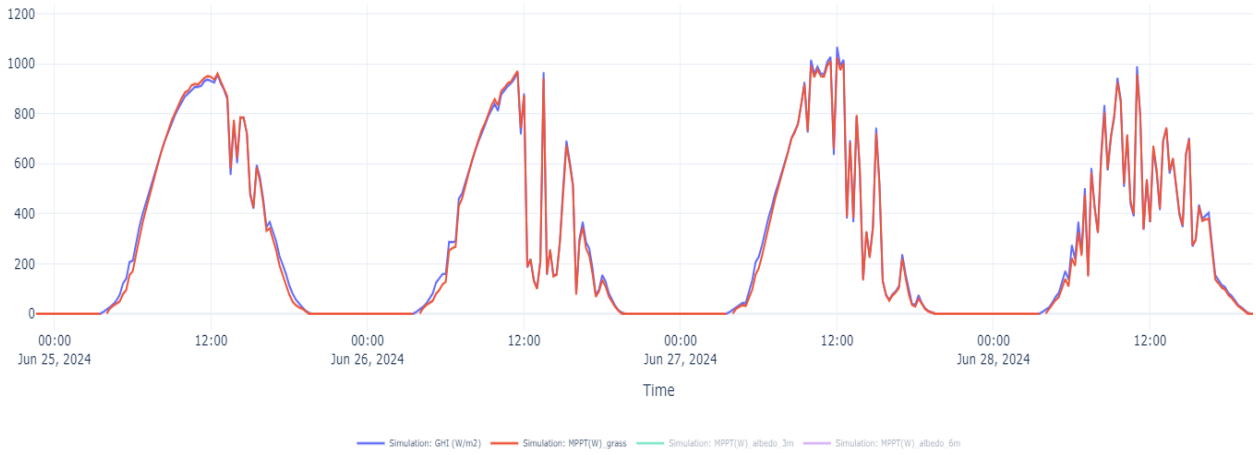


*Figure 36 Field GHI and MPPT Power*

GHI represents the sum of both direct and diffuse sunlight striking a horizontal surface, which directly influences the total energy available for PV generation. Sunsolve's simulation algorithms utilize the Perez model for diffuse transposition and detailed ray-tracing to account for the interactions of light with reflective surfaces and shading elements. As the GHI increases, more photons are available for energy conversion, directly boosting the power output of the MPPTs. This relationship is mirrored in the field results, where the inverters similarly respond to higher irradiance levels with increased power production. Conversely, during cloudy or low-irradiance periods, the reduction in GHI is reflected in both the simulated and actual MPPT outputs. This direct relationship is a fundamental characteristic of PV systems and is well-modeled by Sunsolve's physics-based simulation environment, validated by real-world inverter measurements.

### 4.2.2. Increased MPPT Power with Larger Albedo Boosters

A second critical observation is that the magnitudes of the MPPT power outputs increase progressively with the width of the albedo boosters in both Sunsolve simulations and the actual inverter data. The scenarios consistently show a clear hierarchy in power production:

- Grass < Albedo 3m < Albedo 4m < Albedo 5m < Albedo 6m

This trend is expected, as wider albedo boosters enhance the reflective surface area beneath the bifacial modules, allowing for greater rear-side irradiation. In Sunsolve, albedo effects are simulated through backward ray-tracing, where reflected light from the ground surface is mapped onto the rear side of the bifacial panels. This increase in rear-side illumination results in more electrical power generation, which is similarly captured in the actual inverter outputs.

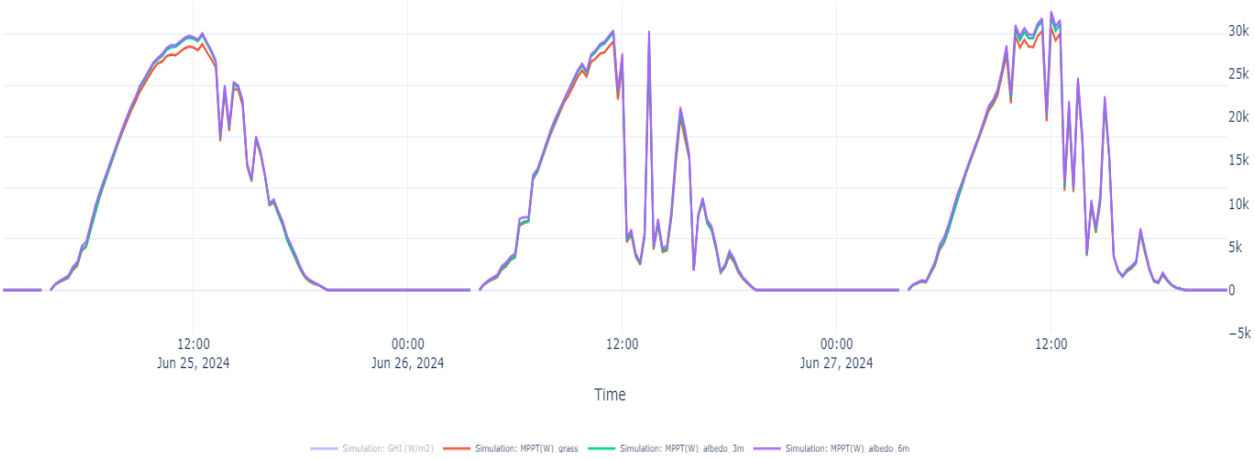


*Figure 37 Albedo Boosters MPPT Power Graph*

Larger booster widths increase the solid angle of reflected light, thereby capturing more diffused and direct sunlight, which is then converted into additional electrical power. This effect is observable not only in the simulation environment but also in real field performance, indicating that the albedo boosters are effectively enhancing bifacial gains as designed. The consistent reflection of this trend in both datasets underscores the reliability of Sunsolve's modeling for rear-side enhancements.

### 4.2.3. Greater MPPT Gain Differences During Diffuse Days

One of the key observations is that the MPPT gain differences between the albedo booster scenarios are more pronounced during diffuse days compared to sunny days. This trend is evident in both Sunsolve simulations and actual inverter data. The primary reason for this behavior lies in the nature of diffuse irradiance and its interaction with the albedo booster sheets.

On diffuse days, sunlight is scattered uniformly across the sky dome, leading to a more isotropic distribution of light. This uniform scattering increases the angular spread at which light reaches the ground surface, thereby enhancing the effectiveness of ground-based reflectors like the albedo booster sheets. Since these reflective surfaces have a much higher albedo than grass, the relative boost in rear-side irradiation is more significant when sunlight is diffused rather than concentrated in a direct beam.

Sunsolve's transposition model effectively captures this scattering effect, allowing it to simulate the increased light availability on the rear side of the bifacial panels during overcast or cloudy conditions. This is confirmed by the field measurements, where MPPT gain values show a marked separation between albedo scenarios under diffuse conditions. The difference in gain is not as prominent during sunny days because direct beam irradiance dominates the incident energy, and the albedo reflection contributes comparatively less to the overall energy yield. In contrast, during diffuse conditions, the widespread angular distribution of light enables the albedo boosters to reflect more light onto the rear surface, thereby enhancing the bifacial gain.

The consistency of these trends across both Sunsolve simulations and the actual inverter data demonstrates the accuracy of the simulation models and the effective contribution of albedo boosters to bifacial energy gains. These findings provide confidence in using Sunsolve as a reliable tool for predicting bifacial performance under variable sky conditions.

### 4.2.4. Actual Weather Data vs. Satellite Weather Data

Upon comparing the actual weather data collected on-site with satellite-derived weather data, several notable differences emerge, particularly in the variability and smoothness of the recorded irradiance values.

Higher Variability in Ground-Based Measurements: The ground-based measurements of Global Horizontal Irradiance (GHI), Diffuse Horizontal Irradiance (DHI), and Direct Normal Irradiance (DNI) exhibit significant short-term fluctuations. These fluctuations are primarily due to the sensors' ability to capture rapid changes in local atmospheric conditions, such as transient cloud cover, aerosol concentrations, and other microclimatic factors. Ground-based instruments provide high temporal resolution data, often recording measurements at intervals as short as one minute, allowing for the detection of these rapid changes.

Smoother Satellite-Derived Data: In contrast, satellite-derived weather data tend to present smoother irradiance profiles with less pronounced short-term variability. This smoothing effect arises from several factors:

- Spatial Averaging: Satellites capture data over large geographical areas, leading to an averaging effect that smooths out localized variations. This spatial resolution

limitation means that small-scale atmospheric phenomena may not be detected in satellite data. [73]

- Temporal Resolution: Satellite observations are typically made at fixed intervals, which may not coincide with rapid changes in atmospheric conditions. As a result, transient events like passing clouds may be underrepresented or missed entirely.
- Data Processing and Smoothing Algorithms: Satellite data often undergo processing that includes the application of smoothing algorithms to reduce noise and fill gaps. These algorithms, such as Fourier transformation and Whittaker smoothing, are designed to highlight long-term trends but can suppress short-term variability .[74]

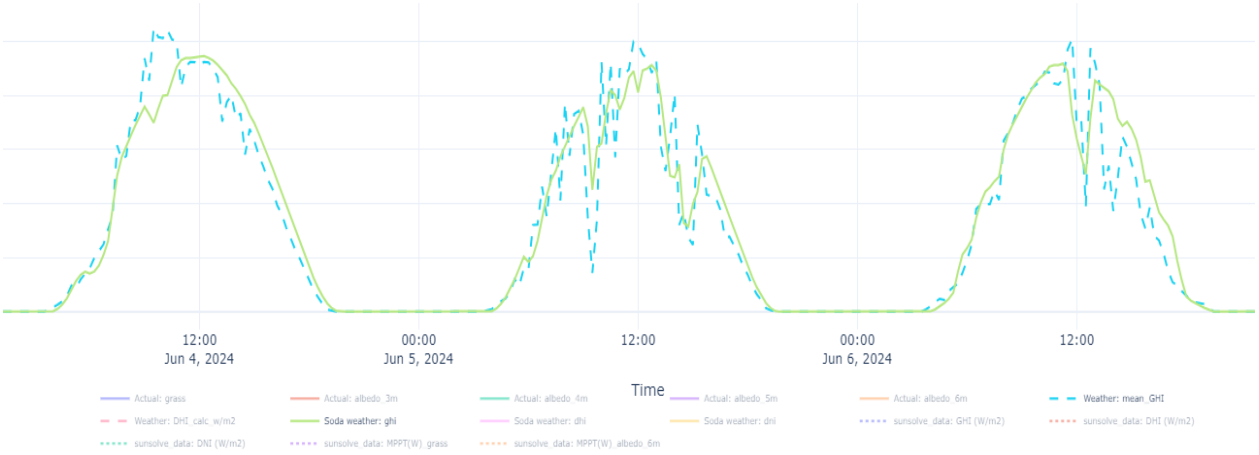


*Figure 38 Actual vs Satellite Weather Data*

Implications for Data Comparison and Validation: Despite these differences, the overall patterns and trends observed in both datasets are generally consistent. This consistency provides a level of validation for the satellite data's accuracy in representing broader climatic conditions. However, for applications requiring high temporal resolution and sensitivity to local atmospheric changes, such as the performance analysis of photovoltaic systems, ground-based measurements offer a more detailed and accurate representation of the actual conditions experienced by the system. Because of this, we chose to move forward with Field weather data for all further analysis and comparisons.

# 5. Results and Analysis

## 5.1. Simulated vs. Actual MPPT Results

In our comparative analysis of simulated and actual MPPT power outputs, we opted to utilize the site-specific weather data for all subsequent simulations and evaluations. This decision was driven by the observation that satellite-derived weather data, while consistent, exhibited significantly smoother irradiance profiles compared to the high-resolution, ground-based measurements obtained on-site. The smoothing inherent in satellite data often fails to capture the rapid fluctuations caused by transient cloud cover and other microclimatic factors, which are critical for accurate modeling of photovoltaic (PV) system performance.

Sunsolve's simulation engine, which heavily relies on Global Horizontal Irradiance (GHI) inputs, demonstrated a strong correlation between GHI and MPPT power outputs. Consequently, the absence of high-frequency irradiance variations in satellite data led to discrepancies in simulated power patterns, particularly during periods of rapid weather changes. Moreover, the actual inverters on-site are subject to power clipping, with a threshold around 26,000 W per MPPT. This clipping effect, not accounted for in the simulations, further accentuated the differences between simulated and actual power outputs when using satellite data.

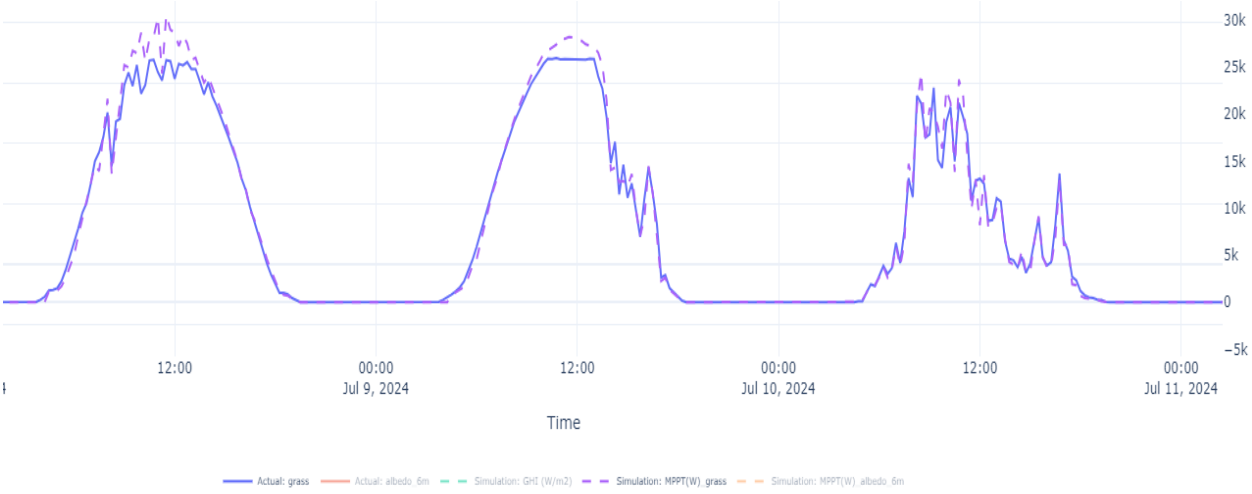


*Figure 39 Simulation vs Actual MPPT Results*

### Comparative Analysis of Simulated and Actual MPPT Power Results

Upon comparing the Sunsolve simulations driven by site-specific weather data against the actual inverter MPPT outputs, several key observations emerged:

1. Alignment in Diurnal Power Patterns: Both simulated and actual datasets exhibited similar daily power generation patterns, reflecting the system's response to the solar

cycle. This alignment indicates that the simulations effectively captured the overall behavior of the PV system under varying irradiance conditions.

2. Discrepancies Due to Clipping: The simulations, not constrained by inverter clipping limits, occasionally projected MPPT power values exceeding the 26,000 W threshold observed in actual inverter outputs. This overestimation is expected, as the simulations model the theoretical maximum power output without considering hardware limitations.
3. Variations in Generation Start and End Times: Minor discrepancies were noted in the initiation and cessation times of power generation, with simulations sometimes starting or ending 15 to 30 minutes earlier or later than the actual data. These variations, corresponding to one or two timestamp differences, were deemed negligible in the context of overall energy yield, as power generation during these periods is minimal.
4. Influence of Inverter Variability on MPPT Outputs: A noteworthy observation was the slight variation in instantaneous power patterns among different albedo booster scenarios (3m, 4m, 5m, and 6m sheets) in the actual data. While simulations maintained consistent base parameters across scenarios, akin to identical MPPTs within the same inverter, the actual data reflected subtle differences. This variation is attributed to the fact that each albedo booster scenario was connected to a different inverter. Even among inverters of the same brand and capacity, variations in MPPT algorithms, firmware versions, and hardware tolerances can lead to differences in power tracking behavior. Additionally, environmental factors such as localized cloud cover and shading can differentially impact inverters based on their physical location and the specific strings connected to them.

## 5.2. Simulated vs. Actual Gain Time Series Comparison

The analysis of gain time series for the different albedo booster scenarios, Albedo 3m, Albedo 4m, Albedo 5m, and Albedo 6m, using the grass scenario as the reference provides significant insights into the reflective enhancements introduced by the booster sheets. Absolute values of gain time series presented in this section are omitted for confidentiality reasons.

### Performance Before and During Albedo Booster Installation

Albedo boosters were installed at the site from June 13, 2024, to July 15, 2024. Before the installation period, the gain time series across all scenarios (3m, 4m, 5m, and 6m) showed no clear distinction. The gains appeared to be primarily influenced by the behavior of individual MPPTs associated with the different inverters rather than any reflective boost. Variability in MPPT outputs across different inverters led to fluctuations where, on some

days, certain inverter setups showed higher power compared to the grass reference, and on other days, they showed lower power. This variability is typical when different inverter MPPTs, exposed to distinct cloud patterns and string configurations, are compared without any engineered reflective surface.

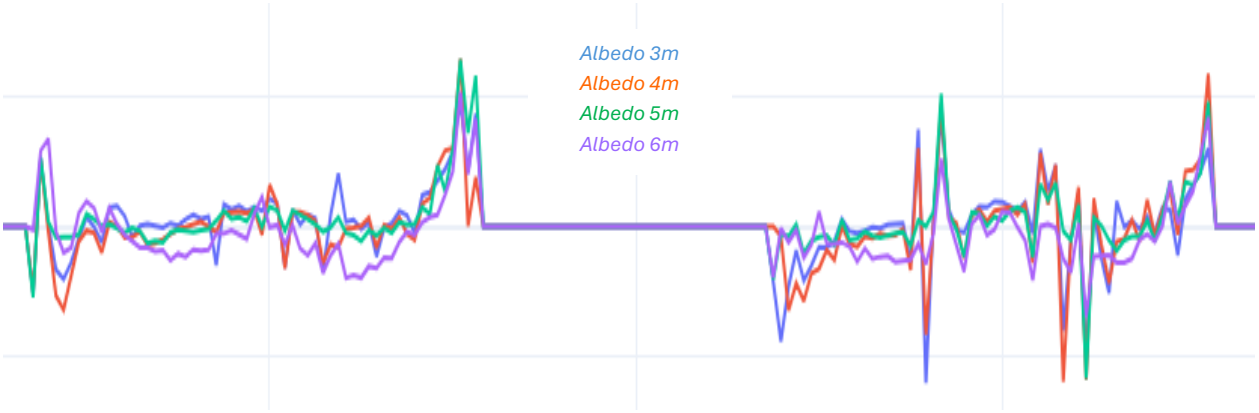


*Figure 40 Inverter gains before Booster Installation for different Booster Scenarios*

We notice from Figure 40 that the gains even below zero quite a lot signifying that the albedo booster inverter's power is going lower than the grass reference inverter's power for many instances.

During the installation period of the albedo boosters, the gains for the various scenarios became distinctly visible. Each albedo scenario demonstrated measurable improvements over the grass reference, with the magnitude of the gains increasing with the booster width:

$$\text{Grass} < \text{Albedo 3m} < \text{Albedo 4m} < \text{Albedo 5m} < \text{Albedo 6m}$$


*Figure 41 Inverter gains after booster installation*

From Figure 41, it's observed that the gains now don't go negative as much as they did before the installation of the boosters.

This validated the efficacy of the albedo booster sheets in enhancing rear-side irradiance, translating directly to increased MPPT power generation. The structured reflectivity of the booster sheets redirected additional light to the bifacial panels, thus confirming their role in boosting energy capture, especially under diffuse conditions.

### Smoothening of Actual Gain Time Series

The actual gain time series exhibited high-frequency fluctuations compared to the simulation outputs. These fluctuations were primarily driven by variations in the behavior of the different inverters associated with each scenario. To address this and facilitate better comparison, we applied a smoothening algorithm to the actual gain time series. This approach helped in aligning the general trends and allowed for more meaningful comparisons with Sunsolve's simulation gains.

On comparing the smoothed actual gains with the simulated gains, the general patterns aligned well; however, specific discrepancies were observed:

- Early morning and late evening deviations: During these low-irradiance periods, even small differences in power output led to large deviations in percentage gain due to the low baseline power levels. For instance, a minor change of 2–3 W during these hours resulted in noticeable percentage shifts in gain.
- Hardware-related fluctuations: Occasionally, the inverters displayed non-typical behavior due to hardware inconsistencies or environmental interferences, further impacting the actual gain percentages. Despite these instances, the overall trends of simulated and actual gains showed strong correlation.

*Figure 42 Smoothened(red) and Actual(green) Gains for Albedo 5-sheets*

### Sunrise and Sunset Gain Patterns

Both the simulated and actual gain time series demonstrated notable spikes during sunrise and sunset periods. This trend is attributed to the lower sun angles during these times, allowing more light to be captured and reflected onto the rear side of the bifacial panels. With the albedo boosters in place, the oblique sunlight is effectively redirected, enhancing rear-side generation.

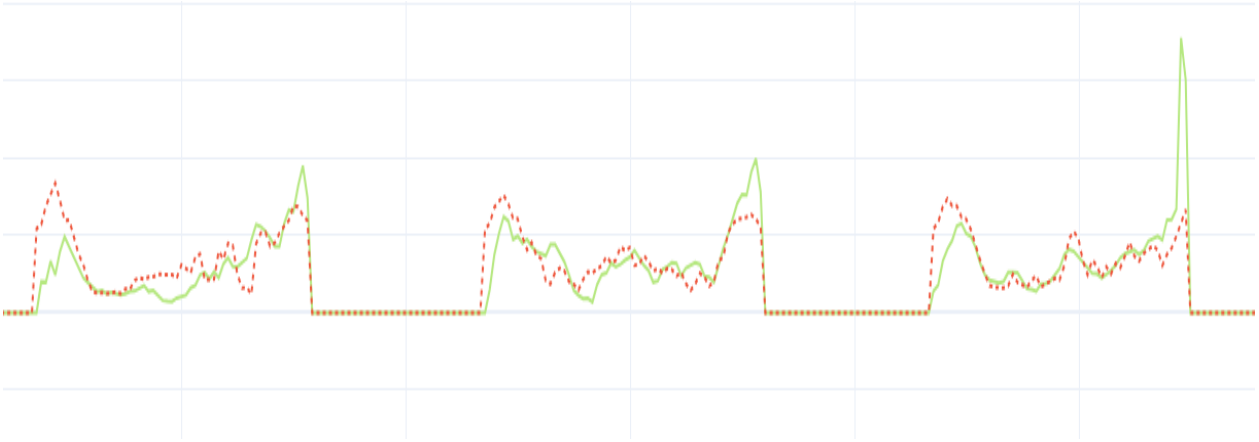

*Figure 43 Edge effect on Actual Inverter Gains (green) compared to simulated*

Interestingly, the actual gain series showed even higher magnitudes during sunset periods. This was primarily due to the edge effect of the installed panel setup. The MPPTs used for our albedo booster set up was part of the edge panel tables. The west side of these panel tables were clear, allowing for greater unimpeded reflection in the evening when sunlight entered at shallow angles. This phenomenon could not be entirely captured in Sunsolve simulations, as its models assume symmetrical panel layouts without specific edge configurations.

### Sunny vs. Diffuse Days

The gain behavior varied notably between sunny and diffuse days:

- Sunny Days: During peak sun hours, the gain reduced slightly, as the direct beam component dominated, and the relative effect of albedo reflection was less impactful. The larger reflective area of the boosters primarily benefited sunrise and sunset periods, where low-angle sunlight was more effectively redirected to the rear side.

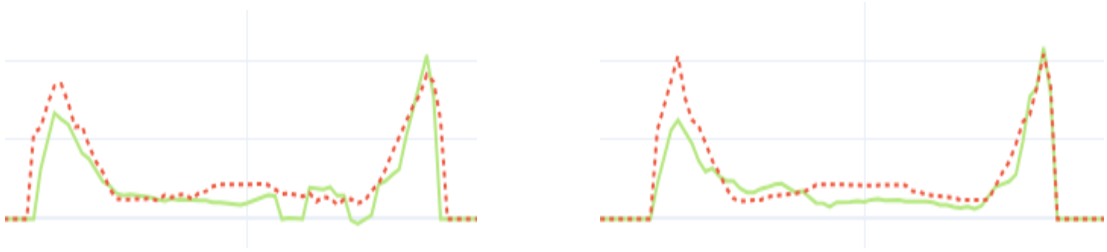

*Figure 44 Gain Pattern for Sunny Days. Simulated (red) vs Actual (green)*

- Diffuse Days: Gains remained more consistent throughout the day. Unlike sunny days, the diffuse irradiance is scattered evenly across the sky, leading to stable rear-side illumination and less dramatic variation between peak and non-peak hours. Notably, the actual gains still demonstrated slight increases during sunset due to the edge reflection effect not captured in simulations. Since the Gain MPPTs belonged to different inverters, the actual gain behavior was also a bit more erratic during diffused days, most probably due to varying cloud cover and hence the varying front and rear irradiance between the different inverters.

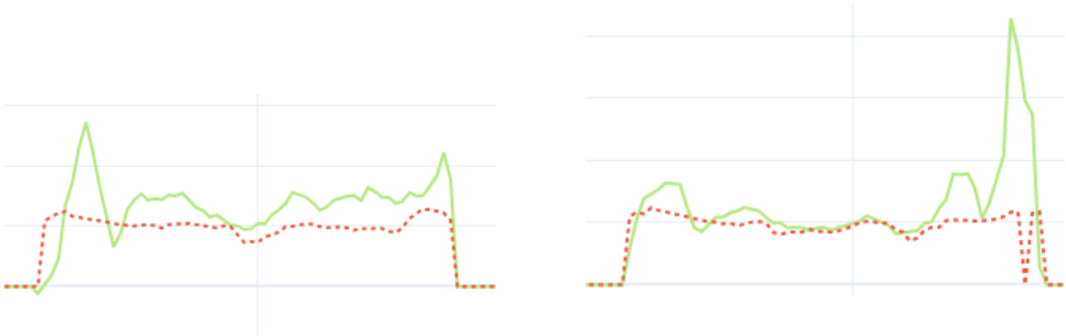

*Figure 45 Gain Pattern for diffused days. Simulated (red) vs Actual (green)*

## Gain Fluctuations Across Different Scenarios

Upon analysis of gain variability across the different albedo booster scenarios, certain trends emerged:

- During sunny days, the gain differences among the various albedo scenarios are relatively minimal, particularly during peak sunlight hours. This is primarily because the direct beam component dominates during these periods, and the influence of ground reflectance is less pronounced compared to the sheer magnitude of direct irradiance striking the module surfaces. However, the gain differences become more noticeable during the mornings and evenings when the sun's angle is lower, and the proportion of light interacting with the reflective sheets increases. In these non-peak

hours, the albedo boosters contribute more significantly to rear-side irradiation, causing slight boosts in gain that are otherwise masked during midday when direct irradiance is strongest.

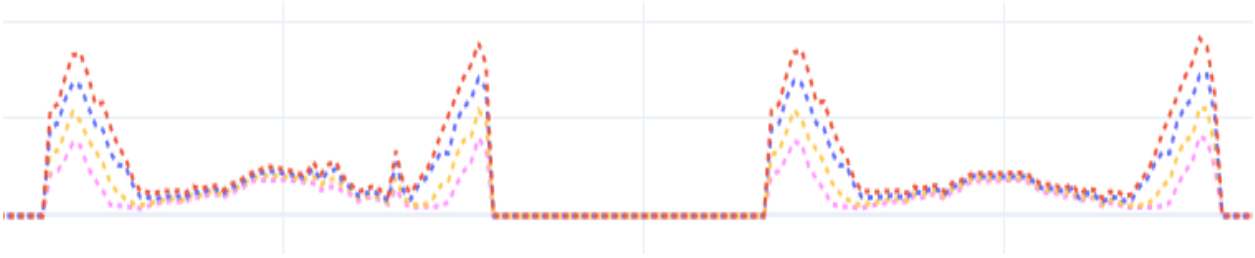

*Figure 46 Simulated Gains for different albedo sheet widths for Sunny days*

- On diffuse days, when sunlight is scattered uniformly across the sky dome, the gain differences between the albedo scenarios become far more significant. Unlike sunny days where direct irradiance overshadows albedo effects, diffuse light strikes the ground reflectors from a multitude of angles, increasing the overall rear-side irradiance captured by the bifacial modules. This omnidirectional scattering allows the high-reflectivity albedo sheets to contribute more consistently and substantially to the total energy yield. As a result, the separation in gains across the 3m, 4m, 5m, and 6m scenarios is much more apparent throughout the day, demonstrating the effectiveness of albedo boosters in enhancing rear-side generation under diffuse sky conditions.

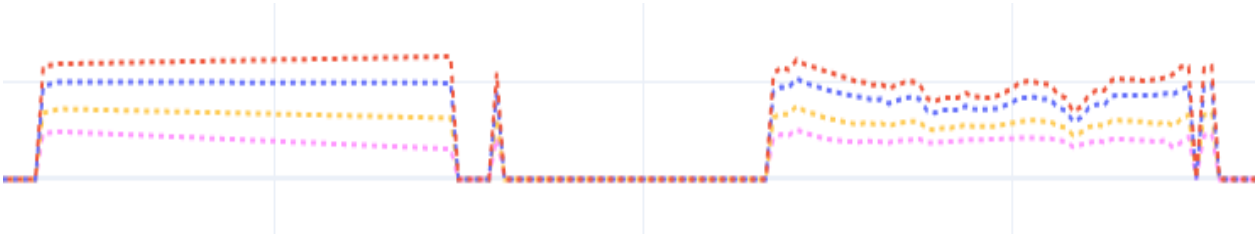

*Figure 47 Simulated Gains for different albedo sheet widths for Diffused days*

- The 6m booster scenario exhibited the least fluctuations in the actual gains compared to its simulation. This was partly because the grass reference inverter (Inverter 8) is geographically closer to the MPPT of the 6m scenario (Inverter 9), leading to more synchronized exposure to cloud cover and irradiance patterns.
- Conversely, the 3m booster scenario showed the highest variability. The MPPT for this configuration (Inverter 14) is located farther from the grass reference inverter, leading to more pronounced differences in irradiance exposure due to varying cloud movement and shadow effects. This spatial separation likely contributed to the intermittent discrepancies in power generation between the grass reference and the 3m scenario, affecting the overall gain patterns.

*Figure 48 Behavior of smoothened gains of Albedo 3m (orange) and albedo 6m (green)*

These observations highlight the impact of inverter placement and environmental interactions on instantaneous gain variability. It also highlights the effectiveness of albedo boosters in enhancing rear-side irradiance, with distinct patterns emerging across sunny, diffuse, and transitional periods. The edge effects observed in the actual data further demonstrate the importance of physical layout in influencing reflective gain, an effect not entirely replicated in Sunsolve's symmetrical simulation environment.

## 5.3. Simulated vs. Actual Gain Scatter Plots

To effectively compare the simulated and actual gain percentages across different albedo scenarios, scatter plots were generated using 15-minute resolution data. However, since the high-frequency nature of actual inverter data often leads to dense and visually cluttered plots, the individual points were made semi-transparent to allow clearer visual interpretation.

Additionally, outliers were filtered to focus the analysis on relevant trends: only data points with actual gain values between −10% and +30% were retained. The extreme values, though relatively few, were mostly attributed to the individual inverter behaviors. Each albedo scenario is mapped to a different inverter located in slightly different physical positions across the site, and each inverter responds independently to cloud dynamics, MPPT configuration, and local shading. These factors occasionally resulted in abnormal gain comparisons that did not reflect the general trend and were thus excluded.

### Scatter Plot Analysis

The scatter plots, once filtered and visualized with transparency, showed distinct and interpretable patterns:

- Each albedo scenario (3 m, 4 m, 5 m, and 6 m) displayed a linear relationship between simulated and actual gain percentages.
- The scenarios with wider albedo boosters appeared progressively higher along the scatter plot axes, aligning with the physical expectation that larger reflective surfaces contribute more to rear-side irradiance and thus enhance overall energy yield.

- Most data points clustered closely around scenario-specific trend lines, indicating a good correlation between simulation and field performance on the 15-minute scale.
- It was also observed that the trend lines had slightly lower slopes compared to the 1:1 (y = x) line, indicating that the actual gain values, while generally in agreement with simulations, often deviated in magnitude.

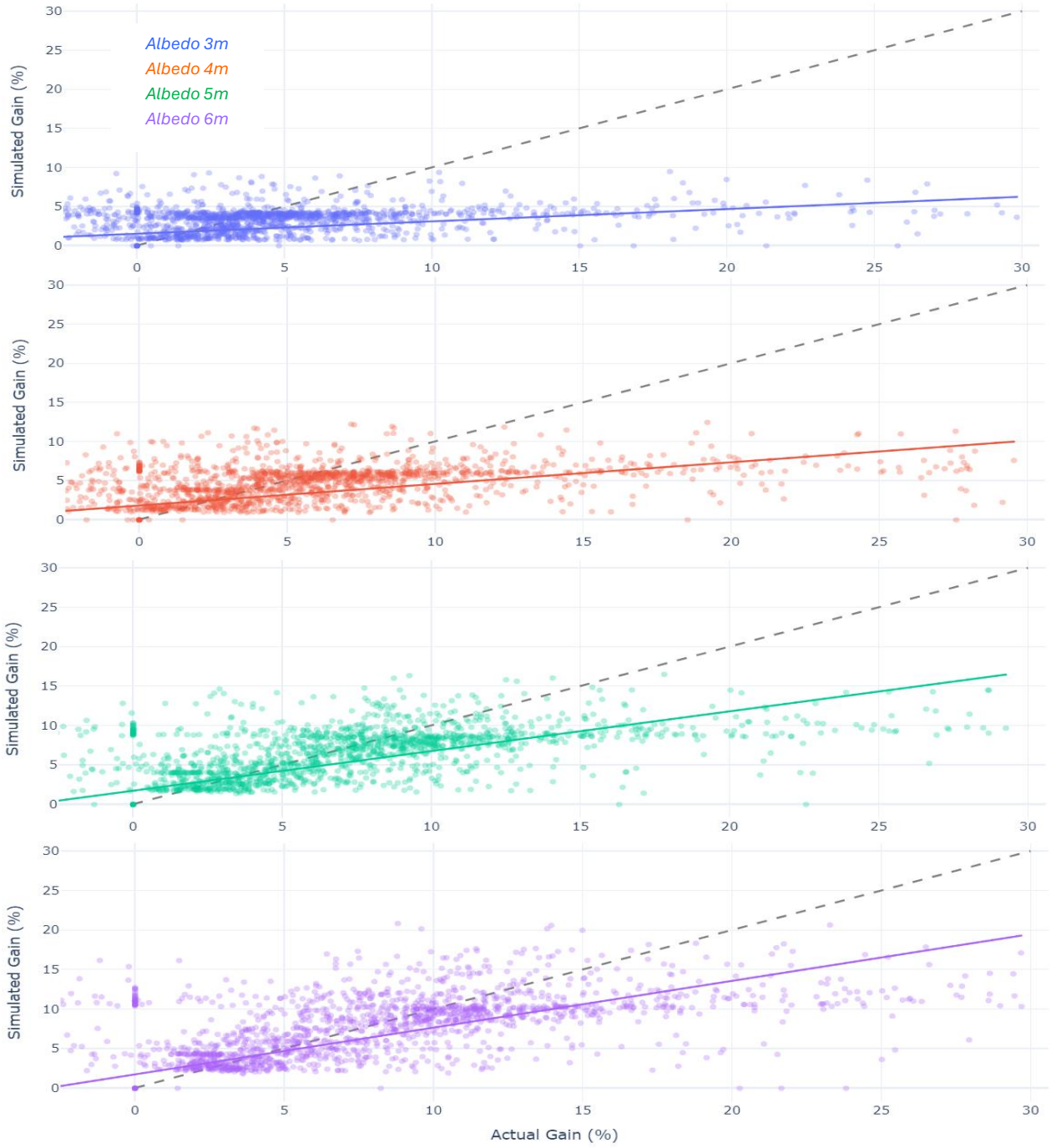


*Figure 49 Albedo Scenarios Scatter Plots*

## Observed Variations and Influencing Factors

Several factors contributed to the differences between simulated and actual gains, particularly to the deviation from the y = x line:

1. Inverter Configuration Differences: The albedo scenarios were assigned to different inverters, each with its own MPPT behavior. These inverters were also located in various parts of the site. As a result, the actual MPPT power output of an albedo-assigned inverter (if it had only grass instead of albedo) could differ significantly from that of the designated grass reference inverter, due to its inherent characteristics and MPPT load. Therefore, the baseline (non-albedo) performance of each inverter would already vary, and the albedo gain is superimposed on that variability. This leads to situations where even with albedo sheets, the inverter's performance could be lower or higher than expected, not because of simulation error, but due to baseline behavioral differences.
2. Spatial Differences Between MPPT Locations: The albedo inverters and the reference grass inverter (Inverter 8) are not co-located. For example, the 3 m scenario (Inverter 14) is placed farther from Inverter 8 than the 6 m scenario (Inverter 9). Consequently, localized irradiance variations, particularly due to passing clouds, impact each inverter differently. This spatial mismatch results in occasional divergence between actual and simulated gain values.
3. Edge Effects in Field Layout: The MPPTs with albedo sheets are generally positioned on edge rows of the array. These rows receive more angled and reflected light, particularly during sunrise and sunset. SunSolve simulations assume symmetric, center-positioned modules, and thus do not account for these edge-enhanced irradiance effects, causing further discrepancy.
4. Outliers Within the Observation Range: A notable outlier occurred on June 16, 2024, when the site inverters were completely offline, resulting in zero actual generation. However, simulations continued to produce output based on modeled irradiance, causing all data points for that day to align vertically along the y-axis. This was an expected anomaly due to operational downtime. Additional minor outliers appeared near the origin (x=0 or y=0), typically during early morning or late evening hours. These instances reflect moments when either the actual or simulated dataset registered near-zero power while the other showed minimal generation, leading to disproportionately high or undefined gain percentages despite very low absolute values.

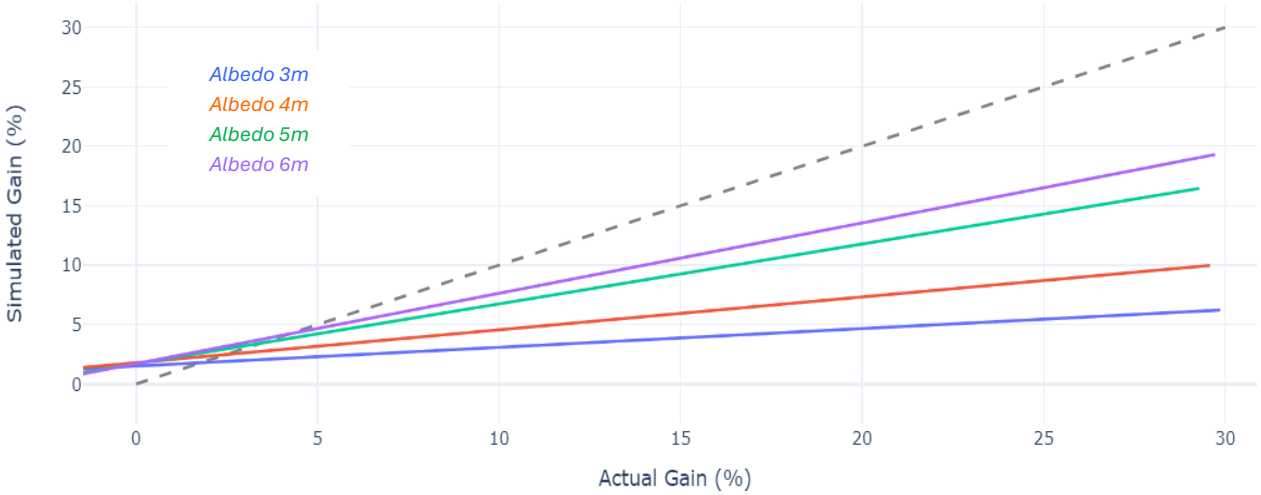


*Figure 50 Trend lines comparison of Albedo Scenario Gains*

The 15-minute scatter plots, with markers and outlier filtering, offered a high-resolution view of the relationship between simulation and real-world performance. The linear trends across scenarios validate the effectiveness of the simulation model. However, the lower-than-unity slope of the trend lines, and cases of actual gains exceeding simulated ones, are primarily explained by inverter-specific behaviors and spatial differences. These findings highlight the need to consider real-world MPPT and inverter heterogeneity when evaluating and validating bifacial simulation models.

## 5.4. Gain Yield Analysis

The Gain Yield Analysis focuses exclusively on the additional energy generation resulting from the installation of albedo booster sheets, using the grass scenario as the baseline reference. By comparing the energy yields of each albedo scenario to that of the grass scenario, we isolate the effect of the reflective sheets, eliminating variations caused by inherent differences in MPPT behavior or inverter configurations. Furthermore, since the analysis is concentrated solely on the added yield from the boosters, clipping effects observed in the actual inverter data are not accounted for. This is a critical distinction, as the clipping limits the maximum output in real conditions, while Sunsolve simulations, unconstrained by such hardware limits, exhibit higher energy yields.

### Analysis of Gain Percentages and Absolute Error

To comply with confidentiality constraints, the analysis is presented graphically. Two separate bar graphs have been generated: one showing actual and simulated energy yield for each scenario, and another displaying the corresponding gain percentages relative to the grass baseline. This allows trends and comparisons to be evaluated without disclosing specific numerical values.

Figure 51 show a clear, consistent increase in both actual and simulated energy as the width of the albedo booster increases, from 3 meters up to 6 meters. This confirms the expected behavior: wider reflective surfaces provide more rear-side irradiance, leading to improved bifacial performance. The gain percentage graph reinforce this trend, showing that both the actual and simulated gains rise proportionally with albedo width. Notably, the simulated gains track the actual values closely, reflecting Sunsolve's effectiveness in modeling the relative impact of albedo boosters, even if it does not replicate field conditions perfectly.

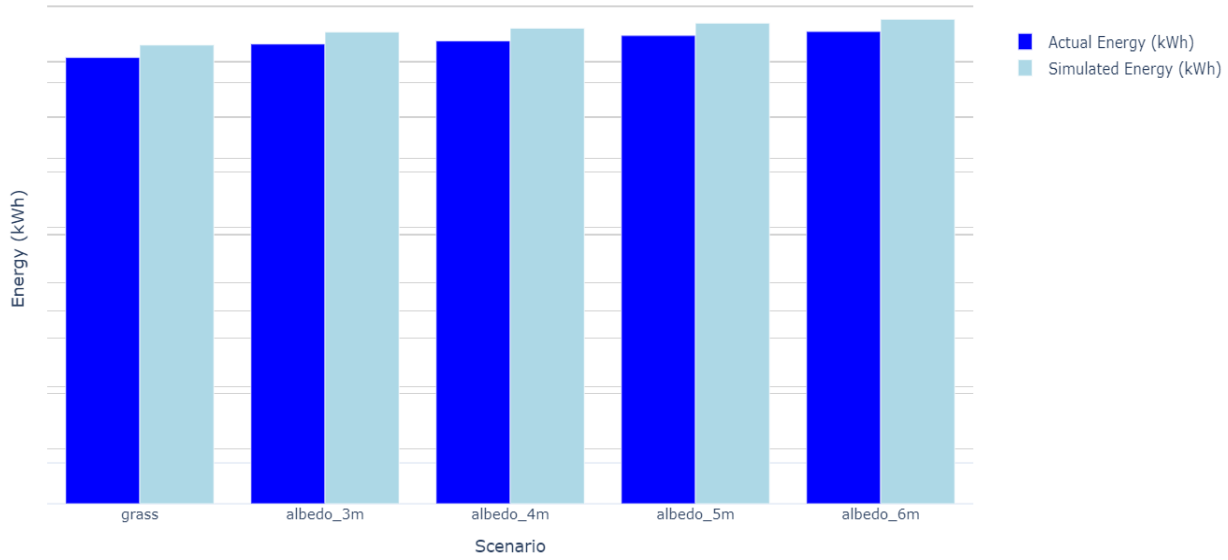


*Figure 51 Actual and Simulated Energy Yield Comparison*

The absolute error between actual and simulated gain is quantified and shown in Figure 52. The Absolute Error % quantifies the difference in percentage points between the actual and simulated gains. Interestingly, the error remains consistently low across all scenarios, with the highest deviation being just -0.20% for the 6m configuration. The Absolute Error % values are negative across all scenarios, implying that the simulated yields are consistently slightly lower than the actual yields. This behavior is somewhat unexpected, as simulations typically overshoot real-world data due to the absence of clipping and perfect environmental conditions modeled in Sunsolve. However, in this case, the opposite is observed, suggesting that the actual reflective performance of the boosters might be marginally better than captured by Sunsolve, possibly due to localized edge effects or minor variations in site conditions that are not fully replicated in the simulation environment.

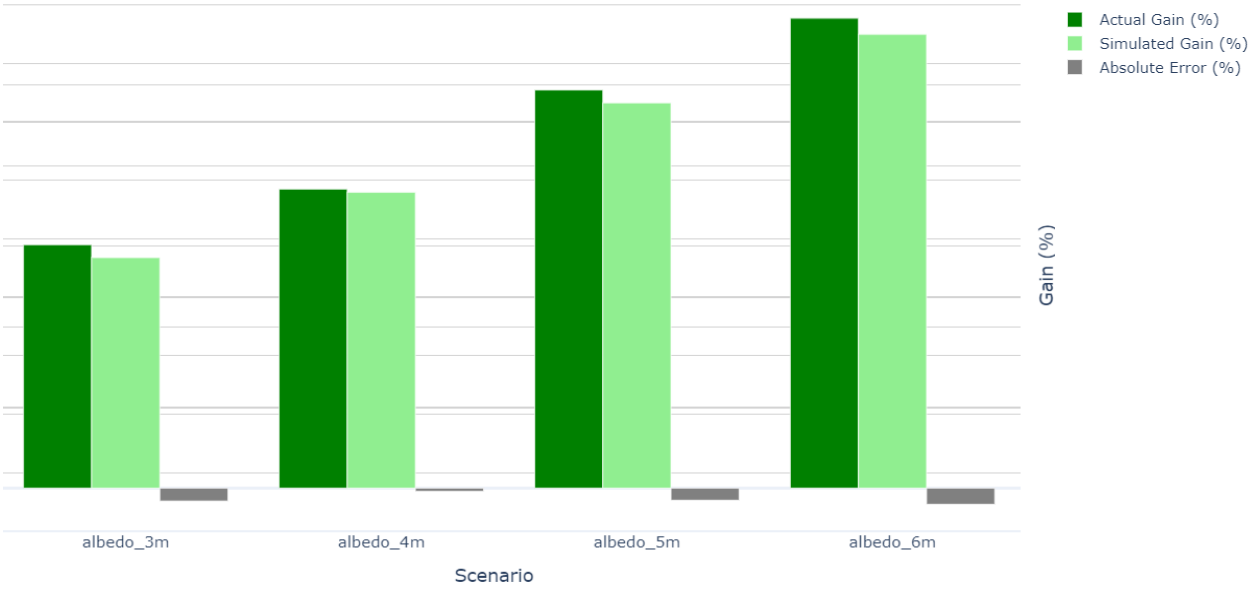


*Figure 52 Gain % and error comparison*

### Key Takeaways

1. Incremental Gain with Albedo Width: Both actual and simulated outputs exhibit a clear upward trend in energy yield and gain percentage as albedo width increases. This validates the expected effect of enhanced rear-side irradiance and confirms Sunsolve's ability to replicate it in relative terms.
1. Minimal Absolute Error with Slight Underestimation in Simulation: The low absolute error values indicate strong agreement between simulated and actual data, though the simulation slightly underestimates the actual gains across all scenarios.
2. Potential for Edge Effects or Local Variations: The consistent underestimation might point to localized edge effects or small-scale site-specific reflectivity enhancements that Sunsolve's model does not entirely capture.

## 5.5. Generation Yield Analysis

In order to accurately compare the simulated and actual generation yields, we first needed to account for clipping in the simulated Sunsolve data. As described in the methodology section, Sunsolve does not inherently model inverter clipping, so we applied a clipping threshold to the simulated results to mirror the physical inverter constraints observed in the actual site data. This adjustment allowed for a fair comparison of energy yields across the various scenarios.

## Analysis of the Yield Results

The results of the energy yield analysis are visualized in Figure 53, which presents the actual and simulated generation yields across all scenarios, along with the percentage error between the two. This visualization offers clear insights into how closely Sunsolve's clipped simulations align with real-world performance for different albedo booster configurations.

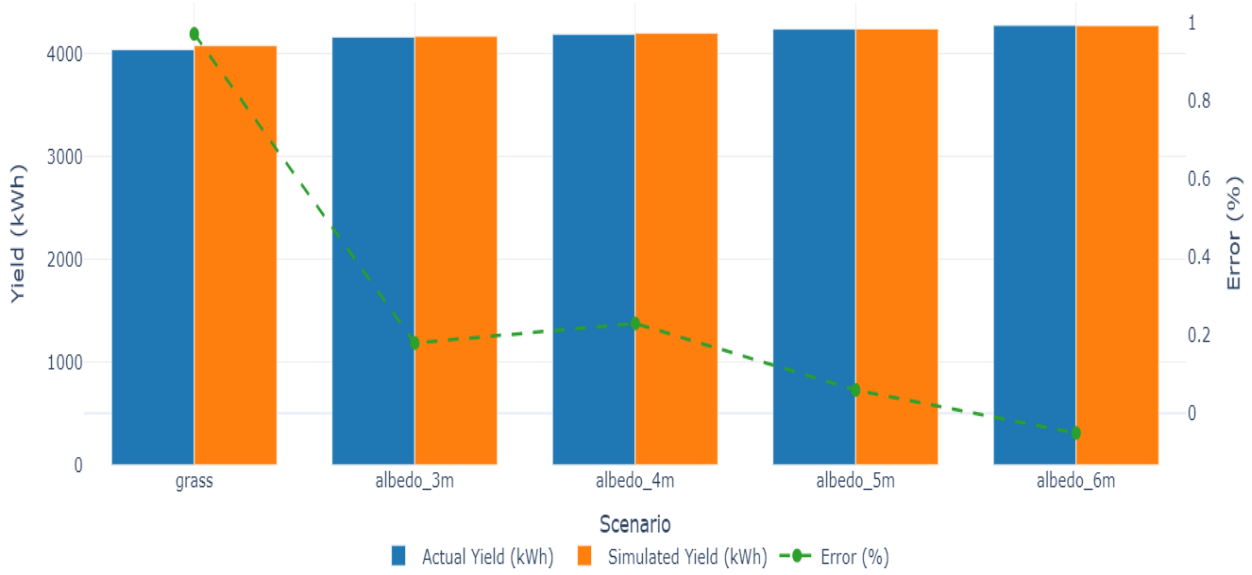


*Figure 53 Generation Yield Analysis*

A consistent pattern is observed: as the width of the albedo boosters increases, the discrepancy between the simulated and actual yields tends to decrease. In the baseline grass scenario, the simulation slightly overestimates the yield, a common occurrence due to idealized assumptions in the model, such as uniform irradiance, absence of soiling losses, and consistent weather conditions. These factors are difficult to replicate in field conditions, where such minor inefficiencies inevitably reduce the actual output.

With the introduction of albedo booster sheets, the alignment between simulation and field data improves significantly. In the narrower booster scenarios, the error percentage drops sharply, indicating a strong agreement between Sunsolve's model and the actual system behavior. This suggests that even modest rear-side irradiance enhancements are being accurately captured by the simulation.

As the albedo boosters become wider, this accuracy continues to improve. In intermediate configurations, the simulated yields remain very close to the actual values, with only minimal error observed. This trend reinforces the notion that Sunsolve is effectively capturing the impact of increased reflective surface area, especially when rear-side irradiance plays a more prominent role in energy generation.

In the widest booster configuration, a unique behavior is observed: the simulated yield is slightly lower than the actual yield. This reversal, where the simulation slightly underestimates performance, suggests that Sunsolve may be slightly conservative in estimating albedo gain at larger booster widths. Such behavior aligns well with the trends discussed in the Gain Yield Analysis section, where actual gains modestly exceeded the simulated ones in the higher-width configurations. This could be attributed to localized edge effects or subtle site-specific factors, such as unexpected reflective enhancements or terrain-induced concentration of light, which may not be fully captured in the simulation model.

Overall, the error percentages across all scenarios are consistently low, highlighting the robustness of Sunsolve's clipped simulation approach. The observed trends further affirm that Sunsolve is capable of accurately modeling rear-side irradiance and energy yield under varying albedo conditions. However, the consistently strong real-world performance of wider boosters, slightly exceeding simulation estimates, suggests that there may be nuanced physical effects at the site that offer marginally higher gains than predicted. These findings emphasize the importance of validating simulation models with empirical data, especially when assessing systems with non-standard surface treatments like reflective boosters.

## 5.6. Evaluation of Error Metrics

The error metrics, RMSE, SMAPE, $R^2$, and RMBE, provide a comprehensive assessment of the alignment between simulated and actual power outputs across different albedo booster configurations and varying weather conditions. Analyzing these metrics reveals distinct patterns and insights into the simulation model's performance.

### Full Dataset Analysis

In the full dataset, which encompasses all weather conditions, the $R^2$ values remain consistently high (around 0.96–0.961) across all scenarios, indicating a strong correlation between simulated and actual outputs. The RMSE values are relatively stable across scenarios, suggesting that the magnitude of errors does not significantly vary with booster width. However, the SMAPE values exhibit slight variations, with the Albedo 5m scenario showing the lowest SMAPE, indicating better proportional accuracy in this configuration.

The RMBE values transition from positive in the Grass scenario (0.967%) to slightly negative in the Albedo 6m scenario (-0.051%). This trend suggests that the simulation model tends to overestimate yields in scenarios without boosters and slightly underestimates in scenarios with wider boosters. This pattern aligns with observations from the gain yield analysis, where simulated gains were marginally lower than actual gains for wider boosters.

| Metric | grass | albedo_3m | albedo_4m | albedo_5m | albedo_6m |
|---|---|---|---|---|---|
| **RMSE** | 1504.084 | 1526.544 | 1520.13 | 1545.108 | 1532.118 |
| **SMAPE (%)** | 30.211 | 30.34 | 32.362 | 29.635 | 31.661 |
| **$R^2$ Score** | 0.96 | 0.96 | 0.961 | 0.96 | 0.961 |
| **RMBE (%)** | 0.967 | 0.178 | 0.225 | 0.063 | -0.051 |

*Table 5 Error metrics - All Days*

## Sunny Days Analysis

Focusing on sunny days, the $R^2$ values improve further (up to 0.986), reflecting the simulation model's enhanced performance under stable irradiance conditions. The RMSE values decrease across all scenarios, indicating reduced absolute errors. This is expected as the sunny days have a much smoother curve compared to diffused and mixed days which have more fluctuations in irradiance. Notably, the SMAPE values are significantly lower in this subset, especially for the Albedo 3m and 5m scenarios, suggesting that the model predicts proportional changes more accurately under clear skies.

| Metric | grass | albedo_3m | albedo_4m | albedo_5m | albedo_6m |
|---|---|---|---|---|---|
| **RMSE** | 1206.599 | 1262.541 | 1272.349 | 1283.597 | 1224.464 |
| **SMAPE (%)** | 24.066 | 19.03 | 25.534 | 20.422 | 21.305 |
| **$R^2$ Score** | 0.986 | 0.985 | 0.985 | 0.985 | 0.986 |
| **RMBE (%)** | 0.644 | -0.673 | 0.376 | 0.061 | -0.272 |

*Table 6 Error metrics - Sunny days*

The RMBE values fluctuate around zero, with both slight overestimations and underestimations observed. This variability indicates that while the model performs well overall, minor biases persist, possibly due to unmodeled site-specific factors or limitations in capturing the exact albedo effects under high irradiance conditions.

## Diffused Days Analysis

On diffused days, characterized by overcast conditions and scattered light, the $R^2$ values remain high (around 0.974–0.978), indicating that the model still captures the general trend of power output. However, the RMSE and SMAPE values increase, reflecting greater absolute and proportional errors. The RMBE values are consistently negative across all scenarios, suggesting a systematic underestimation of yields by the simulation model under diffused light conditions.

This underestimation could stem from the model's limitations in accurately representing the complex scattering and reflection of light in overcast conditions. Diffused irradiance can interact with the albedo boosters in unpredictable ways, enhancing rear-side illumination more than the model anticipates. Additionally, the model may not fully capture the edge effects and localized reflections that become more pronounced under such lighting conditions.

| Metric | grass | albedo_3m | albedo_4m | albedo_5m | albedo_6m |
|---|---|---|---|---|---|
| **RMSE** | 662.396 | 740.64 | 760.15 | 739.792 | 739.551 |
| **SMAPE (%)** | 19.839 | 24.88 | 29.903 | 23.114 | 22.781 |
| **$R^2$ Score** | 0.978 | 0.975 | 0.974 | 0.976 | 0.977 |
| **RMBE (%)** | -5.091 | -6.149 | -6.836 | -6.5 | -6.051 |

*Table 7 Error metrics - Diffused days*

In summary, the error metrics across different scenarios and weather conditions reveal that the simulation model performs well under stable conditions but faces minor challenges in accurately predicting outputs under variable and diffused lighting, Understanding these limitations is crucial for improving the model's accuracy and reliability in diverse operational environments.

# 6. Conclusion and Future Work

## 6.1. Summary of Findings

This thesis set out to evaluate the accuracy of Sunsolve's ray-tracing simulation in predicting the energy yield of bifacial PV systems equipped with multi-width albedo boosters, using real-world performance data from a bifacial PV site in France as a benchmark. The primary goal was to understand the alignment and discrepancies between Sunsolve's simulated results and actual site measurements under varying albedo conditions, as well as to explore the effectiveness of albedo boosters in enhancing energy generation.

The analysis began with a thorough investigation of the site-specific weather data, where multiple pyranometers were strategically placed across different sections of the PV plant. A mean GHI value was derived from these pyranometers, ensuring a representative and calibrated solar input for the simulations. Diffused Horizontal Irradiance (DHI) was then calculated using satellite-derived diffuse fractions, enabling a complete and consistent weather dataset for Sunsolve. This integration allowed for a realistic comparison between simulated and actual inverter outputs, highlighting the impact of real-time weather fluctuations on energy generation.

The evaluation of MPPT power generation revealed that Sunsolve's simulations generally aligned well with actual inverter data, with notable differences arising during instances of power clipping and transient cloud cover, which the simulation did not capture. Despite these discrepancies, the overall power generation patterns, particularly during peak irradiance periods, matched closely, confirming Sunsolve's ability to predict general energy trends effectively. However, slight temporal shifts during sunrise and sunset were observed, primarily due to real-world environmental interactions not fully replicated in the simulation.

A deeper analysis of albedo booster scenarios illustrated clear trends: as the width of the albedo sheets increased, both actual and simulated MPPT power outputs rose proportionally, demonstrating the intended albedo enhancement effect. The simulation successfully captured these trends, although simulated gains were slightly overestimated compared to actual yields. This was attributed to Sunsolve's idealized ray-tracing assumptions and lack of real-world edge effects and site-specific hardware nuances. Interestingly, the 6m albedo scenario showed the least deviation in yield compared to the field data, possibly due to its closer proximity to the reference grass inverter and minimized spatial inconsistencies.

Error metrics across different weather conditions, sunny, diffused, and the full dataset, provided further insights. During sunny periods, the alignment was stronger, with reduced

RMSE and higher $R^2$ values, indicating Sunsolve's robust performance under stable irradiance. Conversely, diffused days introduced more deviation, suggesting that cloud scattering and uneven light distribution are areas where simulation accuracy could be improved. The results consistently showed that spatial variations, inverter-specific behavior, and instantaneous cloud movements contributed to differences between simulated and actual results.

Finally, the gain yield analysis confirmed the effectiveness of albedo boosters in enhancing bifacial PV output, with both actual and simulated data showing increasing yields with larger booster widths. The analysis also highlighted the inherent limitations of simulations in perfectly capturing real-world performance, particularly during rapid weather changes and edge effects on the PV modules.

Overall, the findings validate Sunsolve's capacity to predict general performance trends for bifacial PV systems with albedo enhancement. However, the study also underscores the importance of field-specific adjustments and real-time weather considerations to bridge the gap between simulated models and actual performance. These insights set the stage for targeted improvements in simulation accuracy and field design optimization, paving the way for more reliable and efficient bifacial PV deployments.

## 6.2. Suggestions for Improving Field Setup and Validation

The field setup and validation process, while effective for this study, revealed several areas where improvements could significantly enhance data reliability and the accuracy of simulation comparisons. Addressing these aspects would not only refine the yield and gain analysis but also deepen the understanding of bifacial PV performance under varying albedo conditions.

1. Unified MPPT Allocation for Albedo Boosters: In the current field setup, albedo booster sheets of different configurations (3m, 4m, 5m, and 6m) were distributed across separate inverters and MPPTs. This introduced variations in MPPT algorithms, inverter-specific behavior, and exposure to localized weather effects, making direct comparisons less consistent. For future installations, it would be highly beneficial to place all albedo booster configurations under MPPTs of the same inverter. This would minimize discrepancies caused by inverter-specific behaviors, streamline the power curves for better analysis, and provide more reliable inter-scenario comparisons. With uniform MPPT characteristics, variations would more accurately reflect differences in albedo booster widths rather than inverter-specific behaviors.
2. Integration of Rear Albedo Sensors: One of the key limitations of the current validation process was the inability to directly measure rear-side irradiance, which is crucial for understanding bifacial gain. Integrating rear albedo sensors at the site would allow for

real-time monitoring of the reflected irradiance reaching the back of the panels. This would not only enable more precise validation against Sunsolve's rear irradiance predictions but also improve modeling accuracy by capturing variations in ground reflectivity throughout the day and across different weather conditions. Rear sensors would also help evaluate edge effects and localized shading that currently go unmeasured.

3. Longer Data Collection Periods: The current analysis was limited to a few months of data collection, mainly covering summer months when albedo sheets were installed. While this period was adequate to observe significant trends, a full-year dataset would provide a comprehensive understanding of seasonal variations in albedo performance. Different albedo effects can be expected during winter due to changes in sun angle, ground moisture, potential snow coverage, and varied diffuse irradiance. Extending the experimental campaign would enable the analysis of seasonal effects, including lower solar angles and different cloud patterns, resulting in a more holistic evaluation of the albedo booster impact.
4. Enhanced Ground Characterization: Sunsolve's accuracy is partly dependent on the precision of ground characterization parameters like albedo values and surface roughness. For future experiments, more detailed field measurements of ground albedo, especially under varying weather conditions, would improve simulation fidelity. This could include periodic sampling of albedo values throughout the year to account for environmental changes like soil dampness, vegetation growth, and surface degradation.
5. Cross-Validation with Multiple Simulation Tools: While Sunsolve has proven effective in simulating general trends, cross-validation with additional simulation tools like PVSyst or NREL's SAM (System Advisor Model) could provide more robust verification of results. This multi-model comparison would help identify modeling weaknesses specific to Sunsolve and ensure that observed trends are not artifacts of a single software's assumptions.

Implementing these improvements would significantly strengthen the analysis of bifacial PV systems with albedo boosters, providing deeper insights and more accurate performance assessments. Moreover, it would bridge the current gaps between simulation and reality, enhancing confidence in predictive modeling for future bifacial PV projects.

## 6.3. Future Research Considerations

Building upon the findings and observations of this study, several promising research avenues emerge that could further enhance the understanding and simulation accuracy of bifacial PV systems with multi-albedo surfaces. These considerations not only target the

optimization of field measurements but also the refinement of simulation accuracy through advanced modeling and novel analytical techniques.

1. Integration of Rear Sensors for Enhanced Data Collection: One of the key limitations in this study was the lack of real-time rear-side irradiance measurements. The integration of rear albedo sensors across various booster scenarios would allow for direct monitoring of reflected irradiance hitting the back of bifacial panels. This would enable a more granular comparison with Sunsolve's rear irradiance predictions, bridging the gap between simulated and actual bifacial gains. Moreover, real-time data from rear sensors would help identify shading events, localized albedo fluctuations, and edge effects more accurately. This would not only improve the calibration of Sunsolve models but also validate the effectiveness of different albedo booster configurations under varying sky conditions.

2. Exploration of Diverse Albedo Booster Materials: The current study was limited to specific albedo booster materials; however, future research could broaden this scope by evaluating a range of surface types with distinct albedo characteristics, such as white gravel, reflective membranes, painted coatings, and adaptive materials that dynamically alter reflectivity based on weather conditions. This would enable a more comprehensive assessment of albedo impact and support the optimization of booster material selection tailored to different climates and geographies. Additionally, investigating the spectral reflectance of these materials could reveal which wavelengths most effectively enhance rear-side irradiance, allowing for better alignment with the spectral sensitivity of bifacial modules to maximize yield. Future work could also consider the long-term durability of these materials under open-air exposure, as well as their environmental impact, including potential effects on local biodiversity and ecosystem balance.

3. Determining the Optimal Albedo Booster Width: An intriguing research question that emerged during this study is the existence of an optimal booster width beyond which additional width does not contribute proportionally to energy gains. While the study showed consistent improvement with increased booster width (3m, 4m, 5m, 6m), it is hypothesized that beyond a certain point, the incremental gain diminishes due to the angular limitations of reflected light reaching the panel's rear side. A detailed parametric analysis, combined with simulation and field data, could identify this saturation point, optimizing material usage and cost-efficiency for large-scale installations.

4. Custom Material Integration in Sunsolve: Sunsolve currently provides predefined material properties for albedo surfaces, but further research could explore the custom integration of site-specific reflectance data. This would involve measuring the spectral reflectance of materials at the site and importing this wavelength-specific data into Sunsolve. By creating custom albedo profiles within the simulation, the reflective behavior under different solar

spectra could be accurately modeled. This would help in evaluating not just the quantity but the quality of reflected irradiance, potentially improving the simulation accuracy for bifacial systems. Such capabilities would also allow for the testing of novel materials in a virtual environment before real-world deployment.

5. Machine Learning Applications for Enhanced Prediction and Optimization
Machine learning presents a powerful opportunity to bridge the gap between simulated and actual performance. Advanced predictive models could be trained on historical inverter performance, albedo measurements, and weather data to identify patterns and anomalies more effectively. This would allow for real-time performance prediction and anomaly detection, highlighting underperforming modules or unexpected shading events instantly. Furthermore, machine learning algorithms could be utilized to optimize Sunsolve's ray-tracing parameters, dynamically adjusting settings based on real-time environmental inputs for improved predictive accuracy.

Exploring these research directions could provide substantial advancements in both field measurement accuracy and simulation validation, strengthening the reliability of Sunsolve as a predictive tool for bifacial PV installations. Additionally, it would allow for more optimized system designs and cost-effective albedo booster configurations, enhancing the energy yield and economic feasibility of bifacial PV technology in real-world deployments.

## 6.4. Conclusion

This thesis evaluated the predictive accuracy of Sunsolve’s ray-tracing engine in modeling bifacial PV system performance under varying albedo conditions, benchmarked against field data from a real installation in France. The comparison revealed that Sunsolve was able to simulate energy yield with high fidelity under clear sky conditions, where irradiance was stable and consistent. It reproduced daily MPPT power curves and correctly reflected the diurnal energy generation behavior of the system. Quantitatively, RMSE remained below 6% of the observed MPPT power outputs, and $R^2$ exceeded 0.95 on sunny days, demonstrating Sunsolve’s reliability in accurately predicting bifacial performance across albedo scenarios.

However, a detailed analysis of mismatch periods revealed several sources of discrepancy between Sunsolve simulations and measured site performance. Deviations were most prominent during overcast periods, rapid cloud transients, and inverter clipping events. These discrepancies stemmed from real-world phenomena not fully captured in the simulation, such as rapid diffuse irradiance shifts, microclimatic effects across the PV array, and the simplified assumption of uniform rear-side irradiance. Furthermore, spatial variations in MPPT string responses introduced real-world dynamics that challenged the 1:1 alignment with the simulation's modeled outputs.

The effectiveness of albedo boosters of different widths was clearly demonstrated in both the field data and Sunsolve simulations. Wider boosters consistently resulted in increased rear irradiance capture and higher MPPT power, with both trends and magnitude of improvement largely reflected in the simulation results. Although Sunsolve slightly underpredicted performance gains in highly diffuse conditions, it accurately reproduced the relative differences across booster widths, reinforcing its suitability for modeling the optical impact of reflectors in bifacial system layouts.

To improve the alignment between simulated and actual system performance, this study incorporated site-specific inputs, including ground albedo measurements, accurate panel geometry, and on-site irradiance data. These enhancements reduced simulation error and improved the temporal correlation between modeled and measured outputs. However, the absence of direct rear-side irradiance sensors remained a limiting factor, making it difficult to validate rear-side contributions directly. This underlines the importance of detailed rear irradiance monitoring in future validation campaigns.

Finally, the study explored potential optimizations to Sunsolve's simulation parameters to further enhance predictive accuracy. Refinements in ray density, scene segmentation, and shading resolution reduced noise in simulated outputs and improved numerical stability. Yet, limitations remain in Sunsolve's ability to capture fast-changing sky conditions and the nuanced electrical response of individual MPPTs. Further improvements in weather input resolution, dynamic cloud modeling, and inverter behavior simulation could help bridge this remaining performance gap.

In conclusion, Sunsolve has proven to be a robust and insightful simulation tool for bifacial PV system modeling, particularly for evaluating the impact of reflective surface enhancements. It reliably captured energy generation trends under a variety of albedo conditions and demonstrated strong alignment with measured site data during stable irradiance periods. While the tool's performance decreases under highly variable atmospheric conditions, this study highlights clear pathways for improvement through better input fidelity and more comprehensive validation strategies. The results affirm the growing value of ray-tracing models in bifacial PV design and provide a foundation for more accurate, efficient, and cost-effective system optimization in future research and engineering applications.

# 7. REFERENCES


[1] “Getting Started with SunSolve Yield,” SunSolve. [Online]. Available: https://sunsolve.info/yield/start/

[2] N. Ford and N. Ford, “US solar tracker dominance offers learnings for other markets,” *Reuters*, Aug. 08, 2024. [Online]. Available: https://www.reuters.com/business/energy/us-solar-tracker-dominance-offers-learnings-other-markets-2024-08-08/.

[3] “Passivated Emitter and Rear Cell (PERC),” Millennium Technology Prize. [Online]. Available: https://millenniumprize.org/winners/passivated-emitter-and-rear-cell-perc/

[4] “PERT solar cells.” [Online]. Available: https://sinovoltaics.com/learning-center/solar-cells/pert-solar-cells/

[5] “Heterojunction solar cell,” *Wikipedia*. Feb. 11, 2025. [Online]. Available: https://en.wikipedia.org/w/index.php?title=Heterojunction_solar_cell&oldid=1275243523.

[6] C. Deline, S. MacAlpine, and B. Marion, “Evaluation and Field Assessment of Bifacial Photovoltaic Module Power Rating Methodologies: Preprint”.

[7] “Albedo, the unknown: a green boost for photovoltaic systems,” Enel Green Power. [Online]. Available: https://www.enelgreenpower.com/media/news/2023/11/albedo-photovoltaic-panel

[8] “Albedo,” *Wikipedia*. Mar. 03, 2025. [Online]. Available: https://en.wikipedia.org/w/index.php?title=Albedo&oldid=1278647862.

[9] X. Sun, M. R. Khan, C. Deline, and M. A. Alam, “Optimization and Performance of Bifacial Solar Modules: A Global Perspective,” *Appl. Energy*, vol. 212, pp. 1601–1610, Feb. 2018, doi: 10.1016/j.apenergy.2017.12.041.

[10] amerisolar, “Albedo in Solar Panels,” Amerisolar. [Online]. Available: https://www.weamerisolar.eu/albedo-in-solar-panels/

[11] “Using artificial ground reflectors to boost the efficacy of solar panels.” [Online]. Available: https://techxplore.com/news/2024-05-artificial-ground-reflectors-boost-efficacy.html

[12] S. Golroodbari and W. Van Sark, “On the effect of dynamic albedo on performance modelling of offshore floating photovoltaic systems,” *Sol. Energy Adv.*, vol. 2, p. 100016, 2022, doi: 10.1016/j.seja.2022.100016.

[13] S. Wei *et al.*, “Small reduction in land surface albedo due to solar panel expansion worldwide,” *Commun. Earth Environ.*, vol. 5, no. 1, pp. 1–10, Aug. 2024, doi: 10.1038/s43247-024-01619-w.

[14] “Solar cell,” *Wikipedia*. Apr. 23, 2025. [Online]. Available: https://en.wikipedia.org/w/index.php?title=Solar_cell&oldid=1286956542.

[15] M. Ernst, C.-A. Asselineau, P. Tillmann, K. Jäger, and C. Becker, “Modelling bifacial irradiance – Step-by-step comparison and validation of view factor and ray tracing models,” *Appl. Energy*, vol. 369, p. 123574, Sep. 2024, doi: 10.1016/j.apenergy.2024.123574.

[16] “Revisiting Bifacial Module technology.pdf.” [Online]. Available: https://www.naturalpower.com/mediaLibrary/other/english/2395.pdf?

[17] S. Bouchakour, D. Valencia-Caballero, A. Luna, E. Roman, E. A. K. Boudjelthia, and P. Rodríguez, "Modelling and Simulation of Bifacial PV Production Using Monofacial Electrical Models," *Energies*, vol. 14, no. 14, Art. no. 14, Jan. 2021, doi: 10.3390/en14144224.
[18] G. Noy, "Ray Tracing Techniques in Optical Simulation Software," 3DOptix. [Online]. Available: https://www.3doptix.com/blog/ray-tracing-techniques-in-optical-simulation-software/
[19] S. A. Peláez, C. Deline, B. Marion, B. Sekulic, and J. Stein, "Understanding Bifacial PV Modeling: Raytracing and View Factor Models," *NREL*.
[20] "Project design > Bifacial Systems > 2D Bifacial model conditions," PVSyst. [Online]. Available: https://www.pvsyst.com/help-pvsyst7/bifacial-conditions.htm?
[21] E.-M. Grommes, F. Schemann, F. Klag, S. Nows, and U. Blieske, "Simulation of the irradiance and yield calculation of bifacial PV systems in the USA and Germany by combining ray tracing and view factor model," *EPJ Photovolt.*, vol. 14, p. 11, 2023, doi: 10.1051/epjpv/2023003.
[22] M. Ernst, G. E. J. Conechado, and C.-A. Asselineau, "Accelerating the simulation of annual bifacial illumination of real photovoltaic systems with ray tracing," *iScience*, vol. 25, no. 1, p. 103698, Jan. 2022, doi: 10.1016/j.isci.2021.103698.
[23] J. Kang, J.-H. Jang, C. Reise, and K. Lee, "PRACTICAL COMPARISON BETWEEN VIEW FACTOR METHOD AND RAY-TRACING METHOD FOR BIFACIAL PV SYSTEM YIELD PREDICTION," 2019. [Online]. Available: https://www.semanticscholar.org/paper/PRACTICAL-COMPARISON-BETWEEN-VIEW-FACTOR-METHOD-AND-Kang-Jang/262d775892c33b27dbfeb9a2d82102d27c860e40.
[24] E. M. Tonita, C. E. Valdivia, A. C. J. Russell, M. Martinez-Szewczyk, M. I. Bertoni, and K. Hinzer, "A general illumination method to predict bifacial photovoltaic system performance," *Joule*, vol. 7, no. 1, pp. 5–12, Jan. 2023, doi: 10.1016/j.joule.2022.12.005.
[25] S. Ghafiri, M. Darnon, A. Davigny, J. P. F. Trovão, and D. Abbes, "A comprehensive performance evaluation of bifacial photovoltaic modules: insights from a year-long experimental study conducted in the Canadian climate," *EPJ Photovolt.*, vol. 15, p. 28, 2024, doi: 10.1051/epjpv/2024025.
[26] "HOME - SoDa." [Online]. Available: https://www.soda-pro.com/home
[27] "SunSolve™ - When Accuracy Matters.," SunSolve. [Online]. Available: https://sunsolve.info/
[28] "Can I run a simulation with two albedo on ground?," PVsyst forum. [Online]. Available: https://forum.pvsyst.com/topic/2620-can-i-run-a-simulation-with-two-albedo-on-ground/
[29] the use of cloud computing P. L. C. K. McIntosh, C. B. S. argue that their software can be useful for module makers, T. Suppliers, and P. project developers alike J. Gifford, "The long read: Capturing complexity through the power of the cloud," pv magazine India. [Online]. Available: https://www.pv-magazine-india.com/2020/11/21/the-long-read-capturing-complexity-through-the-power-of-the-cloud/
[30] Sunsolve Yield, "Info0030 - Extracting PVSyst inputs with SunSolve.pdf," *Sunsolve*, [Online]. Available: https://downloads.pvlighthouse.com.au/white-papers/pvsyst-factors/Info0030%20-%20Extracting%20PVSyst%20inputs%20with%20SunSolve.pdf.

[31] “Monte Carlo Ray Tracing: Chapter 38:,” Graphics Compendium. [Online]. Available: https://graphicscompendium.com/raytracing/19-monte-carlo
[32] Steve Marschner, “Monte Carlo Ray Tracing,” Cornell CS4620 Spring 2013 • Lecture 22. [Online]. Available: https://www.cs.cornell.edu/courses/cs4620/2013fa/lectures/22mcrt.pdf
[33] “Transfer-matrix method (optics),” *Wikipedia*. Oct. 21, 2024. [Online]. Available: https://en.wikipedia.org/w/index.php?title=Transfer-matrix_method_(optics)&oldid=1252369244.
[34] “Short-Circuit Current | PVEducation,” PVEducation. [Online]. Available: https://www.pveducation.org/pvcdrom/solar-cell-operation/short-circuit-current
[35] “Physical models used > PV Module - Standard one-diode-model,” PVSyst. [Online]. Available: https://www.pvsyst.com/help-pvsyst7/index.html?pvmodule_model.htm
[36] M. J. Heredia-Rios, L. Hernandez-Martinez, M. Linares-Aranda, M. Moreno-Moreno, and J. F. Méndez, “Analysis of Losses Associated with Series Resistance (Rs) in Simple-Structured c-Si Solar Cells,” *Energies*, vol. 17, no. 7, Art. no. 7, Jan. 2024, doi: 10.3390/en17071520.
[37] “(PDF) Determining Components of Series Resistance from Measurements on a Finished Cell,” in *ResearchGate*, doi: 10.1109/WCPEC.2006.279656.
[38] “ODSOS Lab - What’s the meaning of a light J-V curve?,” ODSOS Lab. [Online]. Available: https://sites.google.com/view/odsos-lab/some-concepts/whats-the-meaning-of-a-light-j-v-curve
[39] Sunsolve Yield, *Running your first simulation in SunSolve Yield*, (Nov. 17, 2023). [Online Video]. Available: https://sunsolve.info/videos/yield_running_first_sim/.
[40] Sunsolve Yield, *Understanding the different types of modules in SunSolve Yield (simple versus complex)*, (Dec. 07, 2023). [Online Video]. Available: https://sunsolve.info/videos/yield_module_types/.
[41] Pv. Team, “Fixed tilt vs tracker system comparison for ground-mounted PV systems,” PVcase. [Online]. Available: https://pvcase.com/blog/fixed-tilt-vs-tracker-system-comparison-for-ground-mounted-pv-systems/
[42] “Choosing PV structures: Trackers vs Fixed vs East-West (Case study inside!) — RatedPower.” [Online]. Available: https://ratedpower.com/blog/choosing-pv-structures/
[43] “Lambertian reflectance,” *Wikipedia*. Oct. 01, 2023. [Online]. Available: https://en.wikipedia.org/w/index.php?title=Lambertian_reflectance&oldid=1178132508.
[44] D. Faiman, “Assessing the outdoor operating temperature of photovoltaic modules,” *Prog. Photovolt. Res. Appl.*, vol. 16, no. 4, pp. 307–315, 2008, doi: 10.1002/pip.813.
[45] “Faiman Module Temperature Model,” PV Performance Modeling Collaborative (PVPMC). [Online]. Available: https://pvpmc.sandia.gov/modeling-guide/2-dc-module-iv/module-temperature/faiman-module-temperature-model/
[46] “Array Thermal losses - PVsyst documentation,” PVSyst. [Online]. Available: https://www.pvsyst.com/help/project-design/array-and-system-losses/array-thermal-losses/index.html#thermal-model
[47] “ChatGPT,” ChatGPT. [Online]. Available: https://chatgpt.com

[48] B. Y. H. Liu and R. C. Jordan, “The interrelationship and characteristic distribution of direct, diffuse and total solar radiation,” *Sol. Energy*, vol. 4, no. 3, pp. 1–19, Jul. 1960, doi: 10.1016/0038-092X(60)90062-1.
[49] “pvlib.irradiance.isotropic,” *PVLib*. [Online]. Available: https://pvlib-python.readthedocs.io/en/stable/reference/generated/pvlib.irradiance.isotropic.html.
[50] N. R. Kamphuis, C. A. Gueymard, M. T. Holtzapple, A. T. Duggleby, and K. Annamalai, “Perspectives on the origin, derivation, meaning, and significance of the isotropic sky model,” *Sol. Energy*, vol. 201, pp. 8–12, May 2020, doi: 10.1016/j.solener.2020.02.067.
[51] “Hay and Davies Sky Diffuse Model,” PV Performance Modeling Collaborative (PVPMC). [Online]. Available: https://pvpmc.sandia.gov/modeling-guide/1-weather-design-inputs/plane-of-array-poa-irradiance/calculating-poa-irradiance/poa-sky-diffuse/hay-and-davies-sky-diffuse-model/
[52] P. G. Loutzenhiser, H. Manz, C. Felsmann, P. A. Strachan, T. Frank, and G. M. Maxwell, “Empirical validation of models to compute solar irradiance on inclined surfaces for building energy simulation,” *Sol. Energy*, vol. 81, no. 2, pp. 254–267, Feb. 2007, doi: 10.1016/j.solener.2006.03.009.
[53] R. Perez, R. Seals, P. Ineichen, R. Stewart, and D. Menicucci, “A new simplified version of the perez diffuse irradiance model for tilted surfaces,” *Sol. Energy*, vol. 39, no. 3, pp. 221–231, Jan. 1987, doi: 10.1016/S0038-092X(87)80031-2.
[54] R. Perez, P. Ineichen, R. Seals, J. Michalsky, and R. Stewart, “Modeling daylight availability and irradiance components from direct and global irradiance,” *Sol. Energy*, vol. 44, no. 5, pp. 271–289, Jan. 1990, doi: 10.1016/0038-092X(90)90055-H.
[55] P. Gilman, “SAM Photovoltaic Model Technical Reference,” NREL, NREL/TP--6A20-64102, 1215213, May 2015. doi: 10.2172/1215213.
[56] “pvlib.irradiance.perez — pvlib python 0.12.0 documentation.” [Online]. Available: https://pvlib-python.readthedocs.io/en/stable/reference/generated/pvlib.irradiance.perez.html
[57] “Perez Sky Diffuse Model,” PV Performance Modeling Collaborative (PVPMC). [Online]. Available: https://pvpmc.sandia.gov/modeling-guide/1-weather-design-inputs/plane-of-array-poa-irradiance/calculating-poa-irradiance/poa-sky-diffuse/perez-sky-diffuse-model/
[58] I. Reda and A. Andreas, “Solar Position Algorithm for Solar Radiation Applications (Revised),” NREL/TP-560-34302, 15003974, Jan. 2008. doi: 10.2172/15003974.
[59] M. Blanco-Muriel, D. C. Alarcón-Padilla, T. López-Moratalla, and M. Lara-Coira, “Computing the solar vector,” *Sol. Energy*, vol. 70, no. 5, pp. 431–441, 2001, doi: 10.1016/S0038-092X(00)00156-0.
[60] J. J. Michalsky, “The Astronomical Almanac’s algorithm for approximate solar position (1950–2050),” *Sol. Energy*, vol. 40, no. 3, pp. 227–235, 1988, doi: 10.1016/0038-092X(88)90045-X.
[61] R. Walraven, “Calculating the position of the sun,” *Sol. Energy*, vol. 20, no. 5, pp. 393–397, 1978, doi: 10.1016/0038-092X(78)90155-X.
[62] J. Spencer, “Fourier series representation of the position of the sun | BibSonomy.” [Online]. Available: https://www.bibsonomy.org/bibtex/d0ca49e4d3dccfcacdcf66df6fe90a76

[63] M. Reno, J. Stein, and C. Hansen, “Global horizontal irradiance clear sky models : implementation and analysis.,” SAND2012-2389, 1039404, Mar. 2012. doi: 10.2172/1039404.
[64] “Physical models used > Solar Geometry,” PVSyst. [Online]. Available: https://www.pvsyst.com/help-pvsyst7/solar_geometry.htm
[65] J. Zimmerman, “Sun-pointing programs and their accuracy,” SAND-81-0761, 6377969, ON: DE81025016, May 1981. doi: 10.2172/6377969.
[66] “Root mean square deviation,” *Wikipedia*. Feb. 16, 2025. [Online]. Available: https://en.wikipedia.org/w/index.php?title=Root_mean_square_deviation&oldid=1276071811.
[67] “Symmetric mean absolute percentage error,” *Wikipedia*. Feb. 25, 2025. [Online]. Available: https://en.wikipedia.org/w/index.php?title=Symmetric_mean_absolute_percentage_error&oldid=1277591083.
[68] “R Squared: Understanding the Coefficient of Determination,” Arize AI. [Online]. Available: https://arize.com/blog-course/r-squared-understanding-the-coefficient-of-determination/
[69] “Mean Bias Error - an overview | ScienceDirect Topics.” [Online]. Available: https://www.sciencedirect.com/topics/engineering/mean-bias-error
[70] “Dijon, France Weather History | Weather Underground.” [Online]. Available: https://www.wunderground.com/history/daily/fr/dijon/IDIJON155/date/2022-8-21
[71] W. Atlas, “July weather - Summer 2025 - Dijon, France,” Weather Atlas. [Online]. Available: https://www.weather-atlas.com/en/france/dijon-weather-july
[72] “Dijon Climate, Weather By Month, Average Temperature (France) - Weather Spark.” [Online]. Available: https://weatherspark.com/y/52152/Average-Weather-in-Dijon-France-Year-Round
[73] R. Urraca, C. Lanconelli, and N. Gobron, “Impact of the Spatio-Temporal Mismatch Between Satellite and In Situ Measurements on Validations of Surface Solar Radiation,” *J. Geophys. Res. Atmospheres*, vol. 129, no. 10, p. e2024JD041007, 2024, doi: 10.1029/2024JD041007.
[74] S. Cros, M. Albuisson, M. Lefèvre, C. Rigollier, and L. Wald, “HelioClim: a long-term database on solar radiation for Europe and Africa,” *Proc. Eurosun*, 2004.